The Directed Heavy Atom Effect:
A Design Principle for Metal-Free Organic Phosphors

by

Onas James Bolton

A dissertation submitted in partial fulfillment
of the requirements for the degree of
Doctor of Philosophy
(Materials Science and Engineering)
in The University of Michigan
2010

Doctoral Committee:

Associate Professor Jinsang Kim, Chair
Associate Professor Lingjie Guo
Assistant Professor Max Shtein
Assistant Professor Anton Van der Ven

For Carrie, Charlotte, and Abby.

Acknowledgements

I first must thank Professor Jinsang Kim. When I first met with Professor Kim I was an under-utilized engineer at a struggling company, possessor of a modest academic record, four years removed from college, and clinging to uncertain hope that I be accepted into graduate school. I can only imagine now what he saw in me then, but nothing in my time at Michigan is more visible than his commitment to support and mentor me. The opportunity he gave me is perhaps the greatest professional, and in some ways personal, gift I have ever received and I will always be in his debt. Thank you, Professor Kim.

Secondly I must thank my colleague, Dr. Kangwon Lee, whose unbridled success in his main research is the only reason I was lucky enough to inherit this most interesting and fruitful project. Without his keen observations none of these findings nor our success with them would have happened. Thank you, Kangwon.

I would also like to thank the members of our research group and my other collaborators. In particular Dr. Hyong-Jun Kim, Dr. Myung-Su Kim, Dr. Eun Jeong Jeong, and Bong-Gi Kim contributed much time as they helped to make devices and new compounds. Dr. Jae Choel Cho taught me the finer points of chemical synthesis. Laura, Rob, Donghwan, and Jisama, I will always treasure your camaraderie. The members of the Shtein Group, Shaurjo Biswas and Steven Morris, were selfless with their time to fabricate devices and move our materials further. Thanks, all.

The small army of undergraduate students that helped me can certainly not be forgotten. In the project's early days Kevin Lin and Matt Gray suffered with me as we struggled to identify the critical compound. Later Jacqueline Harper, Young-Do Kim, Sarah Wang, Sunghyun Jeon, and Kevin Yien helped to take the work to new places and run lots and lots of tests. Lots. Their contributions were all critical. Thanks, guys.

Of course, I thank my family for their support throughout the years. I am the product of their love and guidance and I hope I make them proud. Thanks to my Grandparents and siblings. Thanks to Fred and Jean for helping me juggle science and fatherhood in these last critical months. To Mom and Dad love and thanks for your enduring support. Thanks for band concerts, cars, food/shelter, tuition, and lessons learned as I watched from the kindergarten window.

My daughter, Charlotte, and dog, Abby, didn't contribute a great deal of direct help. In fact, their disregard for my privacy and pointed distain for my focus while writing this seemed, at the time, quite counterproductive. Still, they are both ridiculously cute and having two adorable cherubs at constant play on the center stage of my life gives the entire performance its truest purpose. Hugs and kisses.

Lastly and most importantly, I must thank my wife for whom I dedicate all things I do. My success has come only through her support and patience. Thanks, Carrie. I love you.

Table of Contents

List of Figures

List of Tables

List of Schemes

Abstract

Phosphorescent materials are changing the way organic compounds are used in optical devices. By being more efficient, slower emitting, and uniquely sensitive they are expanding the applicability of organic materials. In order, though, for this trend to include *all* organic materials the critical limitation of an organometallic structure must be overcome. At the time of this publishing, organometallics alone preform well enough for applicational use. Here is presented the Directed Heavy Atom Effect (DHAE), a design principle to realize bright phosphorescence from metal-free organic compounds. By synergistically combining the phosphorescence-enhancing property of the heavy atom effect with the heavy atom directing property of halogen bonding, DHAE achieves organic phosphors with efficiencies competitive to organometallic and inorganic materials. Here the DHAE is attained by cocrystallizing an aromatic aldehyde with an optically inert, halogenated analog. These cocrystals exhibit halogen bonding, which directs the heavy atom to enhance spin-orbit coupling at the carbonyl and activate phosphorescence. The optically inert host isolates the chromophore from self-quenching, resulting in unprecedentedly bright metal-free organic phosphorescence. From this design principle a variety of materials with varying properties are synthesized. Emission color can be tuned in either fine steps of 5 nm or broad chromic steps from blue to green, yellow, and orange. Material modifications, DHAE phosphors with controllable, vapor deposited microstructures or ester functionalization, are also achievable with careful material design presented here. The novel phenomenon of delayed phosphorescence is demonstrated from crystals of pure DHAE chromophore, holding promise for enhancing emissive device efficiencies. To escape design complications, polymeric hosts are presented as an alternative to crystal systems. If well designed, polymer hosts can produce bright phosphorescence even from liquid DHAE-style chromophores by suppressing vibrational dissipation pathways. Finally a broad summation of the work is offered along with ideas about the future direction of DHAE phosphors.

Chapter 1

Introduction and Background

This chapter describes the importance of phosphorescence first by explaining its fundamental differences to fluorescence. It illustrates the pertinent excited state transitions that make phosphorescence possible as well as the measurable values used to examine it and the methods by which they are evaluated. A growing list of commercial applications for which phosphorescent materials are desirable demonstrates the need for more organic phosphors then a brief categorical review of known organic phosphors is presented with their benefits and limitations highlighted. The most important finding in this report is a new design principle to create bright metal-free organic phosphors and the concepts presented in this chapter give the reader the background to understand why this principle works and why the finding is so significant.

1.1 Fluorescence and Phosphorescence

Fluorescence and Phosphorescence are both means by which matter emits light, yet the subtle differences between them make each uniquely useful for specific applications. To understand the novelty of the work presented here one must grasp the differences between them and the electronic states and transitions that govern them. These concepts are explained here at a level of depth sufficient for the average reader. For more complete descriptions of the quantum mechanical basis of atomic electronic states see cited references and texts.[1,2,3,4]

1.1.1 Singlets and Triplets

Electrons are particles with ½ integer spins, they exhibit angular momentum of $\sqrt{3}/2\ \hbar$ (where $\hbar$ is the reduced Plank's constant). These properties define them as fermions and limit their position by Fermi-Dirac statistics. No two electrons can occupy the same quantum state at the same time as per the Pauli exclusion principle, from which Fermi-Dirac statistics are derived. In order for two electrons to share an orbital they must have opposite spins, thereby occupying two separate quantum states. In more complete terms, the total wavefunction of two electrons in an orbital must be anti-symmetric. That is, if the two electrons were to exchange positions their wavefunction would be inverted. This is often stated simply as requiring that two electrons in the same molecular orbital have opposite spins, +½ (↑) and -½ (↓), but the quantum mechanical description of the wavefunction symmetry under particle exchange is more precise.

For any given system of two electrons there exist four possible orientations of their collective spin: ↑↑, ↑↓, ↓↓, and ↓↑. From these four possibilities, only one satisfies the anti-symmetric requirement of the Pauli exclusion principle once we apply particle exchange:

$$S = \frac{1}{\sqrt{2}}\{\uparrow\downarrow\ -\downarrow\uparrow\} =\ 0$$

While the other possibilities yield a net spin of 1 and each is symmetric under particle exchange:

$$S = \frac{1}{\sqrt{2}}\{\uparrow\downarrow\ +\downarrow\uparrow\} =\ 1$$

$$S = \uparrow\uparrow = 1$$

$$S = \downarrow\downarrow = 1$$

These states are named accordingly singlet (S=0) and the three degenerate[5] triplets (S=1). Thus only singlets satisfy the Pauli exclusion principle.

It may be difficult to understand why one case of spin-opposite pairing is a singlet while the other is a triplet. The binary view of spin is a construct that is too simple to fully explain these states. It is important to remember that spin is a three-dimensional property of the rotating electron. Figure 1.1 attempts to use vector representation to illustrate how there exists four possible spin orientations for two electrons. In the rightmost example both electrons are what might be called spin opposite, but their resultant spin is actually non-zero in the xy plane because their dipoles are not out-of-phase. Only when both spins are opposite and out-of-phase do we have a total zero resultant, a singlet state.[6]

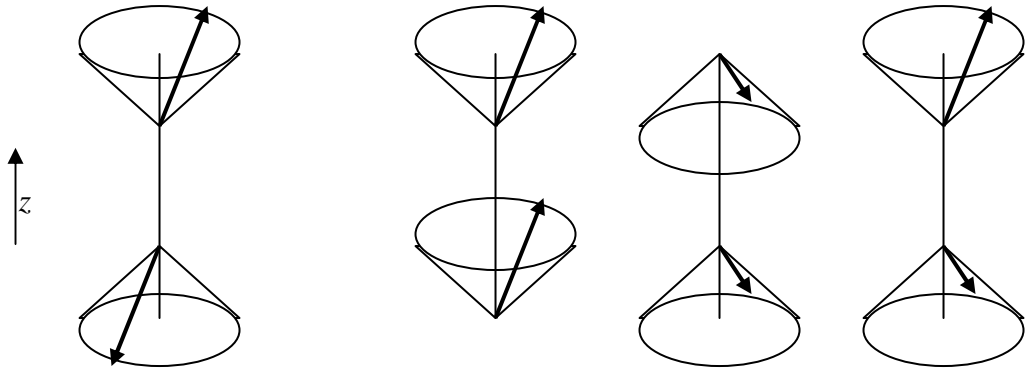

Singlet: electrons are spin opposite and out-of-phase. There is zero resultant.

Triplets: electrons are either spin parallel or in phase. Each has a non-zero resultant.

Figure 1.1 Electron spin diagram showing singlet and triplet states. Recreated from Turro.[3] Precession is important to whether the vectors are perfectly out-of-phase.

In the ground state, all electrons in most organic molecules are sharing orbitals as they are either bonded or coupled as lone pairs. Thus they must be singlets. In excited states, however, spin orientations are no longer restricted because two of the electrons are no longer sharing an orbital. While excited either of those electrons have the freedom to change their spin as they now exist in partially filled orbitals. This process is often referred to colloquially as *flipping* and technically as *intersystem crossing*. Under first order approximations, however, this is strictly disallowed as it does not conserve angular

momentum. The total spin changes from 0 to 1 or vice versa during flipping. As will be discussed later, though, certain second order external effects can mix singlet and triplet states making intersystem crossing possible and in some cases very efficient.

In molecules there exist a large number of orbitals whose wavefunctions can be either antisymmetric (singlets) or symmetric (triplets), though, as stated, ground state configurations for most organic molecules contain orbitals that are all singlets. A theoretically infinite number of singlet states exist for any molecule and are numbered in order of increasing energy, S_1 to S_n. The ground state is often referred to as S_0, since it is also a singlet and the lowest in energy.

Molecules also posses potential triplet state configurations, though they are rarely populated when the molecule is not in an excited state. Triplet states are numbered also by increasing energy from T_1 to T_n. T_0 does not exist for most organic compounds because there is no ground state triplet (molecular oxygen is a notable exception). Ground states in nearly all organic molecules are fully bonded or paired requiring all orbitals to be singlets. Chemists can think of electrons in triplet states as diradicals: the excited state molecule contains two non-bonding, unpaired electrons.

1.1.2 Excited State Transitions

In order to understand the fundamental differences between fluorescence and phosphorescence and to see how we can analyze the materials described in this work it is important to understand what exactly is happening to the electrons of an excited molecule. Described here are the primary actions of an optically active organic molecule. While much of this description applies to non-organic materials as well, this is written with organic molecules in mind. Figure 1.2 illustrates each of the transitions described in this section.

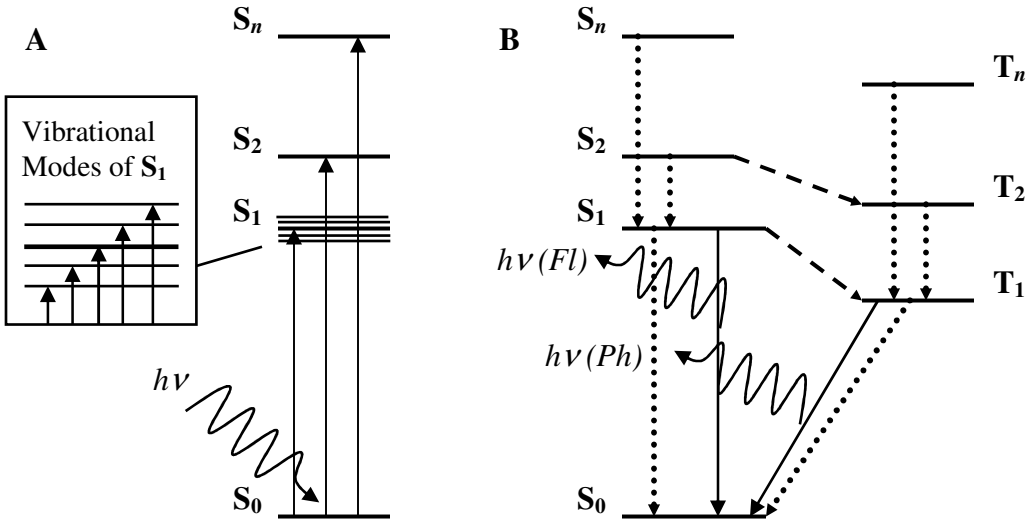

Figure 1.2 Energy diagram showing important excited state transitions. (**A**) Absorption transitions with inset highlighting vibrational modes of S_1 (vibratioanl modes exist but are not shown here for other states). (**B**) Excited state transitions. Quantum transitions are identified by solid arrows, vibrational transitions have dotted lines, and intersystem crossings are dashed. (Note that both transitions from T_1 to S_0 are technically also considered intersystem crossing.)

When an organic molecule is struck by a photon whose energy is equal to the gap between the molecule's ground state, S_0, and any of its higher energy singlet states S_n (where $n > 0$) it may absorb that photon's energy to become excited. The photon acting on the molecule is referred to as the excitation light and the molecule is then in one of its excited states. This process is *absorption*. It is a spin-conserving phenomenon meaning that it allows only for singlet-to-singlet transitions. For many organic molecules the $S_0 \rightarrow S_1$ transition falls with the range of visible light. Higher order transitions, $S_0 \rightarrow S_{1+n}$, are possible but most likely to relax quickly to S_1 by Kasha's Rule.[7] Thus S_1 is typically where the excited state molecule begins its excited state activity. The shorthand representation of absorption is $S_0 + h\nu \rightarrow S_1$.

Once excited by absorption the excited electron undergoes a small amount of *vibrational* relaxation. This is caused by the subtle changes the overall molecular structure undergoes once the two electrons in question are no longer bonded. With the excited electron no longer sharing orbital space with the ground state electron there is less attractive force between their two nuclei. The molecule, like balls connected by springs, shifts to stabilize this new electronic arrangement. This manifests in a slight relaxation of

the excited electron. The small steps via which it does this relaxing are the *vibrational modes* of the excited state. These modes exist for every excited state (including S_0), are usually numerous but small in energy, can be affected by environment and configuration, and are greatly affected by temperature. That last point means that at low temperature nuclear movement is restricted and some, perhaps all, vibrational modes become inaccessible. Figure 1.2 shows vibrational modes as an inset to the energy diagram.

From S_1 there are three possible actions the excited electron can take, which are each depicted in Figure 1.2. The first and often most favorable is *fluorescence*, which is emissive, quantum relaxation from the singlet state. This is most favorable because in S_1 both the excited and ground state electrons are in their original spin orientation, which makes direct quantum relaxation very rapid. For most organic molecules fluorescent relaxation usually occurs in picosecond or nanosecond timescales. In shorthand fluorescence is $S_1 \rightarrow S_0 + h\nu$.

The second route is *internal conversion*, sometimes referred to as *vibrational dissipation*. Just as vibrational modes allow for S_1 to relax somewhat following absorption, there may be sufficient modes to allow S_1 to relax completely to S_0. This may be an internal function or made possible by vibrational interaction with neighboring molecules (solvents for example). The result is that the absorbed photon's energy is eventually lost to vibrational energy, heat. Figure 1.2 shows this route as a dotted arrow. The shorthand is $S_1 \rightarrow S_0 + heat$.

The third most common route to singlet relaxation is *intersystem crossing*. This is the process by which singlets become triplets. It occurs when one or both of the electrons change their spin. The process requires a non-conserving change in spin, forbidden by first order approximations. Changes to the angular momentum of the electron are possible but only by typically weak second order interactions (described in Chapter 2), which make intersystem quite slow and typically uncompetitive with fluorescence and/or internal conversion. Once formed the triplet state itself is more stable than the singlet (with one famous exception[8]) because of Hund's Rule of Maximum Multiplicity.[9] The change in electronic configuration of T_1 is usually more dramatic than that of S_1, causing greater conformational change and enhanced relaxation. Figure 1.2 shows intersystem crossing as a dashed arrow between S_1 and T_1. Its shorthand is $S_1 \rightarrow T_1$.

From T_1 there are roughly the same transitions available that were to S_1. Just as vibrational modes allowed for S_1 to relax slightly, or completely, T_1 has its own vibrational modes to achieve the same. T_1, however, is of much lower energy than S_1 and the possibility of complete relaxation from T_1 to S_0 is much, much greater. Fewer modes are required to completely relax the excited state. Furthermore, because relaxation from T_1 to S_0 requires slower second order interactions, quantum relaxation is very slow and very non-competitive with vibrational decay. This form of internal conversion, $T_1 \rightarrow S_0$ + *heat*, is shown in Figure 1.2 as a zig-zagging line from T_1 to S_0.

Emissive relaxation from T_1 is *phosphorescence*.[10] A photon is emitted as the excited state electron relaxes while returning to its original spin state. Because this process involves intersystem crossing, which requires slow spin flipping, phosphorescent emission is slow to occur following absorption. Thus phosphorescence is observed on a much longer timescale than fluorescence. For organic molecules this is usually microseconds to milliseconds, but can be as long as seconds and beyond. Figure 1.2 shows this transition as a straight arrow with a wavy arrow to indicate the photon. The shorthand is $T_1 \rightarrow S_0 + h\nu$.

Unlike S_1, there is no intrinsic excited state lower than T_1. Thus there is no intersystem crossing from T_1 to a lower excited state. S_1 is, by definition, the lowest energy singlet and T_1 is lower than that. Triplets though are very susceptible to intermolecular interaction, due to their long lifetimes. Numerous lower energy states are possible via these interactions, but they can be thought of simply as additional paths to internal conversion as they almost always lead to vibrational dissipation. It is important to this work, however, to note this susceptibility as triplet isolation is critical to achieving efficient phosphorescence. This is discussed further in chapters 2 and 3.

Now we can understand the critical differences to fluorescence, singlet emission, and phosphorescence, triplet emission. Those key differences are degeneracy, speed, and susceptibility. The degeneracy of the triplet states means that phosphorescent molecules emit light from three excited states, the three states that comprise T_1, while fluorescent molecules emit from only one, S_1. Speed refers to the greatly extended lifetimes of triplets and phosphorescence. Being that the two are orders-of-magnitude separated, phosphorescence is easily distinguished from fluorescence. Finally susceptibility, the

relatively sensitive nature of triplets, often quenched by a wide variety of external stimuli, gives phosphorescent molecules unique properties useful for detection and imaging.

1.2 Characterizations and Methods

In the study of phosphorescent molecules it is critical to understand not only the measurables of the system and how to measure them but also the importance of the measurement condition and technique. This section explains the importance and detail of the data and the methods used to collect them.

1.2.1 Absorption, Emission, and Excitation Spectra

Spectral data can tell a great deal about the excited states of molecules. Absorption spectroscopy will tell us no more than what wavelengths of light the molecule absorbs at relative intensities. It does not give any indication of the excited state transitions other than absorption, $S_0 + h\nu \rightarrow S_{n>0}$. The width and shapes of the peaks seen in the spectrum indicate the vibrational modes of S_1 that are populated, but do not necessarily indicate where S_1 will come to be once it has equilibrated.

Absorption spectroscopy is typically, and in this report, taken by transmittance. A beam of light is passed through the sample and the amount of signal attenuation is measured as the beam wavelength is changed. The relative intensities give a spectrum showing which wavelengths are absorbed by the sample.

Emission spectroscopy is quite simple. It gives the spectrum of light produced by the sample after excitation. In this work, all excitations are achieved by photon absorption. This makes the reported emission *photoluminescent* (PL) emission, luminescence that is excited by photons. Emission spectra tell us final levels of $S_1/T_1$and its vibrational modes, which are represented by the width and shape of the emission peak(s).

Excitation spectroscopy probes the absorption spectrum for those wavelengths that cause the sample to emit. Each wavelength absorbed by the sample raises the ground state electron to a different vibrational mode and singlet state and not all modes/states may lead ultimately to emission. Excitation spectra reveal the emissive states of a chromophore and yield information about the excited-to-ground state transitions where absorption spectroscopy probes only the ground-to-excited state transitions.

Both emission and excitation spectroscopy are measured by exposing the sample to an incident beam of light and measuring the output light coming from the sample. Emission spectroscopy varies the detector wavelength to scan all possible emissions given a single excitation wavelength. Excitation spectroscopy varies the incident light to scan all possible excitations given a single emission wavelength. In both cases the incident beam and detector are oriented at 90^{o} from each other to reduce observation of the incident light. Spectra measured here are done in the steady state, meaning that no dynamic data can be interpreted from the emission or excitation spectra presented.

1.2.2 Quantum Yields

An important measurable for understanding the excited state activity of a molecule is the quantum yield (QY). QY is defined by equation 1.1.

$$\Phi = (\text{photons emitted}) / (\text{photons absorbed}) \quad (1.1)$$

Φ is the QY as a unit-less fraction, a measurement of how efficiently the molecule emits from a certain amount of excitation. Absorption is absolute and all photons that a molecule absorbs lead to an excited state, which must relax somehow. The QY tells us the probability that an excited state relaxes by emission and can yield valuable clues as to the excited state activity of the molecule.

There are several ways to measure QY and there is considerable variance to the style of measurement and resulting number. Because these tests are highly susceptible to variance it is difficult to compare the measurements of different researchers with fine accuracy. Errors between users can be more than ten percent, but careful measurement practice and sound sample preparation can limit this to well below a single percent. As such these numbers must be given with adequate statistical error to be useful and should be compared across measurement method with suspicion.

The use of a standard is quite common for homogenous samples such as solutions and polymer films. The sample's emission intensity is measured against a known standard in the same excitation conditions. Though this method uses a standard, it is still highly dependent on stable conditions between measurements. Excitation light intensity and wavelength, temperature, and all other conditions must be exactly the same to make a comparison between the standard and the sample. This test also assumes and demands

perfect homogeneity of the chromophore in the sample. If either the standard or the sample contains any anisotropy the comparison between them is invalid.

Integrating spheres are often employed to measure QY without the necessity of a standard or the requirement of a homogenous sample. The device is a hollow sphere coated on its inside to be perfectly reflective with only ports for the sample, the excitation light, and the detector inside. The sample is loaded into the sphere and the measurement assumes that all light that enters the sphere or is generated within the sphere (PL emission) exits out the detector port. The intensity difference of the excitation beam when the sample is and is not present in the sphere gives a quantitative value for absorbance by the sample. Emission from the sample can be subtracted from any background emission from the empty sphere to get a quantitative value of emission. The two can be divided to calculate the QY. This method also requires stable conditions between measurements (sample-in and empty sphere, 'blank') and it makes assumptions about the perfection of the sphere and its reflective properties, which is admittedly imperfect as the sphere has at least three ports disturbing its surface.

For the purposes of this report an integrating sphere was used. The samples studied were very inhomogeneous and not viable for measurement by comparison to a standard.

1.2.3 Quantum Lifetimes

The speed at which an excited state molecule exhibits PL emission is measured as a quantum lifetime. The general relationship is given in equation 1.2.

$$I = I_0 e^{(-t/\tau)} \tag{1.2}$$

I is the emission intensity, I_0 is the initial emission intensity, t is time elapsed since excitation, and τ is the *quantum lifetime* in units of time. The excited states experience exponential decay reflective of the stability of the state.

As mentioned, phosphorescence is triplet emission. Triplets require much more time than singlets to emit so phosphorescence typically has a quantum lifetime much longer than that of fluorescence. For organic molecules, τ_{Fl} is typically in a picosecond to nanosecond regime while τ_{Ph} can be microseconds to seconds.

Quantum lifetimes are calculated by measuring the intensity of emission at certain times after the incident absorption light is applied. A decay curve is observed and fit to equation 1.2 to determine τ. Figure 1.3 shows a typical curve for a fluorescent organic

molecule. Pulsed lasers are often used as the light source as they provide short bursts of excitation light (so that the excitation does not interfere with the potentially much weaker signal emission). For short lifetimes, such as those of a fluorescent event, equipment response times can complicate the measurement and must be corrected for. Complicated systems may exhibit several simultaneous emissions, but each can be modeled neatly by equation 1.2, they simply require de-convolution from a single observed decay signal.

The lifetimes reported here were collected using both pulsed laser sources and flash lamps. Flash lamps are slower than pulsed lasers, but they are sufficiently fast for measuring slower phosphorescent lifetimes. Data is fit to equation 1.2 with the lifetime, τ, being the critical measurable.

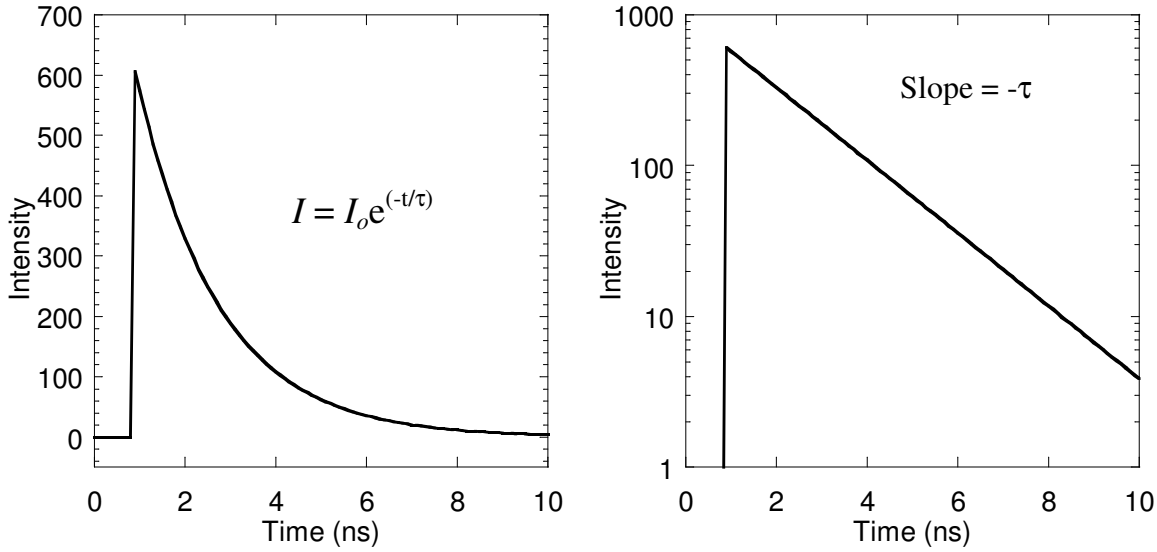

Figure 1.3 Demonstrative Fluorescent Decay Curve. Exponential decay is shown on a linear scale (left) and semi-log (right).

1.2.4 Rate Constants

To understand fundamentally the activity of an excited state molecule and determine which path(s) the excited electron follows it is important to think of all possible actions of the electron as competing rates. As stated before, fluorescence is very fast – the electrons require no additional spin change and the nuclear framework is often not greatly altered from the ground state – so the *rate* at which singlets relax to the ground state by emission is very fast. If one hopes for those singlets to become triplets via intersystem crossing, the rate at which the electrons flip must be competitive with that of the fluorescence. Otherwise no singlets will survive to flip into triplets.

In general the simple relationship between the rate of a transition and the measurable values is given in equation 1.3.

$$k = \Phi / \tau \tag{1.3}$$

The rate, k, of any excited state transition is the ratio of its QY, Φ, divided by the speed at which it acts, τ. For emissive events, fluorescence and phosphorescence, these are easy to measure; τ is the lifetime. This relationship can give us insight into the relative competitiveness of routes vying for the electron.

1.3 Applications for Phosphorescence

The subtle differences between fluorescence and phosphorescence give the later unique advantages in a number of emerging technologies. The critical differences are the degeneracy of the triplet states, the far longer lifetimes of triplets versus singlets, and the sensitivities of triplets to a wider array of quenching conditions. The unique properties of phosphorescent materials are not only opening organic materials to new technologies but also garnering them new popularity in already popular fields.

1.3.1 Organic Light Emitting Diodes

The highest profile application for phosphorescent materials is in the field of organic light emitting diodes (OLEDs). Because of the degeneracy that exists with triplets phosphorescent materials have an advantage over fluorescent materials. In OLEDs excited state electrons are injected (as electrical current) while a ground state electron is extracted. The injected electron must then emit from that excited state. The requirements for fluorescence are strict, the injected excited electron must be in the proper spin configuration to produce light. Technology does not yet exist to control the spin of the injected electron and it may enter the material as a singlet or triplet. This limits the chance that the spins are proper for fluorescence to one-in-four. For phosphorescence there are up to three potential orientations that lead to emission, plus there is energetic impetus for singlets to flip to triplets. Thus it has been hypothesized that phosphorescent materials hold the potential to be three-to-four times more efficient than fluorescent materials in OLEDs.[11] Though measurable device efficiencies have not yet reached the ceiling values of 25 and 75 percent to test this definitively, reports have shown that

phosphorescent OLEDs (PhOLEDs) outpace fluorescent OLEDs in overall device efficiencies by roughly three-to-four times.[12]

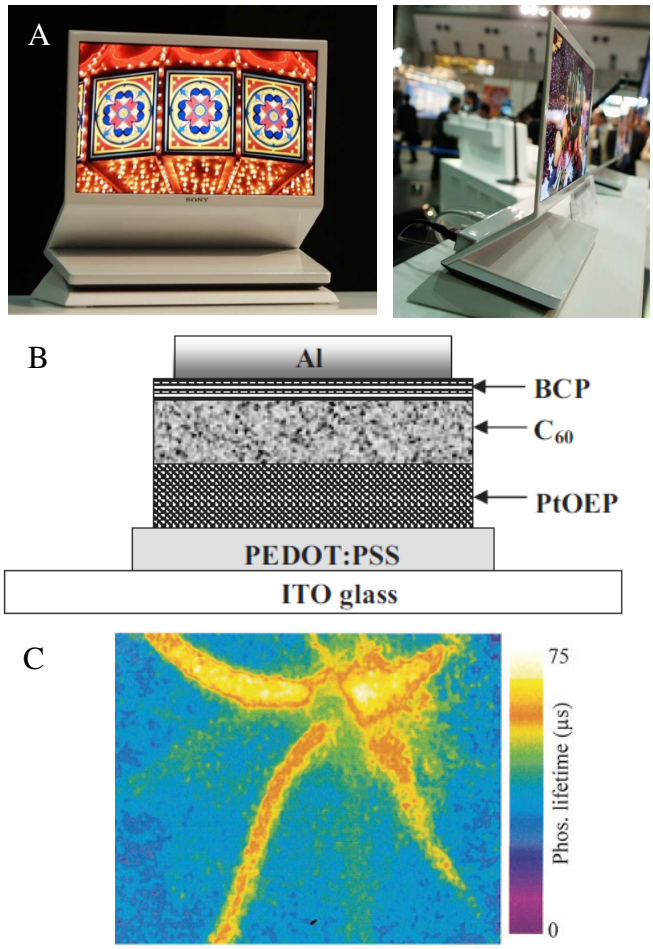

Figure 1.4 A sampling of phosphorescent applications. (**A**) Untra-thin 11-inch Sony PhOLED TV. Image from www.engadget.com. (**B**) Organic PV containing C_{60} as a triplet material. Image from Shao & Yang *Adv. Mater.* **2005**, *17*, 2841. (**C**) Phosphorescent lifetime image of a mouse retina. Image from Wilson et al *Appl. Optics* **2005**, *44*, 5239.

The popularity of PhOLEDs has led to their monopolization of the field and has produced the first commercial products for organic display technologies. An example of a commercial product using organometallic PhOLEDs is given in Figure 1.4(A). The driving force behind the development of organic electronics is versatility of fabrication. Organic compounds do not require the high processing temperatures of ceramic materials (traditional phosphors and LEDs) and provide greater flexibility in device design. Extremely thin displays are already being marketed and the promise of flexible displays

is close at hand. This versatility coupled with high efficiencies has made PhOLEDs popular despite their still suboptimal fabrication costs and working lifetimes.

Commercial and high efficiency academic PhOLEDs are made with organometallic compounds as their emissive component, which presents the field with a number of manageable but intractable challenges and limitations. Fabrication typically requires vacuum thermal evaporation (VTE), sublimation of the compounds by reduced pressure and increased temperatures. A challenge exists in that VTE systems require large vacuum chambers and very low pressures (high vacuums), which are costly to operate and maintain. In this era of large and increasing display size, these systems become even bigger and more expensive.

Broader challenges lie with phosphor design. The family of organometallic chelates useful for PhOLEDs is somewhat limited. Each is basically a collection of organic ligands surrounding a metallic core, typically iridium. Variations to the phosphor are limited to varying the metal, though a select few have dominated this role[13], and changes to the ligand. The color emitted relies upon the Metal-to-Ligand Charge Transfer of the molecule, the transfer of excited state charge from the metal center to the ligand.[14] Thus the metal-ligand bond is critical to the emitted color and QY. Higher energy emission, blue and near-UV light, requires very high-energy metal-ligand bonds, which have poor stability. Pure blue emitting organometallic phosphors have poor QYs[15] and their devices exhibit shorter operating lifetimes.

Achieving long device operating lifetimes remains a challenge to OLEDs. Unlike refractory ceramic phosphors, the organic component of OLEDs make them susceptible to oxidation and decomposition under the relatively extreme conditions of the excited state. Commercial manufacturers have begun reporting device lifetimes that reach up to 30,000 hours of use before losing half of their brightness, though these claims have been disputed to be as low as 17,000 hours.[16,17] Blue and white colors are of particular susceptibility for the reasons mentioned above.

Strategies to improve OLED performance, operative lifetimes as well as other performance metrics, have all revolved around enhanced, though increasingly complex, device architectures. One currently very popular approach has been to add patterning or additional functionality to the emissive layer in order to direct more of the emitted light

outward to the transparent side of the OLED (and thus the viewer).[18,19,20] Organic materials because of their high refractive indices otherwise suffer from strong internal reflection and optical confinement.[21] Other widespread strategies involve preventing degradation of the organic materials by better encapsulation of the OLED[22,23] or further purification of the materials used.[24,25] These strategies are proving successful, but at increased fabrication costs and greater demands on quality control.

Many efforts have been made to improve the usefulness of the emissive material itself (by design rather than purification) though their contributions to the field are greatly overshadowed by the device fabrication schemes mentioned. Chemists face a broad number of targets when designing a better phosphor and have few degrees of freedom to explore. Potential improvements are limited by the requirements of organometallic design. Most improvements achieved come at a cost of complex chemical synthesis, which generally outweighs the benefits and makes material availability difficult for device physicists. Researchers often return to the tried-and-true materials, mundane and commercially available. In fact, tris(8-hydroxyquinolinato)aluminum (Alq3), the emissive material used in the report most often credited as the first OLED is still among the most popular materials used today, over two decades later.[26] Without freedom from organometallic compounds, certain limitations may always be present. For instance, it has been hypothesized that metallic impurities lead to shortened device lifetimes, which is an inescapable condition in organometallic materials.[27] Instabilities at the organic-metal interface of the ligand bonds are also an unavoidable weakness.

While organometallic phosphors are dominating the OLED field, a room for improvement in device cost and operating lifetime remains. Phosphorescent OLEDs out-perform fluorescent OLEDs greatly, but phosphor design is limited to a relatively small family of metal ions chelated to aromatic ligands. Exotic structures have been synthesized to enhance certain device properties, but with more complicated structures come more complicated synthesis and expense.[28,29] Definite boundaries exist in the range of design possibilities for organometallic phosphors.

1.3.2 Photovoltaic Devices

Organic photovoltaics (PVs) hold promise for the fabrication of cheap and versatile solar power. The operating principle in these devices is that an absorbing chromophore collects solar photons to produce excited state electrons. These high-energy electrons are driven through the device to create an electrical current. One of the challenges to organic PVs is getting the excited electron to travel efficiently through the device.[30] Unlike in metals and bulk semiconductors, the electrons in organic materials are tightly bonded and excited states are very easily relaxed by internal conversion or even fluorescence.

The longer the excited state survives, the greater the possibility that it can be driven through the device. Triplets survive much longer than singlets and it has been suggested that triplets would thus have greater diffusion lengths in an organic PV. It has been demonstrated that the inclusion of triplet materials into organic PVs increases the overall power conversion efficiency, presumably because the longer-living excited states (triplets) travel further through the device before they relax or, preferably, reach the cathode.[31] The most popular additive for this is fullerene style polycarbons such as C_{60} and C_{71}, often functionalized to enhance interaction with the absorbing materials.[32]

This approach has become very popular in organic PV design and fullerenes have become nearly ubiquitous in standard device architecture.[33] Figure 1.4(B) shows a typical PV architecture including C_{60}. Contrary to the organometallic phosphors of PhOLEDs, triplet materials for PV design are desired to be non-phosphorescent. Triplets that have long lifetimes, surviving for a long time without experiencing quantum or vibrational relaxation are best. Here there is also a limit in phosphor design. Outside of the organometallic family, there exist very few organic materials that efficiently generate and inefficiently relax triplet states. The popularity of fullerenes speaks to the enhancing properties of triplet materials. The monopolization of fullerenes speaks to the limit in material choice in this role.

1.3.3 Sensors

The broad difference between phosphorescent and fluorescent lifetimes also affords phosphorescent materials with advantages in imaging/sensing applications.[34] Phosphorescent chromophores can be excited with fluorescence but measured on a delay so that no excitation light remains. For example, a phosphor with a millisecond lifetime

can be excited by a pulse with a nanosecond lifetime then measured spectrally a microsecond after the pulse. The fluorescent excitation light will have completely dissipated while the phosphorescent signal remains strong. Thus the signal-to-noise ratio can be improved by reducing background interference.

Another benefit to phosphorescent signaling for sensors is the ability to build images by measuring the lifetimes of the samples rather than just the intensity.[35] With lifetimes in the micro-millisecond range signals are easily measured dynamically. Reductions in phosphor lifetime can be read as a signal to the presence of a quenching analyte, providing a unique method of detection.

Like the applications mentioned prior, the field of phosphorescent sensors is somewhat limited in phosphor design. Organometallic phosphors are bright but limited in design and likely to have unwanted interactions with some analytes due to the presence of the metal and relatively unstable ligand bonds. Metal-free organic phosphors provide some degree of versatility but are very weak emitters, which hinders sensitivity.

1.3.4 Biological Imaging

Though they can live longer, triplets possess some specific sensitivities that singlets do not and these sensitivities have been exploited to design biological sensors. Triplets can be quenched by other triplets in a process known as triplet-triplet annihilation. The quenching effect can be quite subtle with sensitivities suitable for sensor applications.

As it happens molecular oxygen, O_2, exists in a very stable triplet and can quench phosphorescent material quite efficiently. Thus biological oxygen sensors have been designed and tested to measure oxygen levels *in vivo*.[36,37] These sensors can be used to check for the presence of healing wounds and cancerous tissues as there are higher concentrations of oxygen present at these sights. Figure 1.4(C) shows an image taken of a living mouse retina on a lifetime scale using organometallic phosphors as a detecting dye.

The drawbacks to biological phosphorescent sensors mirror that of sensors in general but with the added complication of toxicity. Organometallic phosphors contain heavy metals, which may be detrimental to biological systems.[38] Metal-free phosphors are extremely weak emitting, presenting poor signal-to-noise ratios and with signal intensities not suitable for imaging through tissues.

1.4 Known Organic Phosphors

The primary challenge to organic phosphorescent materials is limit of design. The burgeoning field of organic electronics is driven by the promise of limitless molecular design yet the variety of organic phosphors remains painfully low.

1.4.1 Organometallic Chelates

Organometallic chelates are the most popular organic phosphors being used currently though they are not purely organic and actually derive their usefulness from the decidedly non-organic metal-ligand interaction. This caveat may be inconsequential, however, as their high QYs and short lifetimes have made them nearly ideal for display technologies. In general they consist of a heavy transition metal surrounded by variable organic ligands. The most popular metals used are iridium, platinum, and osmium though iridium remains the distant leader in commercial and academic research. Some popular organometallic phosphors are shown in Figure 1.5(A).

These chromophores are phosphorescent because of the large metal atom, which promotes spin flipping. Organic compounds, purely organic compounds, are neither efficient triplet generators nor are they efficient triplet emitters because their electrons have highly bonded character, giving their electrons strictly singlet character. There is no driving force for spin flipping without the heavy metals present. Thus though these compounds are organic in their ligand structures, it is the metal that provides the rapid $T_1 \rightarrow S_0 + h\nu$ transitional pathway.

Popular organometallic phosphors such as tris(2-phenylpyridine) iridium (Ir(ppy)3) are so because of their excellent combinations of high intrinsic QY, efficient phosphorescence (and limited fluorescence), desirable phosphorescent lifetimes, and, perhaps most importantly, commercial availability due to relatively easy chemical synthesis. Ir(ppy)3 and other iridium chelates are measured to have internal quantum efficiencies (that is, QYs of the materials in devices but not the overall device efficiency) of nearly 100%.[39,40] Iridium chelates also exhibit relatively fast phosphorescent lifetimes in the microsecond regime, which are ideal for display applications that demand refresh rates of 10^3-10^4 Hz. The popularity of these compounds has brought much interesting in development of new analogs, which has led to better synthetic methods of the most basic

members of the family.[41,42,43] Ir(ppy)3 and other iridium chelates are available commercially from catalog and specialty chemical stores.

The popularity of iridium-based chelates also demonstrates the limits to phosphor design. With few options for new metal choices, the development of new organometallic phosphors has focused on ligand design.[25,44] By designing ligands with select excited state energies, the metal-ligand charge transfer is altered and the emission color is changed. Ligand structure can also be used to alter the solid state properties of the chromophore, such as sublimation character, charge transport properties, and surface morphology.[45,46,47] As mentioned this becomes problematic at high energies, such as blue and near-UV emission and often these new ligand designs put large demands on the synthetic chemistry required.

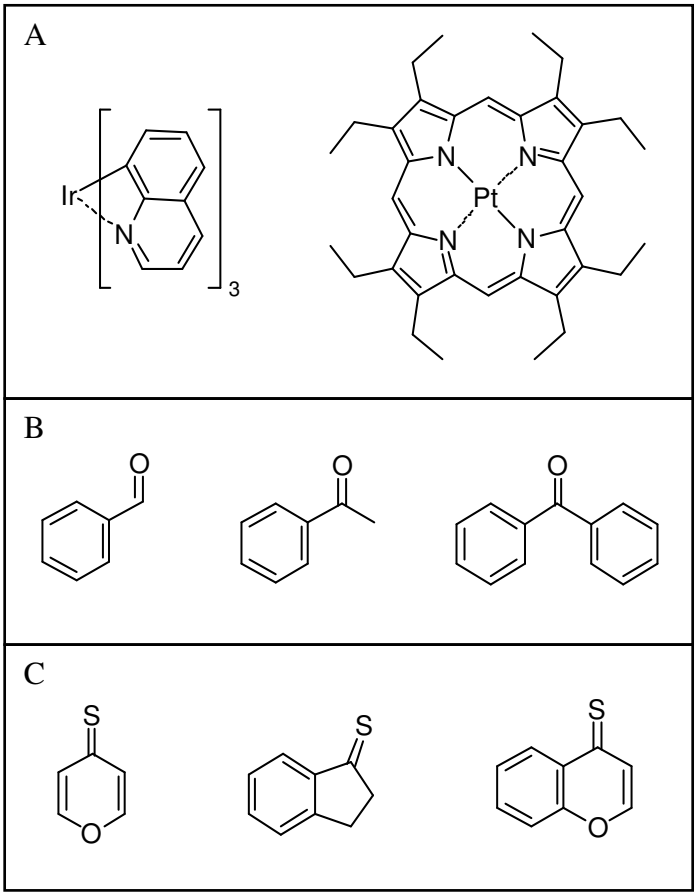

Figure 1.5 Examples of known organic phosphors. (**A**) Organometallic chelates tris(2-phenylpyridine) iridium ($Ir(ppy)_3$) and platinum octaethylporphine (PtOEP). (**B**) Aromatic ketones Benzaldehyde, Acetophenone, and benzophenone (left-to-right). (**C**) Various phosphorescent thiones.

1.4.2 Aromatic Ketones

Aromatic ketones are a broad family of metal-free organic compounds that have been known for decades to be weakly phosphorescent.[48] Figure 1.5(B) shows a collection of simple aromatic ketones known to exhibit detectable phosphorescence. In ways similar to molecular oxygen, which is unusual in that its ground state is a triplet and not a singlet, aromatic ketones have a triplet level that is close in energy to S_1.[49] The well-known and well-studied aromatic ketone, benzophenone, crosses from S_1 to T_1 at nearly one hundred percent efficiency.[3] The reason that these compounds can emit from their triplet states at a rate competitive with other forms of relaxation is the phenomenon of *spin-orbit coupling* active at the carbonyl oxygen.[50] This is discussed in greater detail in Chapter 2.

Despite the knowledge of aromatic ketone phosphoresce, these chromophores have found little use in commercial application and only modest use in academic research. This is due to the extremely low QYs exhibited by these compounds.[51] Measuring at mere fractions of a percent, the brightness of these materials is woefully insufficient for practical applications such as PhOLEDs and sensors. This has been demonstrated in a small number of attempts to build devices from aromatic ketones.[52] However, unlike the other classes of organic phosphor listed here, aromatic ketones do possess promise for broader design as there are not intrinsic limits or strict structural requirements beyond the presence of an aromatic ring and attached ketone. However, Simple compounds like those shown have dominated nearly all academic study because of their simplicity and availability.

1.4.3 Confined Aromatics

Some, non-ketone organic aromatic compounds have also been observed to emit detectable phosphorescence but only when in strictly confined states. These are typically polycyclic compounds such as naphthalene or anthracene whose highly dissociated π–π^* transitions allow for a very modest amount of intersystem crossing. In order for this small population of triplets to emit the chromophores must be very dilute and in extremely rigid matrices. This is achieved through low temperature glasses[53], inclusion into inorganic crystals (so called dye inclusion crystals)[54,55], sequestering chromophores into micelles[56] or macromolecules[57], or adsorption into porous resins or papers.[58]

Like the aromatic ketones these metal-free organic phosphors are extremely weak, and, in addition, they require strict and impractical conditions. These reports are of more scientific value than applicational, though some of their methods have been used in detection schemes.[59] In these cases though, the confinement technique only serves to activate the analyte, which must have intrinsic triplet generation. Room temperature phosphorescence from dye inclusion is also specifically sensitive to the orientation of inclusion.[60]

1.4.4 Thiones

An intriguing class of metal-free organic phosphors exists in a limited family of thione complexes. Typical structures are shown in Figure 1.5(C). These compounds exhibit a host of interesting optical transitions including rare $S_2 \rightarrow S_0$ emission, delayed fluorescence (described in Chapter 5), and room temperature phosphorescence with QYs reported as high as $\Phi_{Ph} = 0.47$.[61] These compounds share many of the attractive qualities of organometallics used in OLEDs; high QY, good candidates for vacuum sublimation, and fast phosphorescent lifetimes (microseconds), however they suffer from photo and thermal stability, plus the undesirable complications of various emission (simultaneous fluorescence and phosphorescence).[62] Many exhibit irreversible redox chemistry, which is devastatingly unattractive for OLEDs or any electronic application. Despite these drawbacks such thiones are being explored for sensing applications such as those mentioned in section 1.3.3 and 1.3.4.[63]

These thiones are intriguing and provide the only known, reasonably practical alternative to organometallic phosphors (in terms of brightness, QY). However, design limitations exist as the emission comes primarily from the thione, which is unalterable. Phosphorescence is intractably in the red regime. Because of this as well as their instabilities, they have not enjoyed the academic nor the commercial popularity of organometallics. Despite some noted outliers their QYs are also relatively low as compared to organometallics. Most thiones reports room temperature phosphorescent QYs in the 0.1 – 0.2 range[64] while the family of popular organometallics are reported to be 0.5 – 1.0.[65] For these reasons the thione family fails to fill the need for a versatile metal-free organic phosphor.

1.5 Conclusions

Though both are mechanisms by which molecules produce light phosphorescence is critically different from fluorescence. Because of the higher degeneracy of triplets, phosphorescent materials provide higher efficiencies in OLEDs. Their longer lifetimes are reported to enhance PV efficiencies as well as provide unique imaging methods and improved signal-to-noise ratios in sensory applications. Also, their unique sensitivities lend their abilities to specialized sensing and biosensing applications. From these advantages, phosphorescent materials are enjoying expanding popularity in new and existing fields. However, despite this great promise, there exist strict limitations to the molecular design of novel phosphorescent materials. The field is restricted, practically, to a narrow family of organometallic compounds.

In order to design new and competitive organic phosphors chromophores must be designed that have very efficient intersystem crossing and that strictly limit vibrational dissipation of the triplet state (thus allowing it to decay emissively). The small families of known organic phosphors provide some direction towards this end, but each is plagued with severe limitations. Organometallics are not readily tunable into the blue and near-UV ranges and also require problematic inhomogeneous metal-organic structures. Aromatic ketones require no metal but exhibit inefficient intersystem crossing and strong vibrational dissipation of their triplets. Confined aromatics require strict environmental conditions and the family of phosphorescent thiones are also marginally efficient and somewhat limited in design.

1.6 References

[1] Griffiths, D.J. *Introduction to Quantum Mechanics* (Prentice Hall, Upper Saddle River, NJ, 2004).
[2] M.A. Baldo *The Electronic and Optical Properties of Amorphous Organic Semiconductors* **2001** Ph.D. Thesis, Princeton University, USA.
[3] N.W. Ashcroft and N.D. Mermin *Solid State Physics* (Brooks Cole, Florence, KY, 1976).
[4] C. Kittel *Introduction to Solid State Physics* (John Wiley & Sons, Hoboken, NJ, 2004).
[5] At extremely low temperatures, single Kelvin, it is possible to distinguish these states dynamically.
[6] Turro, N.J. *Modern Molecular Photochemistry* (University Science Books, Sausalito CA, 1991).
[7] M. Kasha *Disc. Faraday Soc.* **1950**, *9*, 14.
[8] M. Beer and H.C. Longuet-Higgins *J. Chem. Phys.* **1955**, *23*, 1390.
[9] I.N. Levine, *Quantum Chemistry* (Prentice-Hall, Upper Saddle River, NJ ,1991).
[10] G.N. Lewis and M. Kasha *J. Am. Chem. Soc.* **1944**, *66*, 2100.
[11] M.A. Baldo, D.F. O'Brien, Y. You, A. Shoustikov, S. Sibley, M.E. Thompson, and S.R. Forrest *Nature* **1998**, *395*, 151.
[12] M.A. Baldo, M.E. Thompson, and S.R. Forrest *Pure Appl. Chem.* **1999**, *71*, 2095.
[13] A. Kohler, J.S. Wilson, and R.H. Friend *Adv. Mater.* **2002**, *14*, 701.
[14] C.-H. Yang, Y.-M. Cheng, Y. Chi, C.-J. Hsu, F.-C. Fang, K.-T. Wong, P.-T. Chou, C.-H. Chang, M.-H. Tsai, and C.-C. Wu, *Angew.Chem. Int. Ed.***2007**, *46*, 2418.
[15] Y. Kawamura, S. Yanagida, and S.R. Forrest *J. Appl. Phys.* **2002**, *92*, 87.
[16] Sony reports a 30,000 hour average half-brightness time for its XEL-1 OLED television. www.sonystyle.com
[17] J. Sherwood, "Sony OLED TV longevity claim challenged", *Register Hardware*, 13th May 2008.
[18] Y. Sun, and S.R. Forrest *Nature Photonics* **2008**, *2*, 483.
[19] L.S. Liao, K.P. Klubek, and C.W. Tang *Appl. Phys. Lett.* **2004**, *84*, 167.
[20] S. Moller, and S.R. Forrest *J. Appl. Phys.* **2002**, *91*, 3324.
[21] A. Chutinan, K. Ishihara, T. Asano, M. Fujita, and S. Noda, *Org. Elect.* **2005**, *6*, 3.
[22] A.P. Ghosh, L.J. Gerenser, C.M. Jarman, and J.E. Fornalik *Appl. Phys. Lett.* **2005**, *86*, 223503.
[23] Y.G. Lee, Y.-H. Choi, I.S. Kee, H.S. Shim, Y. Jin, S. Lee, K.H. Koh, and S. Lee *Org. Elect.* **2009**, *10*, 1352.
[24] H.G. Jeon, M. Inoue, N. Hirarnatsu, M. Ichikawa, and Y. Taniguchi *Org. Elect.* **2008**, *9*, 903. (This article deals with Alq3 analogs, which are fluorescent, not phosphorescent, but they address purification techniques and the complications that arise.)
[25] S.H. Liao, J.R. Shiu, S.W. Liu, S.J. Yeh, Y.H. Chen, C.T. Chen, T.J. Chow, and C.I. Wu *J. Am. Chem. Soc.***2009**, *131*, 763.
[26] C.W. Tang and S.A. Van Slyke *Appl. Phys. Lett.* **1987**, *51*, 913.
[27] H. Aziz and Z. Popovic *Chem. Mater.* **2004**, *16*, 4522.

[28] Y. You and S.Y. Park *Dalton Trans.* **2009**, *8*, 1267.
[29] E. Baranoff, J.-H. Yun, M. Graetzel, and Md.K. Naseeruddin *J. Organometallic Chem.* **2009**, *694*, 2661.
[30] J.-L. Bredas, J.E. Norton, J. Cornil, and V. Coropceanu *Accounts of Chem. Res.* **2009**, *42*, 1691.
[31] Y. Shao and Y. Yang *Adv. Mater.* **2004**, *17*, 2841.
[32] M. Reyes-Reyes, K. Kim, and D.L. Carroll *Appl. Phys. Lett.* **2005**, *87*, 083506-1.
[33] N.S. Sariciftci, D. Braun, C. Zhang, V.I. Srdanov, A.J. Heeger, G. Stucky, and F. Wudl *Appl. Phys. Lett.* **1993**, *62*, 585.
[34] A.P. de Silva, H.Q.N. Gunaratne, T. Gunnlaugsson, A.J.M. Huxley, C.P. McCoy, J.T. Rademacher, and T.E. Rice *Chem. Rev.* **1997**, *97*, 1515.
[35] W. Zhong, P. Urayama, and M.A. Mycek *J. Phys. D- Appl. Phys.* **2003**, *36*, 1689.
[36] W.L. Rumsey, J.M. Vanderkooi, and D.F. Wilson *Science* **1998**, ***241,*** 1649.
[37] G. Zhang, G.M. Palmer, M.W. Dewhirts, and C.L. Fraser *Nature Materials* **2009**, *8*, 747.
[38] K. K.-W. Lo, P.-K. Lee, and J. S.-Y. Lau *Organometallics* **2008**, *27*, 2998.
[39] C. Adachi, M.A. Baldo, S.R. Forrest, and M.E. Thompson *Appl. Phys. Lett.* **2000**, *77*, 904.
[40] C. Adachi, M.A. Baldo, M.E. Thompson, and S.R. Forrest *J. Appl. Phys.* **2001**, *90*, 5048.
[41] S. Lamansky, P. Djurovich, D. Murphy, F. Abdel-Razzaq, H.E. Lee, C. Adachi, P.E. Burrows, S.R. Forrest, and M.E. Thompson *J. Am. Chem. Soc.* **2001**, *123*, 4304.
[42] S. Lamansky, P. Djurovich, D. Murphy, F. Abdel-Razzaq, R. Kwong, I. Tsyba, M. Bortz, B. Mui, R. Bau, and M.E. Thompson *Inorg. Chem.* **2001**, *40*, 1704.
[43] A.B. Tamayo, B.D. Alleyne, P.I. Djurovich, S. Lamansky, I. Tsyba, N.N. Ho, R. Bau, and M.E. Thompson *J. Am. Chem. Soc.* **2003**, *125*, 7377.
[44] W.-Y. Wong and C.-L. Ho *J. Mater. Chem.* **2009**, *19*, 4457.
[45] P.L. Burn, S.C. Lo, and I.D.W. Samuel *Adv. Mater.* **2007**, *19*, 1675.
[46] J.Q. Ding, J. Gao, Y.X. Cheng, Z.Y. Xie, L.X. Wang, D.G. Ma, X.B. Jing, and F.S. Wang *Adv. Func. Mater.* **2006**, *16*, 575.
[47] G.J. Zhou, W.Y. Wong, B. Yao, Z.Y. Xie, L.X. Wang *Angew. Chemie Intl. Ed.* **2007**, *46*, 1149.
[48] D.R. Kearns and W.A. Case *J. Am. Chem. Soc.* **1966**, *88*, 5087.
[49] R.C. Petterso *Angew. Chem.-Intl. Ed.* **1970**, *9*, 644.
[50] M. Klessinger and J. Michl. *Excited States and Photochemistry of Organic Molecules* (VCH Publishers, New York, NY 1995).
[51] W. D. K. Clark, A. D. Litt, and C. Steel, *J. Am. Chem. Soc.* **1969**, *91*, 5413.
[52] S. Hoshino and. H. Suzuki *Appl. Phys. Lett.***1996**, *69*, 224.
[53] J.R. Ebdon, D.M. Lucas, I. Soutar, A.R. Lane, and L. Swanson *Polymer* **1995***, 36*, 1577.
[54] R.A. Paynter, S.L. Wellons, and J.D. Winefordner *Anal. Chem.* **1974**, *46*, 736.
[55] B. Kahr and R.W. Gurney *Chem. Rev.* **2001**, *101*, 893.
[56] L.J.C. Love, M. Skrillec, and J.G. Habarta *Anal. Chem.* **1980**, *52*, 754.
[57] N.J. Turro, T. Okubo, and C. Chung *J. Am. Chem. Soc*. **1982**, *104*, 1789.
[58] E.M. Schulman and C. Walling *J. Phys. Chem.* **1973**, *77*, 902.

[59] T. Vo-Dinh *Room-Temperature Phosphorimetry for Chemical Analysis: Theory, Instrumentation, and Applications* (Marcel Dekker, New York, NY 1981).
[60] C.A. Mitchell, R.W. Gurney, S.-H. Jang, and B. Kahr. *J. Am.Chem. Soc.* **1998**, *120*, 9726.
[61] M. Szymanski, R.P. Steer, and A. Maciejewski *Chem. Phys. Lett.* **1987**, *135*, 243.
[62] R.C. Evans, P. Douglas, and C.J. Winscom *J. Fluoresc.* **2009**, *19*, 169.
[63] G. Zhang, D. Zhang, S. Yin, X. Yang, Z. Shuai, and D. Zhu *Chem. Comm.* **2005**, 2161.
[64] M. Szymanski, A. Maciejewski, and R.P. Steer *J. Phys. Chem.* **1988**, *92*, 2485.
[65] R.C. Evans, P. Douglas, and C.J. Winscom *Coord. Chem. Rev.* **2006**, *250*, 2093.

Chapter 2

Molecular Design of Metal-Free Organic Phosphors

The main focus of this work is to describe and demonstrate highly efficient metal-free organic phosphors constructed by a design principle called the Directed Heavy Atom Effect (DHAE). This chapter explains the pertinent challenges to organic phosphor design and the tools employed by DHAE to combat them and produce efficient metal-free organic phosphors. The excited state behavior of aromatic ketones is expanded upon from Chapter 1 and specific excited state properties as well as pertinent chemical structures are discussed. Spin-orbit coupling, also critical, is described semi-quantitatively for aromatic ketones and all phosphors in general. The concepts of the heavy atom effect and halogen bonding are explored, both of which are critical components to the DHAE design principle.

2.1 Challenges for Organic Phosphor Design

To design new organic phosphors one must consider the two greatest barriers to achieving phosphorescence, the enhancement of intersystem crossing and the reduction of vibrational dissipation of the triplet. These two criteria are difficult to achieve in metal-free organic materials and are the reason why so few bright, pure organic phosphors are known.[1]

2.1.1 Intersystem Crossing

In order for a molecule to be phosphorescent, it must first efficiently generate triplets. As mentioned, singlet decay by fluorescence is very fast in organic compounds and internal conversion can be as well. Intersystem crossing, on the other hand, is very slow. An efficient phosphor must have an intersystem crossing route that outpaces both fluorescence and internal conversion.

The difficulty to achieving efficient intersystem crossing lies with the fact that an excited state electron changing from singlet to triplet requires a change in angular momentum, which is forbidden by first order approximations. The only means by which this non-spin-conserving change can take place is by second order effects, interactions that are more complex and more difficult to impart into materials by design.[2] Despite their relative ineffectiveness, it is these effects that are responsible for all triplet generation, including those that occur in organometallics. The challenges stands that they are generally very weak/slow in light element organic materials.

2.1.2 Vibrational Dissipation

In order for the triplet to survive long enough to phosphoresce, the molecule must not suffer vibrational dissipation, internal conversion from T_1. Loss of the excited state to heat threatens both S_1 and T_1, though being that T_1 is lower in energy than S_1 fewer vibrational modes are required to relax it completely. Internal conversion of T_1 is generally faster than that of S_1 and stands as the primary reason for low phosphorescent QY from non-metallic organic compounds.

Strategies for reduction of vibrational dissipation vary in success and practicality. The key component to any such strategy is to prevent vibrational freedom of the compound. One popular academic approach is to reduce the temperature of the sample to 77K or lower. At these temperatures nuclear motion is highly restricted and many

weakly or non-emissive room temperature phosphors become very bright. Alternatively, restrictive environments have been employed to far more modest success. As mentioned in Chapter 1, embedding the triplet-generating compounds into crystals, micelles, and even materials as mundane as filter paper have provided detectable phosphorescence. These methods, however, fail to produce QYs suitable for lighting or high contrast imaging applications.

2.2 Directed Heavy Atoms

To achieve both rapid intersystem crossing as well as vibrational suppression the *Directed Heavy Atom Effect* (DHAE) has been developed.[3] It relies on a combination of separate established principles to impart high efficiency phosphorescent emission in metal-free organic molecules at room temperatures and in ambient conditions. At its core are the combined effects of triplet-allowing aromatic ketones, the heavy atom effect, and halogen bonding. In the following sections these three concepts are described along with the means in which they are utilized in the DHAE principle.

2.3 Aromatic Ketones

As described in Chapter 1, aromatic ketones have been known to be weakly phosphorescent organic compounds for several decades.[4] They have been to subject of much scientific investigation and the reasons why this specific family of compounds exhibits competitive intersystem crossing are now well understood. Despite their popularity in research though, attempts to make useful practical devices have not been successful and their role in the field of organic phosphors remains purely scientific.

2.3.1 Intersystem Crossing

Aromatic ketones are defined as having a carbonyl (C=O) moiety attached directly to an aromatic ring or ring system. The carbonyl group is unique in that the lone-pairs on the oxygen do not occupy degenerate sp^2 hybridized orbitals as one might expect. Instead, one lone-pair occupies the unused *p* orbital while the other pair occupies a low-energy *sp* hybridized orbital.[5] This is shown in Figure 2.1 simplified, for clarity, from an aromatic ketone to formaldehyde, which exhibits the same orbitals as aromatic ketones. This arrangement allows for efficient intersystem crossing because it creates $S_1(n,\pi^*)$ and

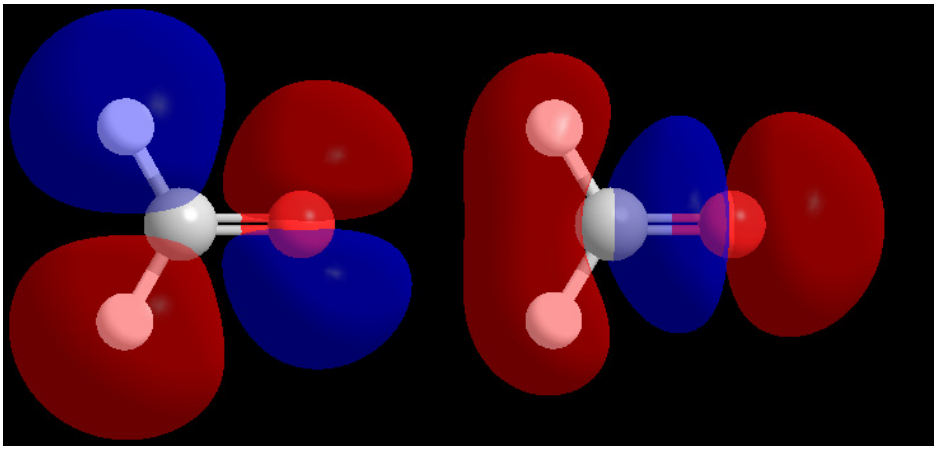

Figure 2.1 Non-bonding molecular orbitals of a carbonyl (formaldehyde). The HOMO level, occupying p (left) and the HOMO-2 level occupying sp (right).

$T_2(\pi,\pi^*)$ states that are very close in energy[6]. Once in T_2 the state transitions to $T_1(n,\pi^*)$, which is very quick as it is a spin-conserving transition. T_1 is much lower in energy than T_2, so $T_1 \rightarrow S_1$ is very unlikely. Figure 2.2 illustrates with rates measured for benzophenone.[7]

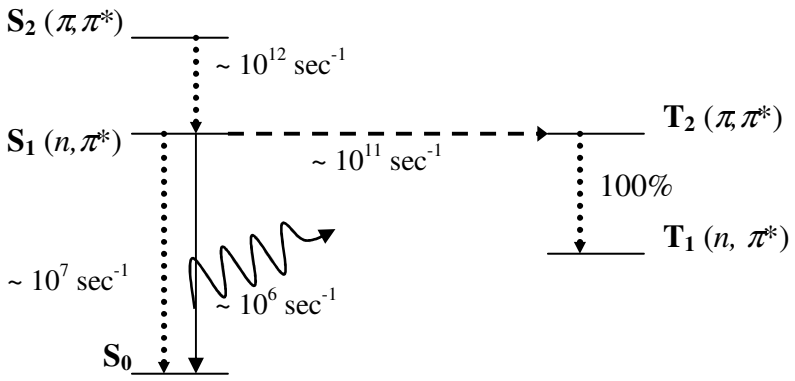

Figure 2.2 S_1-T_2 intersystem crossing in aromatic ketones (benzophenone). Rates shown are those of benzophenone at 77K. S_1 crosses quickly to T_2 because of similar energy and orbital overlap (as well as spin-orbit coupling, described later). T_2 relaxes to T_1 at 100%. T_1 is too low in energy to cross back to S_1.

The efficiency by which the singlets of aromatic ketones become triplets is quite high. For benzophenone the singlet-to-triplet conversions near 100%.[8] Not all aromatic ketones possess such highly efficient intersystem crossing, as will be revealed later, but all can be expected to be at least fairly efficient. This gives aromatic ketones an

advantage for organic phosphor design, they generate triplets readily, but in order to be used in phosphor design these triplets must be allowed to emit.

2.3.2 Spin-Orbit Coupling

In order for triplets to relax emissively to the ground state, S_0, a spin flip must again take place. It is not incorrect to refer to the transition $T_1 \rightarrow S_0$ as intersystem crossing since there it is a non-spin-conserving process. The most prevalent mechanism for spin flipping in organic materials is a phenomenon known as *spin-orbit coupling*.[9] Spin-orbit coupling (also known as spin-orbit interaction or spin-orbit effect) occurs when the spin of an electron is influenced by the electron's motion about a nucleus. Though classical physics is often a poor model for quantum mechanics one can think of electrons as charged spinning particles orbiting around a nucleus. The angular movement of the electron through the magnetic field created by the atomic nucleus can impart an electromagnetic force on the electron causing it to change its spin. This can only occur if the electron is alone in an orbital and thus free from the influences of another electron. The Pauli exclusion principle is absolute.

Spin-orbit coupling is most prevalent in atoms whose nuclei are large. Mathematically, the Hamiltonian for spin-orbit interaction is strongly proportional to the nuclear charge, which is intractably proportional to the size of the atom.[10] A simplified version of this factor is given in equation 2.1.

$$H_{s-o} = -\frac{Z^4 e^2}{8\pi\varepsilon_0 m_e^2 c^2} \boldsymbol{l} \cdot \boldsymbol{s} \tag{2.1}$$

There are two main components to this factor: the coefficient and the dot product. The coefficient is a collection of constants (e is the elementary charge of an electron, ε_0 is the permittivity of the vacuum, m_e is the mass of an electron, and c is the speed of light) and the atomic number of the acting nucleus, Z, to the fourth power. The magnitude of spin-orbit coupling is thus greatly affected by the size/weight/charge of the nucleus. The vector portion is the dot product of the electron's angular momentum, $\boldsymbol{l}$, and spin, $\boldsymbol{s}$. This demonstrates that spin-orbit coupling is critically reliant on the motion of the electron and its spin in the field. Regardless of the nuclear size, non-interacting electron vectors and nuclear fields (a zero dot product) would preclude any triplet formation in the system.

Conversely, Z will never be zero, so even if the $\boldsymbol{l}\boldsymbol{s}$ factor is small, spin-orbit coupling is possible.

It is spin-orbit coupling that facilitates the intersystem crossing necessary for the phosphorescence of all phosphors including organometallic. Because larger nuclei exhibit both greater nuclear magnetic fields and excess orbital space for non-bonded electrons this effect is more pronounced in heavy atoms such as transition metals and large halogens. This, in part, explains why heavy metal organic phosphors like tris(2-phenylpyridine)iridium ($Ir(ppy)_3$) are phosphorescent while light metal chelates such as Tris(8-hydroxyquinolinato)aluminium (Alq_3) are predominantly fluorescent.

Though spin-orbit coupling is strongly proportional to the size of the nucleus involved, it does occur, though not usually very efficiently, for lighter elements. The triplets generated by aromatic ketones can accommodate intersystem crossing from T_1 to S_0 because they exhibit a degree of spin-orbit coupling at the carbonyl oxygen. Rather than drawing its greatest influence from the size of the oxygen atom, it is the orbital arrangement around the carbonyl oxygen that provides favorable spin-orbit coupling. This is what makes aromatic ketones rather unique among light-element organics. The excited state triplet, π^*, mixes weakly with the non-bonded ground state singlet, n, on the cabonyl oxygen. Both orbitals are strongly localized at the oxygen atom, a factor that makes spin-orbit coupling non-trivial as the electron changes energy around a single nucleus. Thus it is spin-orbit coupling that allows aromatic ketones such as benzophenone to exhibit a detectable, but modest amount of phosphorescence. With no heavy nuclei involved, phosphorescence QY remain at fractions of a percent.

2.3.3 Vibrational Suppression

As discussed in section 2.1.2 internal conversion by vibrational modes is far faster, and thus more competitive, than emissive triplet decay, phosphorescence. This is very detrimental to the phosphorescence of aromatic ketones. Though they generate triplets efficiently, they are very weak phosphors. To improve their brightness they are often frozen into glassy solids such as non-crystalline solvents at low temperatures or other rigid matrices. Like the Confined Aromatics described in Chapter 1 Section 1.4.3 removal of the vibrational modes prevents internal triplet conversion, which allows triplet emission to dominate. Most studies of aromatic ketone phosphorescence are measured in

these conditions.[11] Unfortunately though for device design, little-to-no phosphorescence is generated in ambient, concentrated, or room temperature conditions.

2.3.4 Applied to DHAE

One very simple aromatic ketone is benzaldehyde. This molecule consists of a benzene ring substituted by a single formyl group. Figure 2.3 shows this and other pertinent aromatic ketones. Unlike other popular aromatic ketones, benzophenone and acetophenone, benzaldehyde has no additional carbon substitution at the carbonyl making the carbonyl more accessible to extra-molecular interactions. It is the smallest and simples possible aromatic ketone and key to the discovery and earliest applications of the DHAE principle.

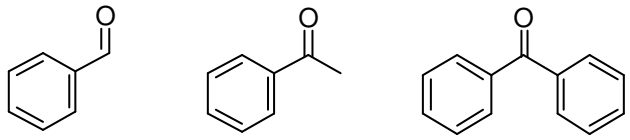

Figure 2.3 Benzaldehyde, acetophenone, and benzophenone (left-to-right).

DHAE relies on an intermolecular interaction at the carbonyl site of benzaldehyde, which is why having as little carbonyl substitution possible is very favorable. Additional groups attached nearby provide some steric hindrance to the species that may otherwise come close enough to interact with the triplet-generating and spin-orbit active moiety, the carbonyl. As is next explained, access to the carbonyl is critical to the DHAE principle. If spin-orbit coupling is to be increased, a greater nuclear charge (Z) must be applied at the carbonyl oxygen. This is why benzaldehydes are used throughout this work.

2.4 The Heavy Atom Effect

Though the ability of an excited state molecule to exhibit intersystem crossing is generally an intrinsic property of its molecular orbitals and not particularly easy to alter for a given molecule, a strategy to promote electron flipping does exist in the *heavy atom effect*. Described here, the heavy atom effect is both a popular means to promote triplet generation, induce spin-orbit coupling, and is an absolutely critical portion of the DHAE design principle.

2.4.1 Background

The heavy atom effect is defined by the International Union of Pure and Applied Chemistry:

> "*The enhancement of the rate of a spin-forbidden process by the presence of an atom of high atomic number, which is either part of, or external to, the excited molecular entity. Mechanistically, it responds to a spin-orbit coupling enhancement produced by a heavy atom.*"[12]

The presence of a heavy atom helps to promote intersystem crossing by providing a heavy/highly-charged nucleus to influence the excited electron (spin-orbit coupling) while mixing its large, unfilled *d* orbitals with those of the excited molecule.[13] It is essentially adding a heavy atom to increase the factor Z from equation 2.1 while also providing a possible improvement to the vector factor, $\boldsymbol{l}\boldsymbol{s}$ (this depends on how the heavy atom is added to the system).

The heavy atom effect is very well established, but usually observed as a rather weak phenomenon. Reports from as early as the 1950s demonstrate that chromophores in iodinated solvents exhibit more triplet absorption (a rare, usually extremely weak $S_0 + h\nu \rightarrow T_1$ transition) than when in light element solvents.[14] Since then innumerable reports utilizing the effect have been recorded often with organic phosphors being halogenated to enhance their very modest phosphorescence to detectable levels.[15,16,17] The effect, though, is always definite but mild. Few numbers are given relating phosphorescent QYs with and without the presence of heavy atoms (data is usually shown as relative spectral intensities), presumably because the final effect is still a very weak signal and perhaps prone to QY measurement errors. The QY enhancement may only be a few fold, which is relatively significant, but unimpressive practically.

2.4.2 Internal and External Effects

Uses of the heavy atom effect generally fall into two classes: internal and external. The internal effect refers to the covalent addition of a heavy atom, usually a large halogen, to the molecular structure itself. Halogens are popular in this role as they are easily substituted for hydrogen in chemical structures. The external effect is the addition of heavy atoms, again usually halogens, to the environment of the chromophore in hope of promoting triplet formation from mixing and collisional interactions. The first is more

elegant and effective, but requires alteration of the intended phosphor, which may not always be feasible. The second is more versatile, but less effective in most cases.

DHAE uses both effects to achieve high efficiency phosphorescence. In practice the heavy atom is usually bromine or iodine, two heavy atoms that can be easily added to organic structures either for the internal effect or to solvent and other environmental molecules for the external effect. In this report bromine is used almost exclusively as it has proved to work very well, for reasons discussed later.

2.4.3 Applied to DHAE

The usual method for achieving the external heavy atom effect has been to add iodinated or brominated molecules to the matrix surrounding the phosphorescent chromophore.[18] These are perhaps the simplest ways to introduce heavy atoms to the sample, and they do work, but they are very indirect. They rely on collisional (in solution) or resonant, solid-state (in glasses) interactions, which are random in the typically used media, unordered systems of solutions and/or frozen glasses.

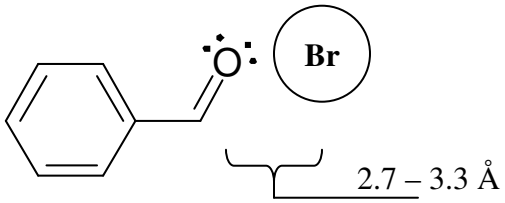

Figure 2.4 Bromine at an ideal position to exert the heavy atom effect and promote spin-orbit coupling in benzaldehyde.

The DHAE principle uses a directed approach to attract the halogen to the chromophore. As described in section 2.3, the critical part of the molecule for phosphorescence is the carbonyl oxygen. It is at this nucleus that we have the intrinsic mixing of triplet and singlet states that makes phosphorescence possible in benzaldehyde and all aromatic ketones. If the heavy atom can interact specifically with that part of the molecule, the heavy atom effect (promoting spin-orbit coupling) would be optimal for the enhancement of phosphorescence. This is why having an accessible ketone is also important. Figure 2.4 illustrates this situation, which is exactly what DHAE achieves. Oriented in this way we later demonstrate how phosphorescent QYs can be increased

from $\Phi_{Ph} < 0.001$ to $\Phi_{Ph} > 0.6$ by employing this design. The means by which this unique orientation is achieved is discussed next.

2.5 Halogen Bonding

Halogen bonding, despite being a fifty-year-old synthon in crystal design, is beginning to receive a great deal of modern attention.[19] It is halogen bonding that allows the DHAE principle to direct the heavy atom to the phosphorescent chromophore in benzaldehydes. Here are described the history, working principles, and identifications of halogen bonding so that the reader can understand the evidence and analysis later in this work.

2.5.1 Background

Discovered in 1954 by Odd Hassel (though evidence had been surfacing since the mid nineteenth century) halogen bonding is a very close analog of hydrogen bonding.[20] An electron deficient species is drawn to an electron rich nucleophile. The interaction is non-covalent, but sufficiently strong to be a directing force in some crystals and semi-ordered solid states. In his most notable work Hassel reported the crystal structure of a 1:1 cocrystal comprised of elemental bromine (Br_2) and 1,4-dioxane. Figure 2.5 shows this structure. The distances measured between the bromine atoms and the neighboring oxygen atoms of the dioxane is 2.71 Å. The sum of the van der Waals radii of both atoms (bromine and oxygen) is 3.35 Å. To observe nuclear distances so far below their van der Waals distance means that clearly there is an attractive force operating between the two. From this report the paradigm of halogen bonding was born, and this reported distance of 2.71 Å remains among the closest, and therefore strongest, halogen bonds cataloged.[21]

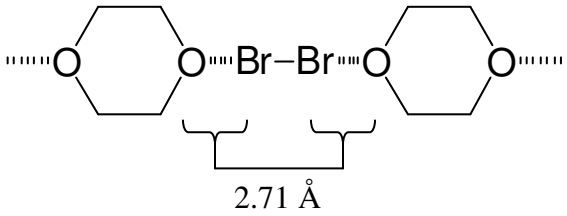

Figure 2.5 Cocrystal structure of bromine and 1,4-dioxane.

In more recent years halogen bonding has become a very popular directing force in the emerging field of crystal engineering.[22] Halogen bonds are being used to design crystals for pharmaceutical and electronic applications.[23,24,25] They are also being used in semi-crystalline liquid crystals for display and electronic technologies and scaffolds for solid state polymerization.[26,27,28] The paradigm is also making its way into non-pharmaceutical biomedical research where halogenated nucleic acids provide unique interactions.[29] Halogen bonding is experiencing rapid growth, fully in parallel to that of crystal engineering.

2.5.2 Electron-deficient Halogens

At first halogen bonding seems counterintuitive as halogens are highly electronegative atoms. One may wonder how halogens can behave as electrophiles. The answer lies in their bonding. Bound halogens are sharing electrons with their partner atoms, which draws electron density away from the halogen at the end opposite the bond. This is most pronounced for larger halogens, bromine and iodide. Figure 2.6 is reproduced from Ho and coworkers and shows this trend as demonstrated by *ab inito* calculations.[30]

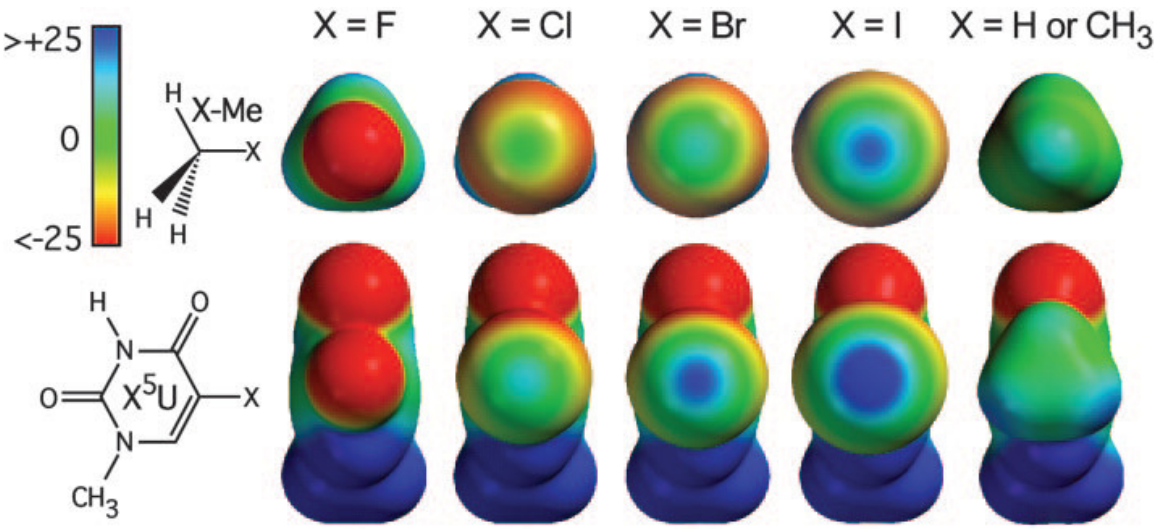

Figure 2.6 Calculated electrostatic potential surfaces of bound halogens. Larger halogens (moving right) and those bound to more electron-withdrawing partners (lower row) exhibit greater partial positive character, far more positive even than hydrogen or methyl (right most). Image is from Ho and coworkers.

Figure 2.6 also shows an important trend that halogens bound to electron accepting groups display a greater positive, and thus electrophilic, character. This allows bound halogens bromine and iodine to be attracted to electron rich nucleophiles. In literature oxygen and nitrogen are the usual nucleophiles as they have lone-pair electrons readily available for donation to this bond.

The arrangement is directly analogous to hydrogen bonding, an electron deficient atom is attracted to an electron rich nucleophile, but halogen bond has two important differences. First, halogen bonds are measured stronger than hydrogen bonds. Second, and possibly more importantly, halogen bonds are much more directional. Hydrogen atoms are wholly electropositive. Halogen bonds, conversely, have only a very select area of electopositivity and it is strongly related to the direction of their covalent bond. Thus halogen bonds are much better suited to crystal design and *directed* interactions. Aside from these two aspects, halogen bonding is a nearly direct analog of hydrogen bonding and all general governing properties applied to each.

2.5.3 Distances and Angles

Because halogen bonding is a much more narrowly accepting interaction, the window of electro-positivity is quite narrow, there are characteristic distances and angles associated with it. Focusing on Br··O halogen bonds, nuclear distances tend to be anywhere from 3.0 – 3.3 Å. Though distances below 3.0 Å (Hassel's 2.71 Å, for example) have been reported, they remain in the minority. Any measured Br··O distance below 3.35 Å is considered evidence of a halogen bond. The distance of the bond is correlated to its strength. The shorter the Br··O distance, the stronger the bond and the more interaction (sharing of orbitals) exists between the two atoms' electrons.

Halogen bonds also exhibit a two characteristic angles. Figure 2.7 shows the angles common to all halogen bonds as well as the distances common to Br··O halogen bonds. Because the region of electropositivity is directly opposite the covalent bond the angle between R-X··O is always nearly 180°.[30] The electrons of the nucleophile (oxygen in this report) are typically sp^2 or sp^3 hybridized and the interaction between them and the halogen follow this orientation. Thus the angles between R'-O··X are usually close to 120°C, though they exhibit more variance than the 180° R-X··O angle.[30] Though the oxygen of a ketone does not have its lone pair electrons in sp^2 orbitals (section 2.3.1) the

halogen bond still behaves at these angles since the p and sp orbitals filled in the ketone are roughly similar in orientation.

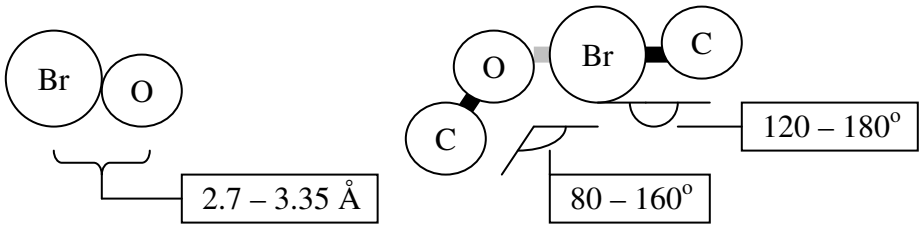

Figure 2.7 Characteristic distance and angles in Br···O halogen bonds.

2.5.4 Applied to DHAE

The halogen bond is a critical piece of the DHAE principle. Directing a heavy atom to the active site of the aromatic ketone facilitates greatly enhanced spin-orbit coupling via the heavy atom effect to promote bright phosphorescence. In an extremely fortunate coincidence, heavy halogens needed for the heavy atom effect are also the most highly active in halogen bonding. The optimal combination of aromatic ketone and heavy atom are brought together by halogen bonding. This good fortune brings together the necessary functionalities of the DHAE design principle.

2.6 Vibrational Limitation

The final piece of DHAE to consider is already achieved by halogen bonding. Vibrational limitation remains an important aspect to enhancing phosphorescence in DHAE. Though we have the ideal combination of the directed heavy atom effect to promote $T_1 \rightarrow S_0$ the threat of vibrational dissipation still looms to reduce the overall phosphorescent QY.

2.6.1 Low Temperatures

One popular strategy to reduce vibrational freedoms is to simply reduce the temperature. Vibrational modes are severely limited at temperatures below 100 K. This is obviously not very practical if we are to use DHAE to design metal-free organic phosphors for commercial applications such as displays, solid state lighting, photovoltaics, and sensors. DHAE-designed phosphors do exhibit very high phosphorescent QYs at low temperature, but this is used later in this report as a purely diagnostic tool.

2.6.2 Polymer/Crystal Embedding

Another strategy is to reduce vibration via the use of a rigid matrix such as a glassy polymer. These methods are more practical than low temperatures, but they are not as effective for a variety of reasons. Even highly rigid, glassy polymers exhibit some degree of vibrational freedom at ambient temperatures and any restriction to vibrational dissipation of the phosphor is strictly external. Polymer embedding is also complicated by the effectiveness of the mixing. Being that the overarching benefit to the DHAE principle is the promise of limitless metal-free organic phosphor design, getting large or complex organic molecules to mix well with polymers can become a great challenge. That, combined with marginal effectiveness makes this approach suboptimal. DHAE-designed phosphors can be enhanced by polymer matrices, as will be demonstrated in Chapter 9, but not to the greatest effect.

Doping organic phosphors into crystals is an approach with mixed success. As mentioned in chapter 1, dye inclusion crystals attempt to confine phosphorescent chromophores into rigid ionic or small molecule crystals in a purely interstitial paradigm.[31] This approach suffers from difficulties in mixing as what is essentially doping organic phosphor molecules into small and dissimilar crystals is a very inefficient process. The use of crystals, however, is not without promise. If both host and dopant are designed to cocrystallize efficiently, the net effect can provide a rigid, vibration-free environment for the phosphor where mixing is far more efficient than in ionic or greatly dissimilar structured crystals. It is in this careful design that the desired aspects of the DHAE principle are brought together and aided by their crystal packing.

2.6.3 Applied in DHAE

By now the critical aspects of the DHAE design principle have been given: halogen bonding directs a heavy atom to interact with the triplet-generating carbonyl in an aromatic ketone. The final important facet of DHAE to understand is the added benefit of the halogen bond in the suppression of vibrational dissipation. When crystallized the halogen bond helps to pack the two moieties very tightly, provided that the halogen bond is reasonably strong. The excited state molecular orbitals of the aromatic ketone are very localized at the carbonyl, which means that the vibrational modes are as well. Having a strong halogen bond nearby means that the carbonyl is essentially pinned down by a very

large neighbor. This prevents vibrational freedom of the excited state and removes the internal conversion pathway to triplet relaxation. This must all be achieved in the crystal state, however, which is a caveat that can make proper design of a DHAE phosphor challenging.

2.7 Conclusions

The DHAE design principle uses solid state halogen bonding to direct the heavy atom effect to the triplet-generating carbonyl site of an aromatic ketone. This technique efficiently combats the two biggest challenges to organic phosphorescence. First, the heavy atom, sharing orbital space with the carbonyl oxygen thanks to the electrostatic interaction of the halogen bond, provides enhanced spin-orbit coupling to promote not only $S_1 \rightarrow T_1$ (technically, $S_1 \rightarrow T_2$ in aromatic ketones) but $T_1 \rightarrow S_0$ as well. Second, the fact that this takes place in a highly ordered crystalline state with the halogen bond closely confining the carbonyl and halogen eliminates many vibrational freedoms at the carbonyl, which reduces non-emissive loss of the triplets. The halogen bonding motif utilized also allows for crystal design, much as is becoming popular in the contemporary field of crystal engineering. The DHAE design principle can be used in conjunction with crystal engineering to design metal-free organic chromophores that contain aromatic ketones and halogens that bond to create bright phosphorescence.

2.8 References

[1] A. Kohler, J.S. Wilson, and R.H. Friend *Adv. Mater.* **2002**, *14*, 701.
[2] Turro, N.J. *Modern Molecular Photochemistry* (University Science Books, Sausalito CA, 1991).
[3] O. Bolton, K. Lee, H.-J. Kim, K.Y. Lin, and J. Kim *Nature submitted*.
[4] J. Ferguson and H.J. Tinson *J. Chem. Soc.* **1952**, 3083.
[5] E.W. Abrahamson, J.G.F. Littler, and K.-P. Vo *J. Chem Phys.* **1966**, *44*, 4082.
[6] M. Kiritani, T. Yoshii, N. Hirota, and M. Baba *J. Chem. Phys.* **1994**, *98*, 11265.
[7] E.H. Gilmore, G.E. Gibson, and D.S. McClure *J. Chem. Phys.* **1952**, *20*, 829; correction, *ibid.*, **1955**, *23*, 399.
[8] T. Itoh *Chem. Phys. Lett.* **1988**, *151*, 166.
[9] M. Koyanagi and L. Goodman *Chem. Phys. Lett* **1971**, *9*, 636.
[10] P.W. Atkins, and R.S. Friedman *Molecular Quantum Mechanics* (Oxford University Press, New York, NY, 1997).
[11] A.M. Turek, G. Krishnamoorthy, K. Phipps, and J. Saltiel *J. Phys. Chem.* A, **2002**, *106*, 6044.
[12] IUPAC Compendium of Chemical Terminology, **1996**, *68*, 2245.
[13]G.G. Giachino and D.R. Kearns *J. Chem. Phys.* **1970**, *52*, 2964.
[14] M. Kasha *J. Chem. Phys.* **1952**, *20*, 71.
[15] M.R. Wright, R.P. Frosch, and G.W. Robinson *J. Chem. Phys.* **1960**, *33*, 934.
[16] A. A. Avdeenko, O. S. Pyshkin, V. V. Eremenko, M. A. Strzhemechny, L. M. Buravtseva, and R. V. Romashkin *Low Temp. Phys.* **2006**, *32*, 1028.
[17] Y. Zeng, L. Biczok, and H. Linschitz *J. Phys. Chem.* **1992**, *96*, 5237.
[18] S.P. McGlynn, M. Kasha, and T. Azumi *J. Chem. Phys.* **1964**, *40*, 507.
[19] S.K. Ritter *Chemical & Engineering News* **2009**, *87*, 39.
[20] O. Hassel *Nobel Lecture* June 9, 1970.
[21] P. Metrangolo and G. Resnati, G. *Chem. Eur. J.* **2001***, 7*, 2511.
[22] P. Metrangolo, F. Meyer, T. Pilati, G. Resanti, and G. Terraneo *Angew. Chem.-Intl. Ed.* **2008**, *47*, 6114.
[23] X.Y. Lu, T. Shi, Y. Wang, H.Y. Yang, X.H. Yan, X.M. Luo, H.L. Jiang, and W.L. Zhu *J. Med. Chem.* **2009**, *52*, 2854.
[24] A.R. Voth and P.S. Ho *Curr. Topics in Med. Chem.* **2007**, *7*, 1336.
[25] H.M. Yamamoto, Y. Kosaka, R. Maeda, J. Yamaura, A. Nakao, T. Nakamura, and R. Kato *ACS Nano* **2008**, *2*, 143.
[26] H. L. Nguyen, P. N. Horton, M. B. Hursthouse, A. C. Legon, and D. W. Bruce, *J. Am. Chem. Soc.* **2004**, *126*, 16.
[27] P. Metrangolo, C. Präsang, G. Resnati, R. Liantonio, A. C. Whitwood, and D. W. Bruce, *Chem. Commun*. **2006**, 3290.
[28] A. Sun, J.W. Lauher, and N.S. Goroff *Science* **2006**, *312*, 1030.
[29] A.R. Voth, F.A. Hays, and P.S. Ho *PNAS* **2007**, *104*, 6188.
[30] Auffinger, P., Hays, F.A., Westhof, E., and Ho, P.S. *Proc. Natl. Acad. Sci.* **2004**, *48*, 16789.
[31] B. Kahr and R.W. Gurney *Chem. Rev.* **2001**, *101*, 893.

Chapter 3

The Directed Heavy Atom Effect at Work in Substituted Benzaldehydes

Now that the details of the DHAE design principle are clear, this chapter demonstrates its application via the molecule 2,5-dihexyloxy-4-bromobenzaldehyde (Br6A). This compound exhibits the properties required for DHAE to succeed. It is an aromatic ketone, a substituted benzaldehyde, and its crystals exhibit strong halogen bonding. By being halogenated Br6A molecules have not only the added benefit of an internal heavy atom effect, but also can halogen bond among themselves in the solid state to further enhance spin-orbit coupling at the carbonyl. This allows Br6A to form bright phosphorescent crystals. In this chapter we present this compound in specific exploring its photophysical and solid-state properties.

3.1 Introduction

The ultimate goal of the DHAE principle is to give researchers the freedom to design metal-free organic phosphors that are easy to synthesize and purify, are stable for device applications, and are practically bright.

3.2 Results and Discussion

2,5-dihexyloxy-4-bromobenzaldehyde (Br6A) is a simple, non-conjugated organic compound easy to synthesize in large quantities by a variety of synthetic routes.[1] Figure 3.1 shows the chemical structure of Br6A. The compound is a substituted benzaldehyde with a bromine atom para to the ketone and alkoxy substituents elsewhere on the aromatic ring. In order to ensure that no optical observations were the result of impurities, metallic or otherwise, batches of Br6A were purified stringently as described in section 3.3.2. Br6A exhibits very interesting photophysical properties based on its environment and state.

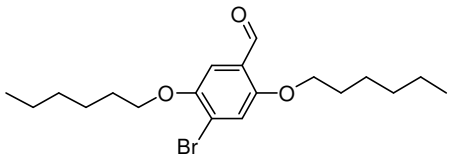

Figure 3.1 Chemical structure of Br6A.

3.2.1 Crystal Structure

The DHAE requires that the aromatic ketone exhibit halogen bonding. This can only be determined by single crystal x-ray diffraction (XRD). Br6A is a crystalline solid at room temperatures. Large crystals (dimensions over 1 mm) can be grown from a slowly evaporated methanol solution. Crystals were grown in this manner and submitted for single crystal XRD to Dr. Jeff W. Kampf in the department of chemistry, University of Michigan. Figure 3.2 shows the crystal structure of Br6A.

Evidence that there is a strong halogen bond active in crystals of Br6A exists in the close nuclear distances between the bromine and oxygen atoms. This distance measures 2.86 Å, which is among the shortest, and therefore strongest, halogen bonds reported.[2] The angle measured between C=O··Br is 126^{o} and that of O··Br-C is 180^{o}, which are also consistent with literature. From this we see that not only is halogen bonding present and directed to the carbonyl oxygen, as is optimal, but also that the halogen bond is particularly strong. This is important as it means also that the tight crystal may have

greatly reduced vibrational freedom at the carbonyl. From this we can see that the halogen bond is successful. Thus the structural goals of the DHAE design principle are working, an aromatic ketone is halogen bonding to put a heavy atom extremely close to the carbonyl oxygen. Excited state activity must next be examined using optical analyses to determine if the DHAE is working.

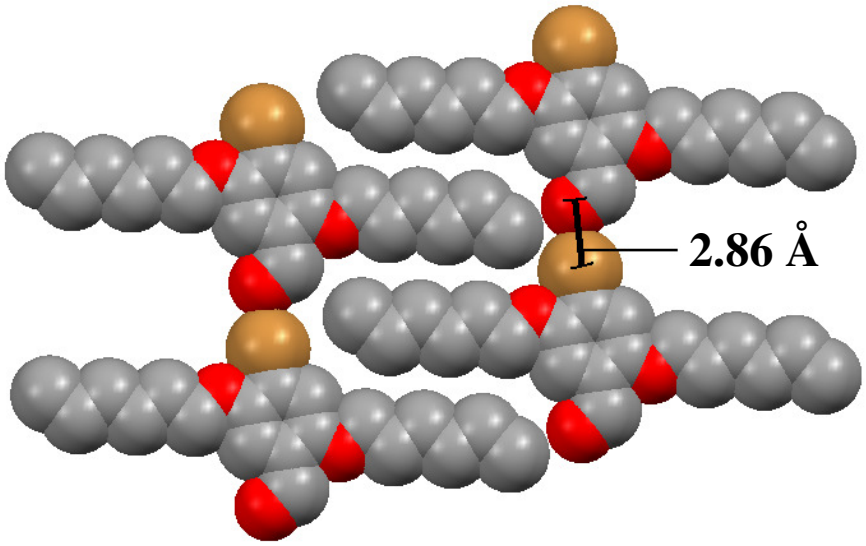

Figure 3.2 Crystal structure of Br6A.

3.2.2 Photophysical Properties: Solution

Because Br6A is among a family of popular aromatic ketones that have been studied for decades, we can assume a great deal about its excited states. By comparing it to benzophenone, for instance, we see that the transitions are well studied.[3] First, the lowest unoccupied molecular orbital represents the transition from non-bonding to π*, $S_1(n,\pi^*)$. However, the absorption transition from S_0 to S_1 is not allowed because the orbitals do not overlap. S_2 is the π-π* transition, which is allowed. T_2 is the triplet state π-π* transition and T_1 is n-π*. Figure 3.3 illustrates this situation with hypothesized chemical structures.[4] Thus, the lowest energy absorption we would expect to see is actually $S_0 \rightarrow S_2$, and not $S_0 \rightarrow S_1$, which is more common among organic compounds.

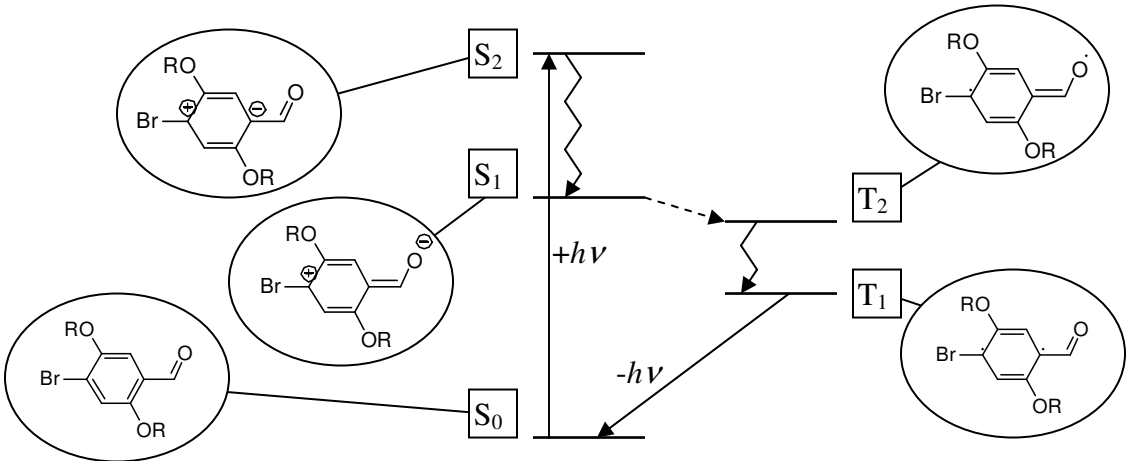

Figure 3.3 Hypothesized energy diagram of Br6A. (Gaps are not drawn to scale.) Following the event arrows: (**S_0**) in the ground state Br6A rests in its lowest energy resonance structure. (**S_2**) The π-π* transition takes S_0 directly into S_2 because of the orbital overlap in the aromatic ring. (**S_1**) However, a lower-energy singlet exists when the negative charge is at the oxygen atom. S_2 quickly relaxes to S_1. (**T_2**) orbital overlap and a small energy barrier promote intersystem crossing between S_1 and T_2. (**T_1**) The radical is stabilized by the higher substitution in a quinoid orientation.[4] T_2 quickly relaxes to T_1, which can emit if it survives long enough.

Br6A has a wide range of solubility, dissolving very well in non-polar solvents such as hexanes as well as modestly in alcohols such as methanol. In solution the UV absorption, photoluminescent (PL) excitation and PL emission of Br6A give us clear insight into its excited state. Figure 3.4 shows the solution state photophysical properties of Br6A.

As shown the UV-absorption spectrum of Br6A in methanol solution exhibits three distinct peaks at λ^{max} = 230 nm, 265 nm, and 350 nm. These are presumably the corresponding $S_0 \rightarrow S_4$, $S_0 \rightarrow S_3$, and $S_0 \rightarrow S_2$ transitions, respectively (remember that $S_0 \rightarrow S_1$ is forbidden so it does not exhibit an absorption band). Kasha's rule states that for most, if not all, chromophores fluorescence is only derived from S_1 and phosphorescence only from T_1.[5] Thus we can disregard the $S_0 \rightarrow S4$ transition (wholly) and $S_0 \rightarrow S_3$ (mostly) for the purposes of this analysis. The $S_0 \rightarrow S_2$ transition, however, is important in our analysis of the Br6A excited state. It represents the transition from π to π* (anti-bonded) and is the primary excitation route to all Br6A emission.

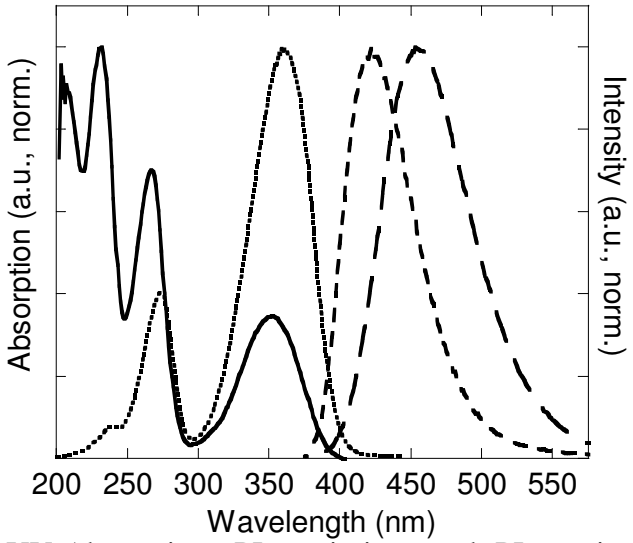

Figure 3.4 UV-Absorption, PL emission, and PL excitation of Br6A in chloroform and methanol solutions. UV-Abs in methanol (solid), emission in chloroform (short dash), emission in methanol (long dash), excitation in chloroform (dotted). (Excitation in methanol is identical to that in chloroform.)

Solutions of Br6A exhibit fluorescent emission whose QY and emission spectrum are variable with the solvent used. As shown in Figure 3.4 chloroform solutions of Br6A emit with a λ^{max} = 425 nm. Solutions in methanol emit at λ^{max} = 460 nm, significantly red-shifted from chloroform. In both cases the solution is excited with 365 nm light. This shift is apparent in polar, protic solvents such as alcohols and water (used as a co-solvent, Br6A is insoluble in pure water). This is presumably due to hydrogen bonding acting on the carbonyl oxygen and is not seen from polar aprotic solvents such as acetonitrile and acetone.

As explained in Chapter 2, the excited state of aromatic ketones is localized at the carbonyl, thus interactions like hydrogen bonding acting at that site greatly affect the emission and excited state activity. Chloroform solutions exhibit PL QYs of Φ_{Fl} = 0.005 with quantum lifetimes measured at τ = 0.5 ns. Methanol solutions exhibit Φ_{Fl} = 0.128 with longer lifetimes of τ = 2.4 ns. If we use equation 1.3 we see that the fluorescent rates, the rates at which the $S_1 \rightarrow S_0 + h\nu$ transition take place, are k_{Fl}^{CHCl3} = 10 MHz and k_{Fl}^{MeOH} = 53 MHz. Fluorescence from methanol solution is over five-times faster than that from chloroform solution. Longer wavelength emission from methanol solution indicates that the hydrogen bonding stabilizes the S_1 state, which lowers its

energy and thus the bandgap. This lowering of energy presumably puts S_1 somewhat below T_1, reducing intersystem crossing and raising Φ_{Fl} as compared to chloroform.

Figure 3.4 shows the PL excitation of Br6A in chloroform solution. Excitation in methanol solution is identical, which indicates that the solvent interaction is with the excited state, not the ground state. The longer wavelength excitation band fits well into the 350 nm absorption band indicating that fluorescent emission is derived from all vibrational modes of that transition. Notice also a small portion of the absorption band at 265 nm is included in the excitation spectrum. This is interesting as it indicates that only the lower energy portion of the vibrational states of S_3 may lead to emission from S_1. Conversely, it appears that all modes of S_2 may relax to S_1 and emit because the shape and position of the excitation matches well to the $S_0 \rightarrow S_2$ absorption. As $S_n \rightarrow S_1$ transitions are assumed to be very fast (~10^{-12} sec)[6] and once relaxed to S_1 the electron has no memory of its route and is no different than those excited directly to S_1, we must assume that the states of S_3 that do not excite fluorescent emission must lead to another end. These high-energy absorptions may lead to reaction or decomposition of the chromophore.

3.2.3 Photophysical Properties: Crystals

Crystalline Br6A exhibits bright green phosphorescence. Figure 3.5 shows typical crystals as well as a sampling of PL emissions. Because the DHAE principle only works when the chromophore is in perfect order, its crystal, samples of poor crystallinity do not emit strong phosphorescence. In Figure 3.5 three spectra are given representing samples of varying crystal quality. One is taken from a sample grown from a dropcast of a chloroform solution. These produce extremely fast-grown crystals of very poor quality, taking only seconds to form. As such the emission spectrum shows dominant fluorescence with a λ^{max} = 420 nm and only a soft shoulder in the phosphorescent region around 500-530 nm. A second sample is grown from a methanol recrystallization at -12°C, which allows for slightly slower-growing crystals and, thus, more highly crystalline samples. These crystals grew over the course of minutes. This sample produces a fairly even mix of fluorescence and a now clear peak of phosphorescence at λ^{max} = 500-530 nm. The last sample is grown from methanol recrystallization at room

temperature. These crystals are grown over the course of 24 hours and are the highest quality crystals in this study. As such, they show dominant phosphorescence with minor fluorescence. This clearly demonstrates the importance of high order in the DHAE principle. Attempts were made to quantify crystal quality by enthalpy using differential scanning calorimetry. A slight trend was seen, but high error rendered the results inconclusive.

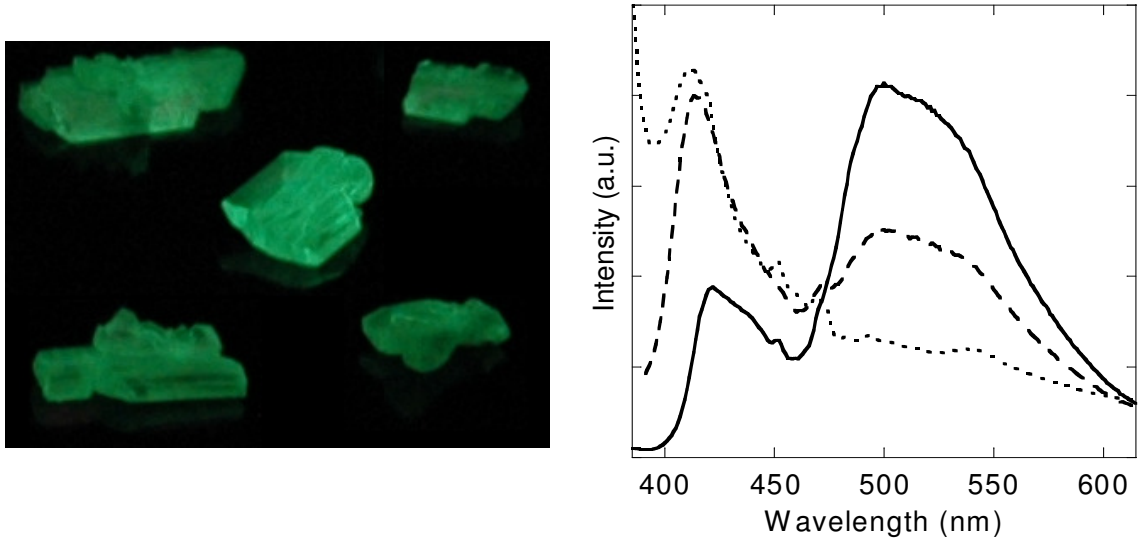

Figure 3.5 Photo and PL emission spectra of solid state Br6A in various crystal qualities. Dropcasts (dotted), fast recrystallization (dashed), and slow recrystallization (solid). Crystals shown in photo are all grown from slow recrystallization.

There are two ways by which we can know that this green emission is phosphorescence. Firstly, it is red-shifted from the blue fluorescence. We know that the blue fluorescence is the $S_1 \rightarrow S_0 + h\nu$ transition (Kasha's rule). By definition there can be no lower singlet state. Only a triplet or intermolecular species could exist at a lower energy. To rule out intermolecular interaction we freeze a toluene solution of Br6A in liquid nitrogen at 77K, making a frozen glass. In this condition there can be no intermolecular interaction as the chromophore is diluted to an optical density of 0.1 (ca. 0.85 μM). There is also greatly reduced vibrational dissipation of T_1 so we can see exactly what energy T_1 is at by the observed phosphorescent emission. As Figure 3.6 shows, emission from Br6A in glassy toluene solution at 77K is identical to the green portion of the emission from room temperature crystals. Thus we can conclude that both emissions are phosphorescence from T_1.

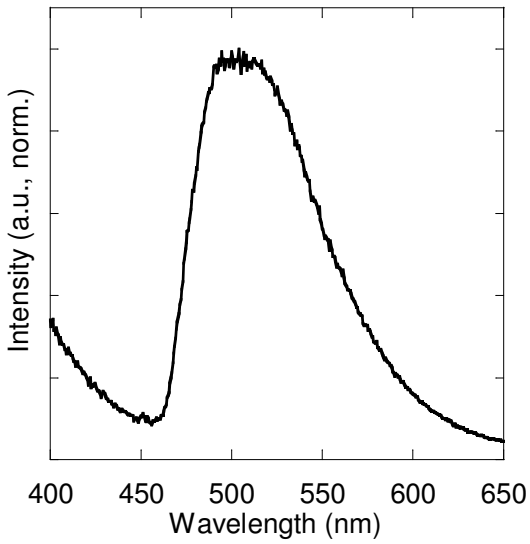

Figure 3.6 PL emission of Br6A in glassy toluene at 77K. The sample was excited with 360 nm light.

The other determining measurable is quantum lifetime. A dropcast sample of Br6A was measured on a strobe laser system. A pulsed laser excites the sample and a strobic detector measures the emission intensity as a function of time. Figure 3.7 shows the decay curve as measured. Remembering equation 1.2 we can fit the curve (at least the long-lived portion) to an exponential decay to solve for a reasonable quantum lifetime, τ. Fluorescent lifetimes are typically in the pico-to-nanosecond range so detecting anything longer points strongly to phosphorescence. As shown these samples measured 5.4 milliseconds, which is several orders of magnitude slower than fluorescence. From this, clearly, the green emission is phosphorescence. (The spectral differences rule out any possible delayed fluorescence.)

Finally we examined the QY of these crystals to understand how efficiently our triplets are emitting. In solution and any non-crystalline state the phosphorescent quantum yield, Φ_{Ph}, is practically zero as no phosphorescent emission is detected. We cannot, therefore, make a measurement of the improvement of Φ_{Ph} due to the DHAE principle. As discussed the phosphorescent emission strength is closely tied to the crystal quality. High quality crystals (slowly dropcast from methanol solution at room temperature) were measured using an integrating sphere to exhibit QY of $\Phi_{Ph} = 0.029$ (2.9%). Not outstandingly high, but a marked improvement from zero. Lower quality

crystal samples (dropcasts) measured much lower, typically in the range of Φ_{Ph} = 0.001-0.01 (0.1-1%).

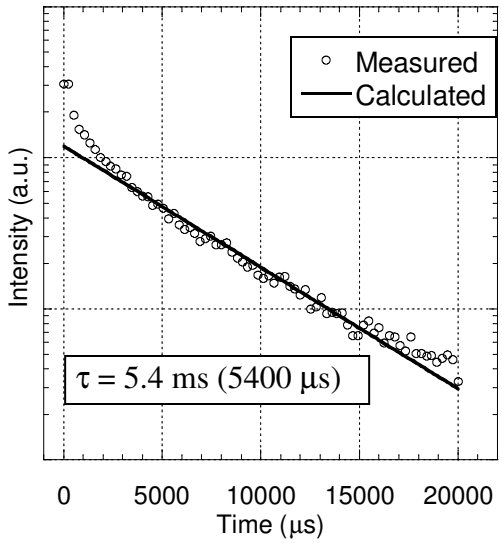

Figure 3.7 Phosphorescent lifetime measurement of Br6A crystals.

3.3 Experimental

3.3.1 General Methods

All chemicals used were purchased from Sigma Aldrich and used without further purification. Deuterated solvents for NMR were purchased from Cambridge Isotope Laboratories. Proton NMR was conducted on a Varian Inova 500 using $CDCl_3$ solvent with chemical shifts identified relative to 0.05 v/v% tetramethylsilane standard (0.00 ppm). Anhydrous tetrahydrofuran was generated by refluxing over sodium metal and benzophenone collected only from deep purple solution.

UV Absorption measurements were collected using a Varian Cary 50 Bio spectrometer with solution state samples held in a quartz cuvette. PL emission, excitation, and quantum yield data were collected using a Photon Technologies International (PTI) Quantamaster system equipped with an integrating sphere. Quantum lifetime data was collected using a PTI LaserStrobe. Quantum lifetime calculations were carried out on the FeliX32 software partnered with the PTI equipment. XRD was conducted using a Bruker SMART APEX CCD-based X-ray diffractometer as described below.

3.3.2 Synthesis and Characterization

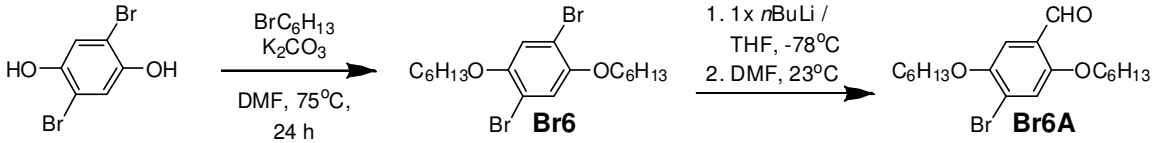

Scheme 3.1 Synthetic Route to Br6A.

Synthesis of 2,5-dihexyloxy-1,4-dibromobenzene (Br6). 2,5-dibromohydroquinone (1 equiv.) and 1-bromohexane (2.5 equiv.) is loaded into a two-neck round bottomed glass flask and dissolved into dimethylformamide (ca. 1 ml solvent / g dibromohydroquinone). Potassium carbonate (3 equiv.) is added and the flask is sealed under nitrogen, stirred, and heated to 75°C for 24 hours. The reaction is then cooled, filtered, and rotovaped at high temperature to remove all solvents. The product is purified by column chromatography with hexanes. White crystals were collected at yields of 70-80%. For Br6, ^{1}H NMR (500 MHz, $CDCl_3$): δ 7.05 (s 2H), 3.91 (t 4H), 1.76 (m 4H), 1.43 (m 4H), 1.33 (m 8H), 0.91 (m 6H).

Synthesis of 2,5-dihexyloxy-4-bromobenzaldehyde (Br6A). 2,5-dihexyloxy-1,4-dibromobenzene (Br6, 1 equiv.) is loaded into a two-neck round bottomed glass flask and vacuum purged with argon three times. Anhydrous tetrahydrofuran is added by syringe (ca. 25 ml solvent / g Br6) and the vessel is placed into a bath of dry ice and 2-propanol (-78°C). *n*-Butyllithium (1 equiv.) is added dropwise via syringe and the reaction is stirred at -78°C for 1 hour. Anhydrous DMF (4 equiv.) is then added and the reaction is allowed to warm to 23°C over three hours. The reaction is quenched carefully with water and extracted with diethylether. The organic layer is collected and dried over $MgSO_4$ before being filtered and rotovaped to remove solvents. Purification is done by column chromatography with ethylacetate:hexane (1:30) eluent followed by successive recrystallizations from methanol and acetonitrile at 23°C. White crystals were collected at yields of 50-70%. For Br6A, ^{1}H NMR (500 MHz, d_6-DMSO): δ 10.29 (s 1H), 7.53 (s 1H), 7.23 (s 1H), 4.09 (t 2H), 4.01 (t 2h), 1.73 (m 4H), 1.42 (m 4H), 1.30 (m 8H), 0.87 (m 6H).

Crystal Structure of Br6A. *The following analysis was conducted and report written by University of Michigan Department of Chemistry staff crystallographer Dr. Jeff W. Kampf as a paid service.* Colorless blocks **Br6A** were grown by slow evaporation of a methanol solution at 25 deg. C. A wedge-shaped crystal of dimensions 0.27 x 0.22 x 0.15 mm was cut from a larger mass and mounted on a Bruker SMART APEX CCD-based X-ray diffractometer equipped with a low temperature device and fine focus Mo-target X-ray tube (λ = 0.71073 A) operated at 1500 W power (50 kV, 30 mA). The X-ray intensities were measured at 85(1) K; the detector was placed at a distance 5.055 cm from the crystal. A total of 4095 frames were collected with a scan width of 0.5° in ω and 0.45° in phi with an exposure time of 15 s/frame. The integration of the data yielded a total of 33365 reflections to a maximum 2θ value of 56.72° of which 4669 were independent and 4444 were greater than $2\sigma(I)$. The final cell constants (Table 3.1) were based on the xyz centroids of 9960 reflections above $10\sigma(I)$. Analysis of the data showed negligible decay during data collection; the data were processed with SADABS and corrected for absorption. The structure was solved and refined with the Bruker SHELXTL (version 6.12) software package, using the space group P1bar with Z = 2 for the formula $C_{19}H_{29}O_3Br$. All non-hydrogen atoms were refined anisotropically with the hydrogen atoms placed in idealized positions. Full matrix least-squares refinement based on F^2 converged at R1 = 0.0225 and wR2 = 0.0606 [based on I > 2sigma(I)], R1 = 0.0241 and wR2 = 0.0615 for all data.

- Sheldrick, G.M. SADABS, v. 2007/4. Program for Empirical Absorption Correction of Area Detector Data, University of Gottingen: Gottingen, Germany, 2007.
- Sheldrick, G.M. SHELXTL, v. 6.12; Bruker Analytical X-ray, Madison, WI, 2001.
- Sheldrick, G.M. CELL_NOW, Program for Indexing Twins and Other Problem Crystals, University of Gottingen: Gottingen, Germany, 2003.
- Sheldrick, G.M. TWINABS, v. 1.05. Program for Empirical Absorption Correction of Area Detector Data, University of Gottingen: Gottingen, Germany, 2005.
- Saint Plus, v. 7.34, Bruker Analytical X-ray, Madison, WI, 2006.

Table 3.1 Crystallographic Data for Br6A.

Name	**Br6**
Formula	$C_{19}H_{29}BrO_3$
Space Group	P-1
Cell Lengths	**a** 9.5083(8) **b** 9.6863(8) **c** 10.9481(9)
Cell Angles	α 68.5630(10) β 85.8470(10) γ 84.9170(10)
Cell Volume	934.004
Z, Z'	**Z**: 2 **Z'**: 0
R-Factor (%)	2.25

3.4 Conclusions

The DHAE principle works in Br6A. This simple substituted, halogenated benzaldehyde exhibits strong halogen bonding in its crystalline solid. This halogen bonding brings the bromine atom of one molecule very close to the carbonyl oxygen of its neighbor showing an interatomic spacing that indicates a non-covalent electronic interaction. In solution, Br6A is fluorescent blue and exhibits solvatochromic properties with protic solvents. Fluorescent quantum yields in solution are between 0.5 and 12% indicating that singlet-to-triplet intersystem crossing is intrinsically quite efficient and highly competitive with emissive singlet decay (fluorescence).

Once crystalline, Br6A exhibits green phosphorescence whose brightness is correlated to the quality of the crystal. Well-ordered crystals exhibit strong phosphorescence that is noticeably dominant over fluorescent emission with phosphorescent quantum yields measured as high as 2.9 %. Quantum lifetimes of these crystals are measured to be in the millisecond regime, clearly indicating emission from a long-lived triplet state. Low temperature emission of Br6A in glassy toluene solution agrees with room temperature crystals to remove the possibility that the green emission is the result of a long-lived intermolecular phenomenon.

Here we demonstrate the DHAE design principle succeeding to active phosphorescent emission from a room temperature, nonmetallic organic compound. Br6A is non-phosphorescent at room temperatures *unless* it is crystallized to exhibit strong halogen bonding. Phosphorescent quantum yields are good, immeasurably better than otherwise, but still, frankly, far from competitive with established organometallic phosphors.

3.5 References

[1] O. Bolton, K. Lee, H.-J. Kim, K.Y. Lin, and J. Kim *Nature submitted*

[2] P. Auffinger, F.A. Hays, E. Westhof, and P.S. Ho *Proc. Natl. Acad. Sci.* **2004**, *48*, 16789.

[3] E.H. Gilmore, G.E. Gibson, and D.S. McClure *J. Chem. Phys.* **1952**, *20*, 829; correction, *ibid.*, **1955**, *23*, 399.

[4] The idea that the structure of T_1 is a quinoidal diradical comes from computations done in the following reference: S.T. Park, J.S. Feenstra, and A.H. Zewail *J. Chem. Phys.* **2006**, *124*, 174707.

[5] M. Kasha *Disc. Faraday Soc.* **1950**, *9*, 14.

[6] Turro, N.J. *Modern Molecular Photochemistry* (University Science Books, Sausalito CA, 1991).

Chapter 4

Cocrystallization for Enhanced Brightness from DHAE

In order to enhance the QY of Br6A crystals a cocrystallization motif can be employed. By diluting the Br6A chromophore into an optically inert "host" crystal we can remove the possibility of triplet-triplet annihilation and excimer formation. The caveat is that the host crystal must exhibit the same halogen bonding of Br6A. This is critical to efficient emission. Here we present a simple addition to the DHAE design principle to build suitable host compounds. By replacing the aldehyde moiety of Br6A (or many other aromatic aldehydes, as is demonstrated in Chapter 5) with a bromine atom an optically inert material suitable for cocrystallization is made. For Br6A this host is 1,4-dibromo-2,5-dihexyloxybenzene (Br6). When cocrystallized with Br6A, QYs of Br6A solids can be increased from a modest 2.9% to a robust 68%. By utilizing cocrystallization DHAE organic phosphors can achieve QYs competitive with organometallics though, as is discussed here, cocrystallization can be complex and achieving optimal QY requires some precision.

4.1 Introduction

In Chapter 3 the DHAE principle was demonstrated, working in high quality crystals of pure Br6A. Though this finding is quite significant for designing nonmetallic phosphors and holds great promise for new classes of material, QYs of 2.9% are far from sufficient if these are to compete with organometallic phosphors. There are two most probable reasons for the low QYs in these crystals, and both are derived from saturation of the chromophore. Two well-known quenching mechanisms are triplet-triplet annihilation and excimer formation. Triplet-triplet annihilation occurs when two triplets, usually two neighboring triplet excited state molecules, interact to relax each other non-emissively (though this occasionally leads to repopulation of higher energy singlet states which may then emit fluorescence).[1] Excimer formation occurs when the excited state of one molecule interacts with a ground state neighbor to dimerize and reduce the overall system energy. Triplet excimers are notoriously quenching because triplets are normally fairly low in energy, making their excimers more so.[2,3] Both of these mechanisms are intermolecular. Crystals of pure Br6A represent the most concentrated state possible of the chromophore, making these mechanisms very favorable. The probability of chromophore-chromophore interaction is unity.

Just as for known organic phosphors (organometallics included) dilution of the chromophore is critical to achieve high QY emission. By diluting the chromophore intermolecular interactions are prevented, allowing triplets to emit rather than die from triplet-triplet annihilation or relax vibrationally by triplet excimer formation. Prior to our report of the DHAE principle, chromophore order was not sought in phosphors. In PhOLEDs organometallic chromophores are diluted into host materials by carefully controlled vapor deposition. The phosphor is randomly oriented (or at least their order is not controlled). In existing studies of nonmetallic phosphors, samples are typically chromophores liberally diluted into glassy solutions, unordered by definition. DHAE, however, uses careful controlled order to greatly outpace these mixed state phosphors in brightness. So successfully diluting a DHAE phosphor must be done in a similar but optically inert crystal, one that exhibits the same halogen bonding character but will not generate its own triplets nor form excimers with the phosphorescent chromophore. A fitting "*host*" is required.

Fortunately a very simple alteration to the DHAE chromophore allows for the design of an ideal host material. The aldehyde moiety, CHO, is roughly the volumetric size of a bromine atom. Replacing the aldehyde with bromine makes a nearly spatially perfect analog. Removing the aldehyde also greatly alters the optical properties of its chromophore, as it is a strong auxochrome. As discussed at length earlier, the carbonyl imparts very unique optical properties on its molecule: S_1 and S_2 are greatly reduced in energy, $S_0 \rightarrow S_1$ absorption is extremely weak, and triplet generation is very efficient by intersystem crossing. Replacing the aldehyde with bromine removes these unique optical characteristics making a highly non-phosphorescent chromophore that has much higher energy excited states. Thus, swapping aldehyde for bromine would yield a compound that is both very similar in size, shape, and volume but is also optically inert (higher energy).

4.2 Optical Results and Discussion

Applying this addendum to the DHAE principle for the purposes of Br6A, we get 1,4-dibromo-2,5-dihexyloxybenzene (Br6).[4] Figure 4.1 shows the chemical structure of Br6. Br6 is a highly crystalline white solid that forms block shaped crystals readily from a variety of methods. Enhanced crystallinity versus that of Br6A is likely due to the higher symmetry of the compound. Br6 is highly soluble in low and moderate polarity solvents and very slightly soluble in alcohols. It is slightly less polar than Br6A, which is probably why it has better solubility in perfectly non-polar hexanes and worse in highly polar methanol, though on a general scale both Br6 and Br6A have very similar polarity and solubility.

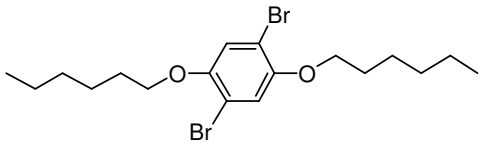

Figure 4.1 Chemical Structure of Br6.

4.2.1 Photophysical Properties: Br6

To ensure that Br6 is optically non-interfering with Br6A we first look at its personal optical characteristics. Br6 is nonemissive in both solid and solution at room

temperature. It has a single identifiable absorption band at λ^{max} = 300 nm. This is presumably the $S_0 \rightarrow S_1$ transition, which is the typical lowest energy absorption for non-carbonyl compounds (remember that Br6A having no $S_0 \rightarrow S_1$ absorption is unusual). This is shown in Figure 4.2.

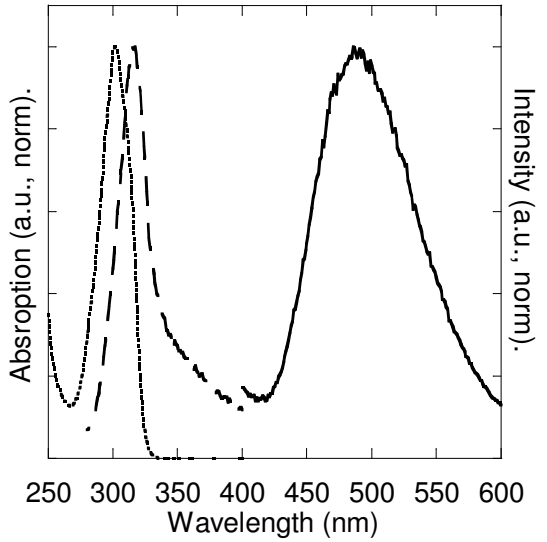

Figure 4.2 UV-absorption, PL excitation, and PL emission of Br6 at various temperatures. UV-abs at 298 K (dotted), PL emission at 77K (solid), and PL excitation at 77K (dashed)

The lack of fluorescent emission from Br6 is intriguing. To relax S_1 via internal conversion would require either a very large number of small vibrational modes or several large ones, neither of which is highly likely. Though Br6 contains no carbonyl, it can still generate triplets via the internal heavy atom effect. There are two heavy atoms, bromines, attached to the central chromophore. As it happens, this is the case.

At 77K Br6 emits bright green phosphorescence when excited at 310 nm whether in solution or crystal states. Figure 4.2 shows the pertinent spectra. Reductions in temperature remove vibrational modes, but they do not directly affect intersystem crossing or emissive transitions. Thus to see phosphorescent emissive become active only at low temperature means that Br6 is an efficient triplet generator and we can deduce that, probably, $\Phi_{S1 \rightarrow T1} \approx 100\%$ because $\Phi_{Fl} \approx 0\%$. Internal conversion of $S_1 \rightarrow S_0$ + *heat* is not common in solid aromatics (such as Br6 crystals).[5] At room temperature all S_1 state Br6 crosses into T_1 only to relax non-emissively. This means that Br6 is a triplet

generator, however its excitation of 310 nm is well higher in energy than the 360 nm that excites triplets in Br6A. There is sufficient separation to produce triplets in Br6A selectively in cocrystals and prevent interspecies triplet-triplet annihilation between Br6A and Br6.

4.2.2 Photophysical Properties: Cocrystals

Br6A and Br6 cocrystallize readily, which is discussed in great detail in the next section. First we look at the optical properties of these cocrystals to see that the DHAE principle is succeeding. Figure 4.3 shows a photograph of cocrystals grown from the slow evaporation of a hexane solution containing a 0.01 weight percent mixture of Br6A/Br6, irradiated here with 365 nm light. Clearly, bright green emission is exhibited.

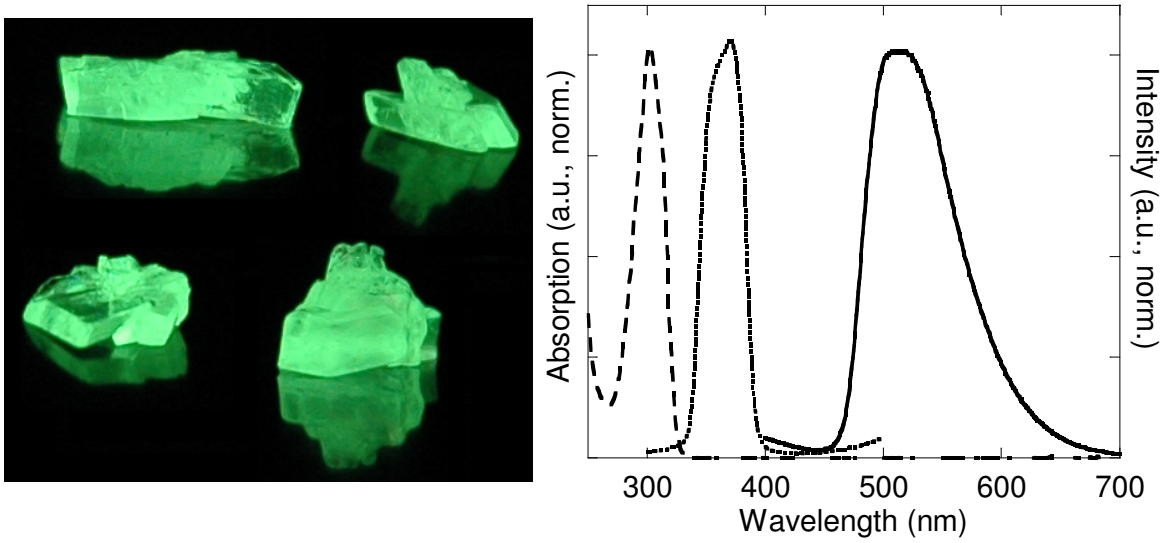

Figure 4.3 Photo, UV-absorption, PL emission, and PL excitation of solid-state Br6A/Br6 cocrystals. UV-abs (dashed), PL excitation (dotted), PL emission (solid).

Figure 4.3 also shows the spectral analysis of these crystals. UV absorption yields a single peak at λ^{max} = 300 nm, which is the absorption of the Br6 component alone. This is understandable as Br6 constitutes 99.99 weight percent of the crystal. The three-peak absorption of Br6A is drowned out by the signal from Br6. In stark contrast, PL excitation of these crystals shows only a single, clean peak at λ^{max} = 360 nm, which is completely separate from the absorption peak. This is also understandable. PL excitation measures only those wavelengths that, once absorbed, lead to emission. Though Br6A is

a very minor component in these crystals, it is the only one emitting light. Thus despite its lack in numbers it dominates the sample optically.

PL emission measured from these cocrystals is the same broad green peak at λ^{max} = 500-530 that we see from pure Br6A crystals. Unlike in pure crystals of Br6A however there is no fluorescent peak seen in the 400-450 nm range. In Br6A crystals the fluorescent peak is due to the unordered portion of the sample. In Chapter 3 it is demonstrated that the fluorescence peak is reduced by higher quality crystallization. Here it is removed completely. This is likely due to the high crystallinity of Br6 and the low quantity of Br6A present. Highly ordered Br6 drives Br6A to crystallize more effectively than it does itself and that small amount of Br6A that does not cocrystallize is dominated by the resultant phosphorescence (remember that Br6A fluorescence exhibited QYs of only Φ_{Fl} = 0.5-12%, with the lower limit of that range measured in aprotic conditions like those here). Emission from cocrystals exhibits a quantum lifetime of τ = 8.2 milliseconds, a timescale that can only imply phosphorescence.

We can tell, optically, that these two species are cocrystallizing or at least that Br6A is orderly substituted into the Br6 crystals. First, we know that strict order is required to produce phosphorescence. In solution, molten, and glassy states (at room temperatures) Br6A/Br6 mixtures do not emit phosphorescence. Only the crystalline solid does. If order were not required, we should see phosphorescence from molten and glassy states where there is ample but random Br6-Br6A contact, but we do not. Second, emission for the cocrystals is polarized. Figure 4.4 shows a thin single cocrystal of ca. 0.01 wt% Br6A/Br6. In one panel the emission polarizer is turned at 90^{o} relative to its position in the other panel. As can clearly be seen in the right panel, when the polarizer is perpendicular to the chromophores in the crystal the emission to the camera is greatly reduced. Edge effects and internal reflectance still randomize the light at the crystals edges, but in the center this effect is clear. This proves that the Br6A molecules are ordered in the cocrystal because a random orientation would not yield polarized emission.

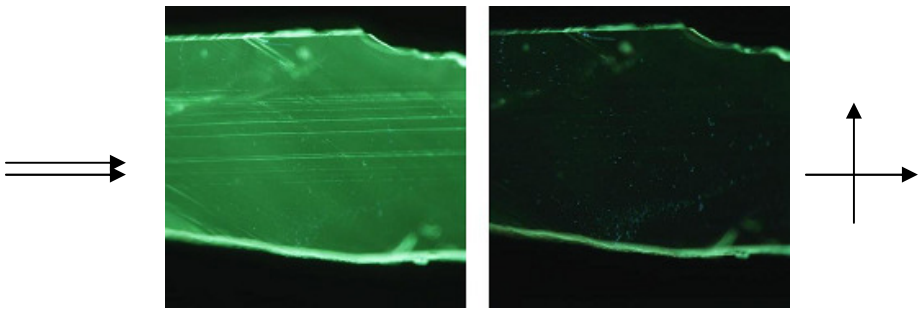

Figure 4.4 Polarized emission of Br6A/Br6 cocrystal.

From the optical analysis we can see that the goals of cocrystallization are met: the compounds cocrystallize readily (this will be explored more in a moment) and the host does not interfere optically. Exciting the cocrystals at 365 nm excites only Br6A. Br6 is totally unaffected and remains in its ground state. Crystals excited at 300 nm produce no detectable emission at room temperature (not shown).

4.3 Cocrystallization

Despite their similarities, there are several considerations in creating well ordered and well mixed cocrystals of Br6A and Br6.[6] As there are several means to crystallize small organic molecules, the cocrystal system is rife with variables. Here we seek to understand the effect of various conditions: Br6A concentration, crystal forming method, and crystal forming conditions to name a few. QY is directly proportional to the quality of mix and cocrystallization. Br6A that is not included in the cocrystal will still absorb but produce no phosphorescence, reducing QY. If we are to optimize QY, we must optimize cocrystallization.

4.3.1 Crystal Comparisons

Earlier it was assumed that emissive crystals are truly cocrystalline given what we know of the DHAE principle and the fact that the emission is polarized. Analyzing further we observe the Br6 crystal structure via XRD. Figure 4.5 shows the pertinent crystal packing of Br6. We can see that there is a very similar motif to that of Br6A. Rings are packed in plane with close contact between halogen substituents. Bromine atoms are distanced from neighboring bromines by only 3.3 Å. The bromine-bromine van der Waals distance would be 3.7 Å, indicating that there is a halogen-halogen

interaction acting to attract bromine atoms.[7,8] This is a non-covalent interaction very similar to the halogen bonding seen in Br6A. Also, if we use the nearest aromatic carbons as a common measurable, we can see that the aromatic rings are spaced laterally in both Br6A and Br6 crystals at exactly 6.9 Å. Thus, in plane parallel to the rings, Br6A and Br6 crystals are strikingly similar, nearly identical aside from the structural differences of each molecule. This is likely due to the very similar volumetric sizes and bonding natures of aldehyde (CHO) and bromine. From this it is clear why Br6 makes such a good candidate for cocrystallization with Br6A.

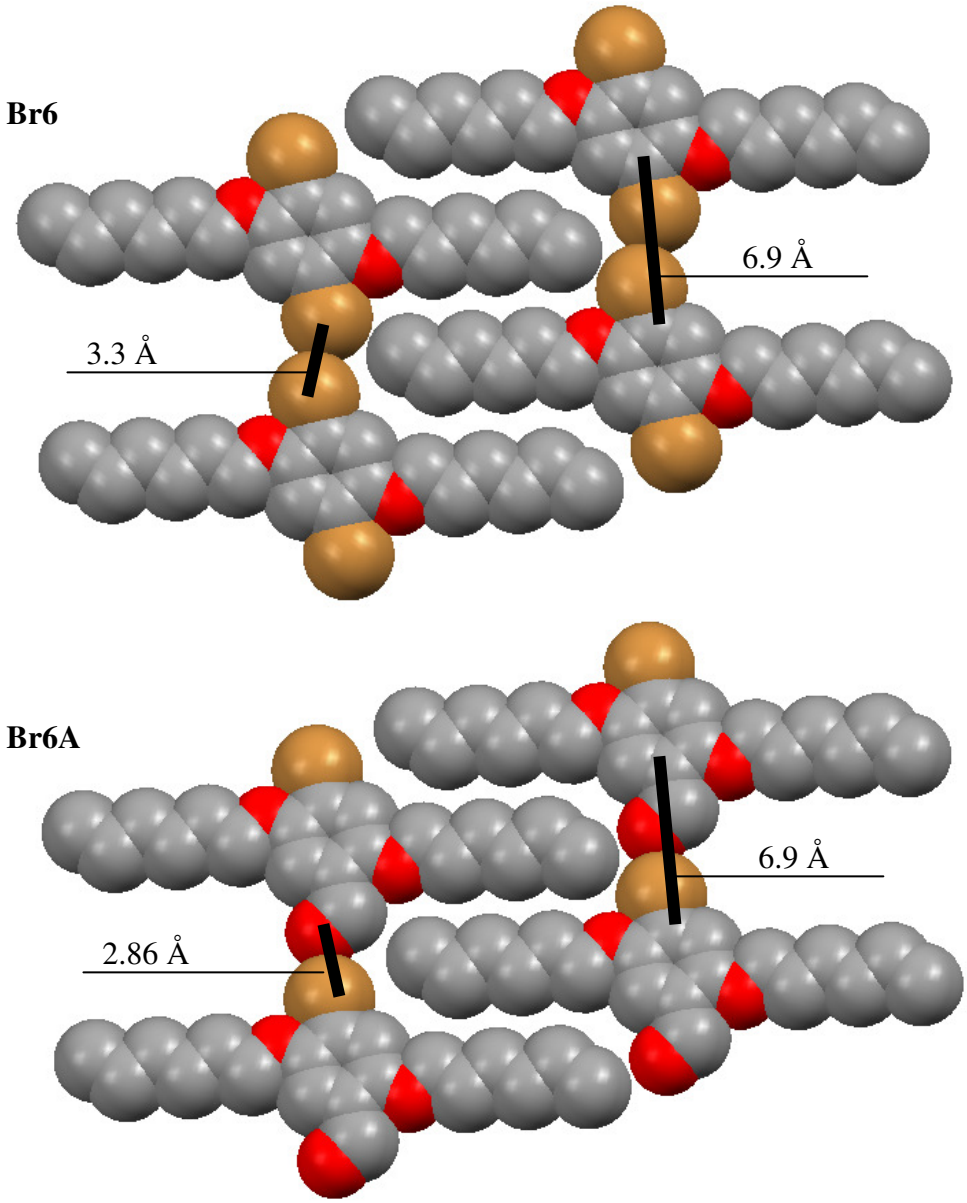

Figure 4.5 Crystal structures of Br6 and Br6A.

Looking now at the other dimension of the crystals we see a more dramatic difference. Figure 4.6 shows a view of Br6 and Br6A crystals highlighting their packing in the direction perpendicular to the rings. Br6A exhibits some degree of π-π stacking with the benzaldehyde groups stacking in a head-to-toe manner. This puts the aromatic chromophores roughly 3.5 – 3.7 Å, which is sufficiently close to generate excimers.[9] Crystals of Br6, on the other hand, exhibit a perfectly staggered crystal with no π-π stacking. The aromatic rings are over 9 Å apart, making excimer formation impossible. This aspect of Br6 makes it all the more attractive as a host material. Not only does it isolate Br6A molecules from one-another, it isolates them from all chromophores (facially) to help deter any possible Br6A-Br6 excimers as well.

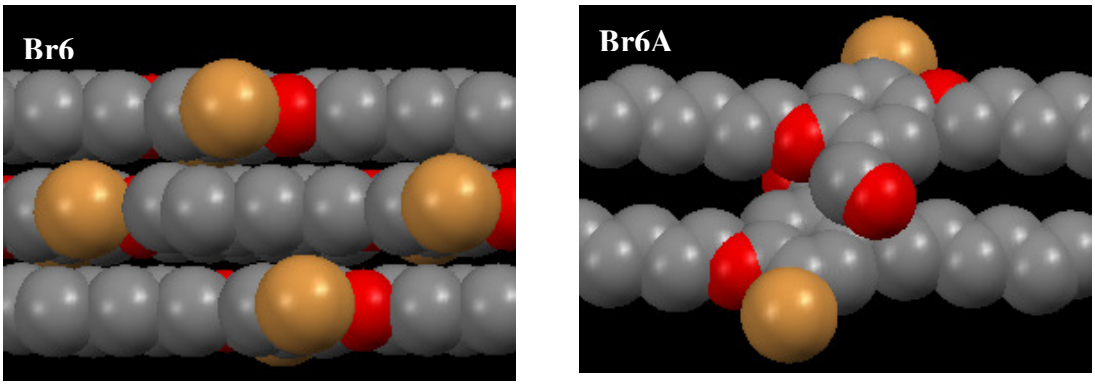

Figure 4.6 Comparing other crystal dimensions of Br6 and Br6A.

Now knowing the specific crystal structures of Br6 and seeing how they compare so favorably to Br6A the assumption of cocrystallization is justified. Cocrystals grown from the slow evaporation of chloroform containing a 10 weight percent mixture (as solids) of Br6A and Br6 were analyzed by XRD and shows a unit cell identical to crystals of pure (non-emissive) Br6. This indicates that the entire sample had taken on the form of the Br6 crystal structure despite the fact that as much as one tenth, by weight, was Br6A.

4.3.2 Cocrystallization Efficiency

Achieving efficient cocrystallization is the greatest challenge to producing high QYs. The amount of Br6A used has a profound effect on the final QY, not only because of possible saturation but also in the dynamics of cocrystallization. Several samples were dropcast for QY measurement from chloroform solutions of various Br6A/Br6 mixes. Figure 4.7 shows the relationship observed from these samples. Notice that an optimum exists at a weight fraction of 0.01 (one weight percent) Br6A. Here cocrystals achieved

Φ_{Ph} = 55.9 ± 3.3 %. The error is rather high because of unavoidable inconsistencies in sample preparation. Furthermore, it is suspected that minor purity differences may have an enormous effect on cocrystal QY. An earlier batch of Br6A and Br6, synthesized two years prior to the material used to generate Figure 4.7, produced Φ_{Ph} = 67.7 ± 2.0 % when mixed at one weight percent. Being that later batches were cleaner as synthetic and purification techniques improved, and after reviewing the data many times, our suspicions lie with the possibility that a minor, unnoticeable impurity may have facilitated better cocrystallization for reasons unknown. So, despite recent irreproducibility of these high numbers, we believe that QYs can reach 68%, and we feel comfortable to report it here.

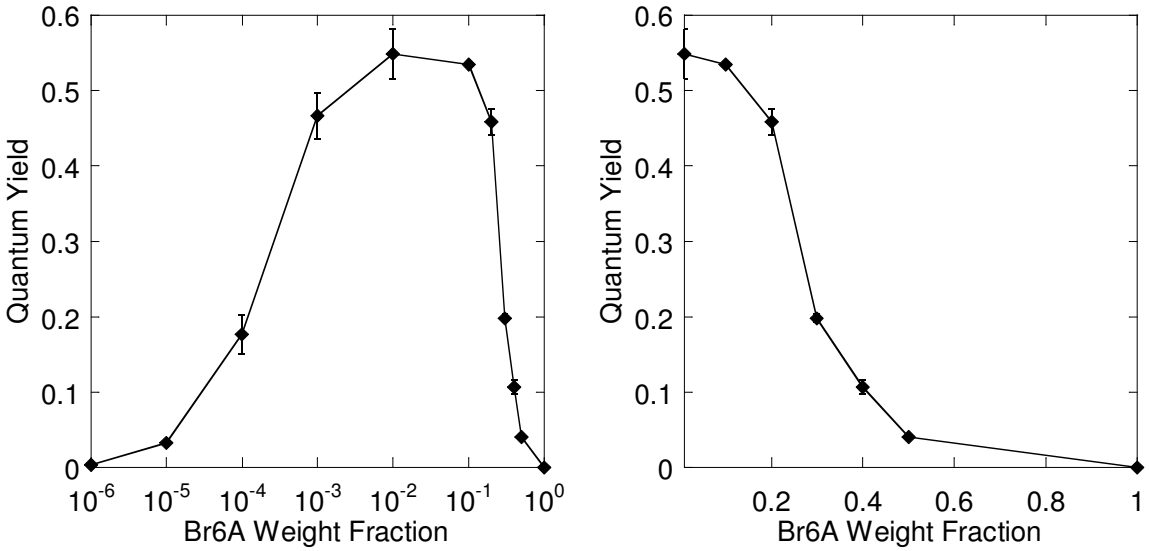

Figure 4.7 QY versus Br6A content in dropcast cocrystals.

At high concentrations of Br6A there is a precipitous drop in QY, which is to be expected. As Br6A become saturated in the crystals Br6A-Br6A contact becomes more likely, which means that excimer formation and possibly triplet-triplet annihilation becomes more probable. We have seen already that even the best crystals of pure Br6A only exhibit QYs of 2.9%, so we should expect a trend toward that as we near a 1.0 weight fraction of Br6A.

Low concentrations of Br6A trend toward zero, which is at first counterintuitive. On a logarithmic scale this trend leads sigmoidally from the apex at 0.01 to zero at 0.000001 weight fractions. This seems strage because at concentrations that are sufficiently low to

prohibit Br6A-Br6A interactions we would not expect QY to drop. Since QY is simply a ratio of photons emitted to photons absorbed and only Br6A is involved photonically (as demonstrated in the previous section) crystals in which Br6A accounts for one-in-one-thousand molecules should not differ from those where it is one-in-ten-thousand? There is little possibility that the emission is based on a Br6A-Br6A interaction, as the chance of a Br6A-Br6A pair at weight fractions of 0.01, 0.001, and 0.0001 are very small (2%, 0.2%, and 0.02% respectively), much smaller than the QYs seen (55.9%, 46.6%, and 17.7%). The drop in QY can only be from complications of cocrystallization.

We hypothesize that at low concentrations of Br6A (in the dropcasting solution) there is little driving force for the Br6A to solidify until nearly all solvent is evaporated. At that point the vast majority of the Br6 has grown into large, high purity crystals reducing the chance of Br6A inclusion. Thus a large portion of the Br6A in these mixes ends up unordered or in homo crystals of Br6A, which exhibit low QY due to efficient excimer formation. The only other suggesting evidence is photos taken of dropcast Br6A/Br6 cocrystals showing that the nucleation sites are noticeably brighter, suggesting better inclusion/cocrystallization during the fast nucleating portion of the crystal formation timeline. Figure 4.8 shows some examples.

To combat these complications other methods of cocrystallization can be used, though attempts to obtain accurate QY measurements from them were unsuccessful. One promising method is solvent-based recrystallization. At elevated temperature, both Br6A and Br6 are quite soluble in alcohols such as methanol. If cooled slowly and carefully, free of vibration and shock, large (millimeter dimensions) and noticeably bright crystals are generated. Also, slow evaporation from good and volatile solvents such as chloroform or hexane produced exceptionally large crystals, some with centimeter scale dimensions. Crystals grown from co-melts of Br6A and Br6 were very small in feature size due to fast crystallization. Their QYs could be reliably measured, but they did not perform as well as dropcast ssamples. Both Br6A and Br6 have fairly low melting temperatures (55-65^{o}C) but do not recrystallize until much cooler (36 and 51^{o}C, respectively), making this form of crystal growth highly unpredictable.

To our extreme chagrin though the large, bright, solution-grown crystals produced very unreliable QY data and after much work we are still unable to explain nor correct it.

As described in Chapter 1, other forms of QY measurement are very unreliable with non-homogenous samples such as crystals, so with the failure of the integrating sphere method, we must leave this study unfinished.

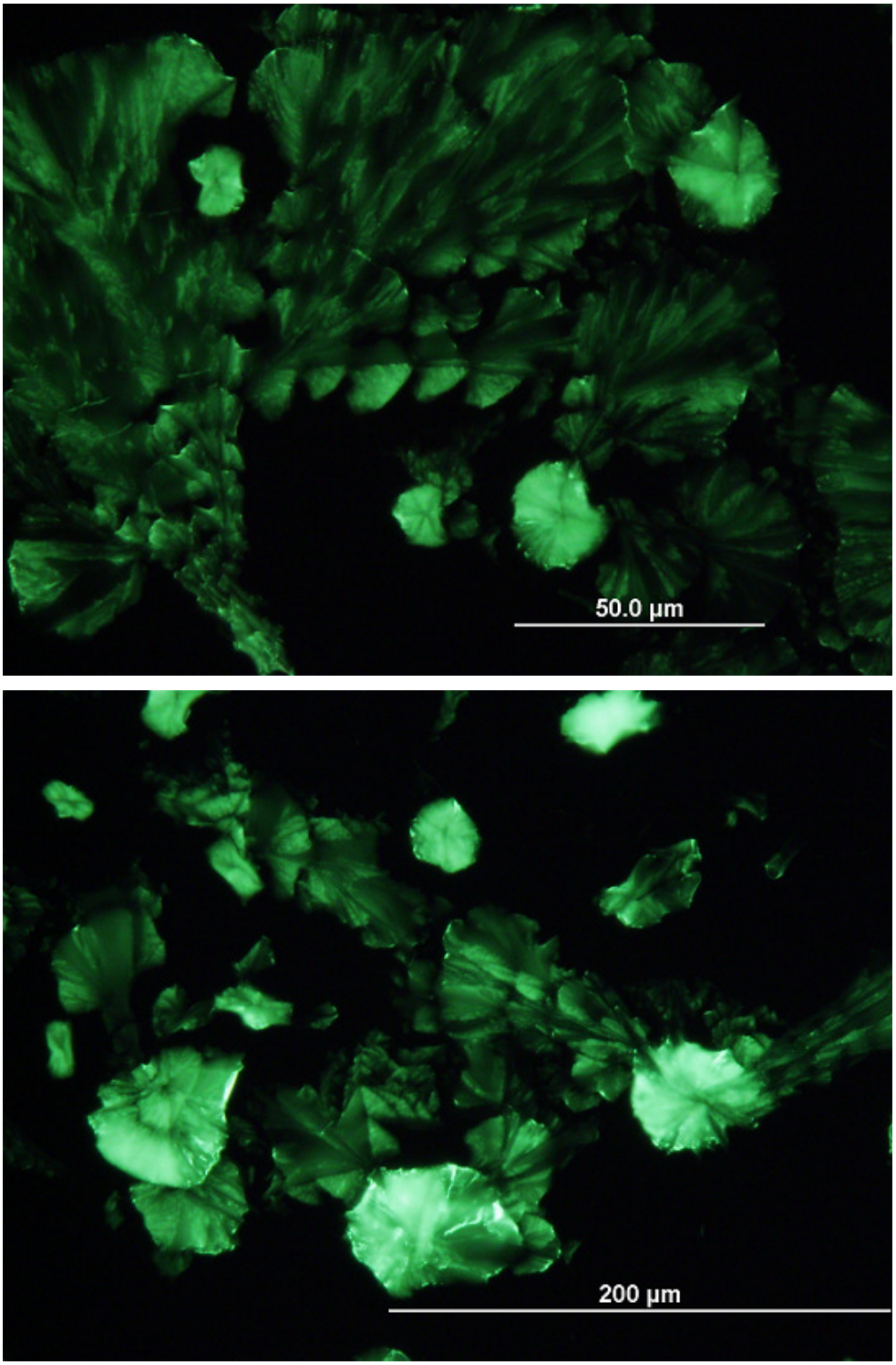

Figure 4.8 Photos of Br6A/Br6 dropcasts magnified to show bright nucleation sites.

4.3.3 Size Constraints

To demonstrate the effect of inclusion in another way, a series of Br6 and Br6A analogs were designed and synthesized. Figure 4.9 shows these compounds, Br4(A) – Br8(A). Each compound has a different length to its alkoxy substiutents from butyl (four carbons) to octyl (eight). A matrix of combinations was dropcast from chloroform solutions each containing 0.01 weight fractions of the aldehyde versus the dibromo compound hosts. Samples were measured for QY as well as dropcast onto frosted glass cubes (to homogenize the highly crystalline emission) and photographed. The QY data and photo are also shown in Figure 4.9.

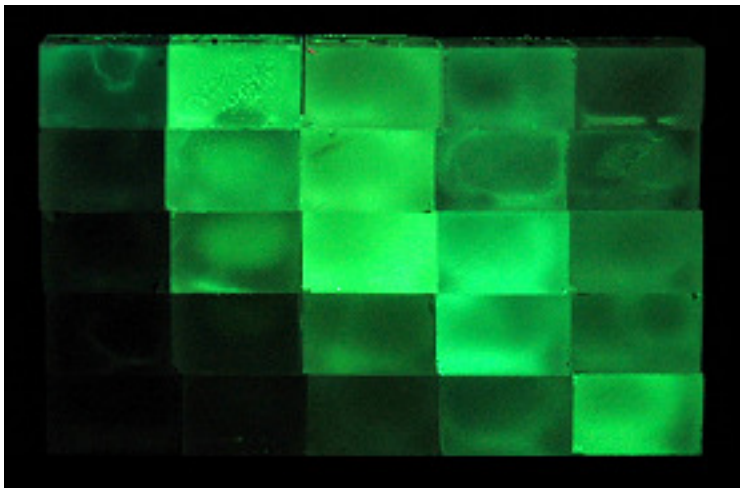

	Br4	Br5	Br6	Br7	Br8
Br4A	27.5%	54.7%	25.8%	21.7%	10.0%
Br5A	14.9%	59.7%	39.8%	33.3%	14.1%
Br6A	4.1%	45.9%	55.6%	50.3%	22.4%
Br7A	1.1%	25.7%	34.0%	61.2%	40.9%
Br8A	1.5%	7.4%	9.9%	44.8%	54.8%

Figure 4.9 Photos of Br4-Br8 and Br4A-Br8A as well as QYs measured from a series of their mixed crystals.

Notable features include the bright line (and high QY numbers) that make a diagonal across the matrix. The brightest samples came from those whose host material was matched to the aldehyde. This, by now, is entirely expected as we have well established

the working principles in the DHAE principle. There is one exception, however, in Br4A. Br4A/Br4 cocrystals exhibit only Φ_{Ph} = 29.5% while Br4A/Br5 cocrystals do better at Φ_{Ph} = 58.6%. This is attributed to an intrinsic lower crystallinity in Br4, which was apparent by a noticeably different crystal structure to the dropcasts.

The second useful feature to this data is the fact that we do observe some phosphorescence, sometimes reasonably bright, from mismatched cocrystals. Though the diagonal is brightest, several combinations achieve QYs of 20 to 40%. A clear trend can be seen that larger hosts accept smaller aldehydes much more readily than smaller hosts accept larger aldehydes. The matrix in the photo is practically dark in its lower left corner, where larger aldehydes are attempting to cocrystallize with smaller hosts. The opposite corner is also dim, but not completely dark. The quantitative data supports this as well. Compare Br6A in Br8, Φ_{Ph} = 24.0%, to Br8A in Br6, Φ_{Ph} = 10.6%.

This study demonstrates a few important things. First, it reinforces the ideas of cocrystallization being based on structural and volumetric similarity between the aldehyde and host. Second, it shows the relatively accepting character of the Br*N* family of compounds. Phosphorescence is reasonably bright from cocrystals that are not ideally matched. Third, it shows that the halogen bond / halogen-halogen interaction motif exhibited by Br6A and Br6 is active in all variants, even weakly emissive Br4. This will be critical as we attempt to design new phosphors. Crystal structures are notoriously difficult to predict from chemical structure. The fact that each variant presented here behaves as desired gives us as starting point as we attempt to design new phosphors.

4.4 Experimental

4.4.1 General Methods

All chemicals used were purchased from Sigma Aldrich and used without further purification. Deuterated solvents for NMR were purchased from Cambridge Isotope Laboratories. Proton NMR was conducted on a Varian Inova 500 using $CDCl_3$ solvent with chemical shifts identified relative to 0.05 v/v% tetramethylsilane standard (0.00 ppm). Anhydrous tetrahydrofuran was generated by refluxing over sodium metal and benzophenone collected only from deep purple solution.

UV Absorption measurements were collected using a Varian Cary 50 Bio spectrometer with a solution samples held in a quartz cuvette. PL emission, excitation, and quantum yield data were collected using a Photon Technologies International (PTI) Quantamaster system equipped with an integrating sphere. Quantum lifetime data was collected using a PTI LaserStrobe. Quantum lifetime calculations were carried out on the FeliX32 software partnered with the PTI equipment. XRD was conducted using a Bruker SMART APEX CCD-based X-ray diffractometer as described below. Optical micrographs were collected using an Olympus BX51 optical microscope equipped with a Mercury lamp UV light source and Olympus DP71 color digital camera.

4.4.2 Synthesis and Characterization

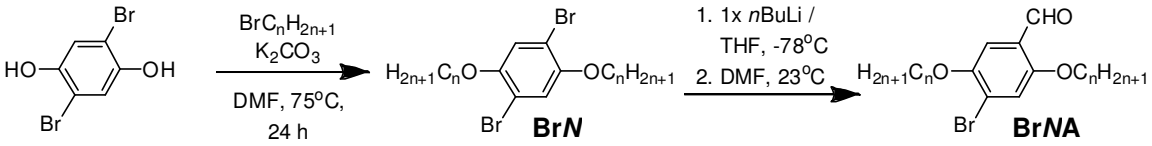

Scheme 4.1 Synthetic Route to Br6A. (n = 4 - 8)

Synthesis of 2,5-dihexyloxy-1,4-dibromobenzene (Br6) and variants Br4-Br8. 2,5-dibromohydroquinone (1 equiv.) and 1-bromo-n-alkane (2.5 equiv.) are loaded into a two-neck round bottomed glass flask and dissolved into dimethylformamide (ca. 1 ml solvent / g dibromohydroquinone). Potassium carbonate (3 equiv.) is added and the flask is sealed under nitrogen, stirred, and heated to 75°C for 24 hours. The reaction is then cooled, filtered, and rotovaped at high temperature to remove all solvents. The product is purified by column chromatography with hexanes. White crystals were collected at yields of 70-80%. For Br6, ^{1}H NMR (500 MHz, $CDCl_3$): δ 7.05 (s 2H), 3.91 (t 4H), 1.76 (m 4H), 1.43 (m 4H), 1.33 (m 8H), 0.91 (m 6H).

Synthesis of 2,5-dihexyloxy-4-bromobenzaldehyde (Br6A) and variants Br4A-Br8A. 2,5-dialkyloxy-1,4-dibromobenzene (Br*N*, 1 equiv.) is loaded into a two-neck round bottomed glass flask and vacuum purged with argon three times. Anhydrous tetrahydrofuran is added by syringe (ca. 25 ml solvent / g Br6) and the vessel is placed into a bath of dry ice and 2-propanol (-78°C). *n*-Butyllithium (1 equiv.) is added dropwise via syringe and the reaction is stirred at -78°C for 1 hour. Anhydrous DMF (4

equiv.) is then added and the reaction is allowed to warm to 23°C over three hours. The reaction is quenched carefully with water and extracted with diethylether. The organic layer is collected and dried over $MgSO_4$ before being filtered and rotovaped to remove solvents. Purification is done by column chromatography with ethylacetate:hexane (1:30) eluent followed by successive recrystallizations from methanol and acetonitrileat 23°C. White crystals were collected at yields of 50-70%. For Br6A, ^{1}H NMR (500 MHz, d_6-DMSO): δ 10.29 (s 1H), 7.53 (s 1H), 7.23 (s 1H), 4.09 (t 2H), 4.01 (t 2h), 1.73 (m 4H), 1.42 (m 4H), 1.30 (m 8H), 0.87 (m 6H).

Crystal Structure of Br6. *The following analysis was conducted and report written by University of Michigan Department of Chemistry staff crystallographer Dr. Jeff W. Kampf as a paid service.* Colorless plates of **Br6** were grown from a methanol solution at 25 deg. C. A crystal of dimensions 0.40 x 0.36 x 0.06 mm was mounted on a standard Bruker SMART 1K CCD-based X-ray diffractometer equipped with a LT-2 low temperature device and normal focus Mo-target X-ray tube (λ = 0.71073 A) operated at 2000 W power (50 kV, 40 mA). The X-ray intensities were measured at 108(2) K; the detector was placed at a distance 4.912 cm from the crystal. A total of 4095 frames were collected with a scan width of 0.5° in ω and phi with an exposure time of 20 s/frame. The integration of the data yielded a total of 15030 reflections to a maximum 2θ value of 56.64° of which 2332 were independent and 2189 were greater than 2σ(I). The final cell constants (Table 4.1) were based on the xyz centroids of 5428 reflections above 10σ(I). Analysis of the data showed negligible decay during data collection; the data were processed with SADABS and corrected for absorption. The structure was solved and refined with the Bruker SHELXTL (version 6.12) software package, using the space group P1bar with Z = 1 for the formula $C_{18}H_{28}O_2Br_2$. All non-hydrogen atoms were refined anisotropically with the hydrogen atoms placed in idealized positions. The molecule lies on an inversion center in the crystal lattice. Full matrix least-squares refinement based on F^2 converged at R1 = 0.0190 and wR2 = 0.0497 [based on I > 2sigma(I)], R1 = 0.0213 and wR2 = 0.0506 for all data.

- Sheldrick, G.M. SADABS, v. 2007/4. Program for Empirical Absorption Correction of Area Detector Data, University of Gottingen: Gottingen, Germany, 2007.

- Sheldrick, G.M. SHELXTL, v. 6.12; Bruker Analytical X-ray, Madison, WI, 2001.
- Sheldrick, G.M. CELL_NOW, Program for Indexing Twins and Other Problem Crystals, University of Gottingen: Gottingen, Germany, 2003.
- Sheldrick, G.M. TWINABS, v. 1.05. Program for Empirical Absorption Correction of Area Detector Data, University of Gottingen: Gottingen, Germany, 2005.
- Saint Plus, v. 7.34, Bruker Analytical X-ray, Madison, WI, 2006.

Table 4.1 Crystallographic Data for Br6A.

Name	**Br6**
Formula	$C_{18}H_{28}Br_2O_2$
Space Group	P-1
Cell Lengths	**a** 6.8032(10) **b** 8.117(3) **c** 9.659(3)
Cell Angles	α 108.27(3) β 106.91(3) γ 96.94(2)
Cell Volume	471.218
Z, Z'	**Z**: 1 **Z'**: 0
R-Factor (%)	1.9

4.4 Conclusions

An additional piece to the DHAE design principle is introduced: cocrystallization. An ideal host material is designed by replacing the aldehyde moiety on the aromatic ketone with a bromine atom. This yields a compound that is both a strong candidate for cocrystallization with the aldehyde (because of their pronounced structural similarity) and one that is also likely to be optically non-interfering because it will have a higher energy excited state. Here we demonstrate this in Br6 as well as Br4-Br8. Bromine is applied specifically because it more closely fits the volumetric size of the CHO moiety than does iodine (or chlorine for that matter, though chlorine would be a poor choice regardless as it is a worse halogen bonding halogen and provides much poorer heavy atom effect). When cocrystallized with this host, halogen bonding is still actively directing the heavy atom effect but intermolecular quenching effects, mostly excimer formation, is prevented to increase QYs to well over Φ_{Ph} = 50% and have been measured as high as 68%. This represents a twenty-five-fold increase in QY as compared to the crystal DHAE phosphors of pure aldehyde (Chapter 3).

Though this addendum to the DHAE principle greatly increases QY to make it competitive with established organometallic phosphors, the necessity of excellent cocrystallization presents a number of variables. The mixing study presented suggests that optimal aldehyde contents are in the range of one-to-ten weight percent. Higher aldehyde concentrations lead to excimer formation while lower concentrations make efficient cocrystallization difficult. Solution-based crystallization methods may produce higher QYs, but limitations to accurate measurement prevented their full study.

We now understand the full DHAE design principle: aromatic aldehydes, halogen bonding, the heavy atom effect, and cocrystallization. For the remainder of this work the ideas and findings presented here and in chapter 3 will define the approach we take to making metal-free organic phosphors. Hosts will be designed as demonstrated here and mixtures will be attempted first at one weight percent aldehyde. To the reader, the DHAE design principle is now fully defined.

4.6 References

[1] R.E. Kellogg *J. Chem. Phys.* **1964**, *41*, 3046.
[2] J.B. Callis, J.M Knowles, and M. Gouterma *J. Phys. Chem.* **1973**, *2*, 154.
[3] M.A. Slifkin and A.O. Al-Chalabi *Chem. Phys. Lett.* **1974**, *29*, 110.
[4] O. Bolton, K. Lee, H.-J. Kim, K.Y. Lin, and J. Kim *Nature submitted.*
[5] Turro, N.J. *Modern Molecular Photochemistry* (University Science Books, Sausalito CA, 1991).
[6] O. Bolton, K. Lee, K.K. Yien, K.Y. Lin, S.M. Wang, M.T. Gray, J.W. Kampf, and J. Kim *manuscript in preparation.*
[7] I. Csoregh, T. Brehmer, P. Bombicz, and E. Weber *Crystal Engineering* **2001**, *4*, 343.
[8] K. Tanaka, D. Fujimoto, and F. Toda *Tetrahedron Lett.* **2000**, *41*, 6095.
[9] S. A. Jenekhe & J. A. Osaheni *Science* **265**, 765, (1994).

Chapter 5

Principles for Color Tuning

In this chapter the DHAE principle is utilized to design and synthesize a series of metal-free organic phosphors to achieve emission in various colors. This demonstrates the broader applicability of the DHAE and does so to create materials that have applicational value as well. First we show how minor modifications to the aldehyde chromophore can be used to fine-tune the phosphorescent emission of the crystals. Secondly we show how more dramatic changes to the chromophore allow for more dramatic changes to the emission color. The strategy is based on electron density. Chromophores with more electron donating character have higher highest occupied molecular orbitals, which raise the ground state energy to narrow the bandgap and red-shift the emission. This works conversely as electron density is reduced, blue-shifting emission. Here we produce colors from blue to orange and explain the details of a failed attempt to achieve red.

5.1 Introduction

In order for the DHAE principle to be a valuable finding, it must be applicable to a wide variety of compounds. Though organometallic compounds are somewhat limited in their design freedom they are still more variable than only the Br*n*A/Br*n* family demonstrated thus far. If we can apply DHAE to other systems, then we should be able to alter the emission these metal-free phosphors emit, as well as other properties, by synthesizing new compounds that have the required aspects for DHAE.

The biggest challenge to designing a DHAE phosphor is trusting that the crystal will exhibit the necessary halogen bonding. Though the halogen bonds in Br6A are decidedly strong and halogen bonding is becoming a very popular synthon in crystal engineering, simple structural design cannot guarantee that halogen bonding will occur in crystals. Because of this we begin our exploration of new DHAE phosphors by making simple changes, only as dramatic as necessary. Minor alterations will hopefully lead to compounds that crystallize in a motif similar to Br6A/Br6.

5.2 Fine Tuning

The first and simplest alteration made was to change the 4 position of Br6A, which is the bromine atom in Br6A. In crystals of pure Br6A this position is critical as it generates the halogen bonding. However, in cocrystal we can change this halogen (on the chromophore) to others or remove it entirely and still achieve halogen bonding in the crystal, because it will come from the host material. This produces an interesting study on the electronic states of the aldehyde chromophore and provides a means to fine tuning.

5.2.1 Halogen Variations

Four additional compounds are synthesized: 2,5-dihexyloxy-4-chlorobenzaldehyde (Cl6A), 1,4-dichloro-2,5-dihexyloxybenzene (Cl6), 2,5-dihexyloxy-4-iodobenzaldehyde (I6A), and 1,4-diiodo-2,5-dihexyloxybenzene (I6).[1] These compounds are direct analogs to Br6A and Br6 with either chlorine or iodine replacing bromine in all instances. Their chemical structures are shown in Figure 5.1. These compounds were designed to probe both the efficacy of halogens other than bromine as well as change the electron density of the benzaldehyde chromophore. Chloroform is smaller and has less electron density to donate to the benzaldehyde ring than does bromine. Iodine has more. We would expect

the ground states to exist at energy levels according to this trend: ClA6 the lowest, I6A the highest, and BrA6 in between them.

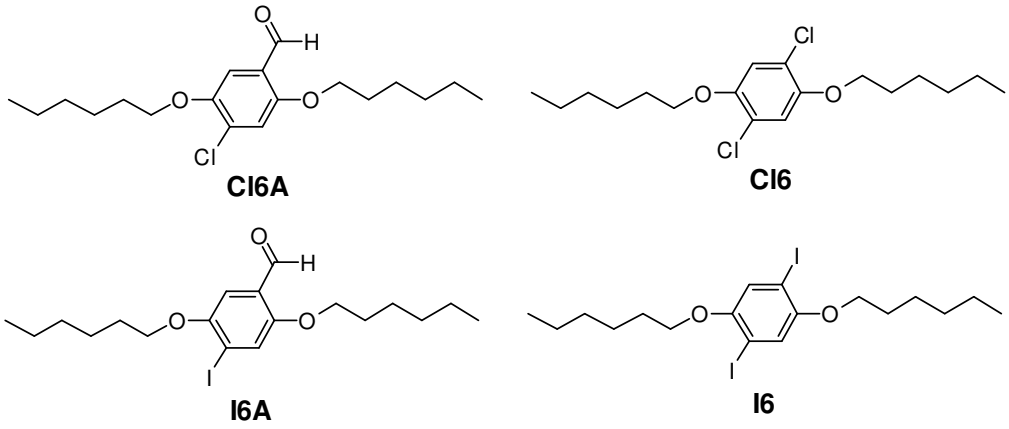

Figure 5.1 Chemical structures of Cl6A, Cl6, I6A, and I6.

Testing the first aspect of this study proved complex. A mixing matrix was designed to test each of Cl6A, Br6A, and I6A in each host Cl6, Br6, and I6. Samples were dropcast onto a glass substrates to form cocrystals from chloroform solutions containing one weight percent aldehyde, the balance host. Samples with Br6 as the host were by far the brightest. Samples with Cl6 as the host exhibited very weak but visible emission. Samples with I6A as the host were non-emissive at first but began to exhibit some emission after several days for reasons unknown. This finding is somewhat surprising, but telling. Contrary to the findings demonstrated by mixed crystals of Br(4-8)A / Br(4-8) from Chapter 4, the large I6A aldehyde produces better phosphorescence when cocrystallized with smaller host Br6 than when with ideally sized host I6. This may be because I6A does not exhibit sufficient halogen bonding, or may crystallize in a different motif altogether. The observation of latent phosphorescence some time after crystal formation is very interesting, but was not explored for lack of time.

PL emission spectra were collected from the brightest samples, whose hosts were Br6. Figure 5.2 shows the emission spectrum of each when excited at 365 nm. Elegantly, each different halogen alters the aldehyde ground state to shift the emission in discrete 5 nm steps. Chlorine donates less electron character than bromine so Cl6A has a ground state below that of Br6A meaning that the gap between T_1, which is unaffected by the halogen because it receives no electron donation in the excited state, and S_0 is greater.

Cl6A has a slightly larger bandgap than Br6A and, thus, bluer emission. Iodine donates more than bromine so I6A has a redder emission than Br6A for the same reasons.

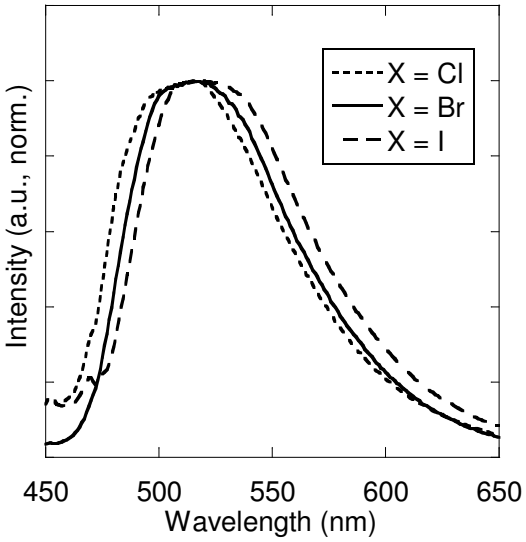

Figure 5.2 PL emission spectra of Cl6A, Br6A, and I6A each cocrystallized with Br6 at roughly one weight percent.

These findings give a means to perform fine color tuning in DHAE phosphors. Clearly the benzaldehyde chromophore is very sensitive to even very subtle changes in electron density. Here we achieve unexpectedly precise fine-tuning since the 5 nm steps are imperceptible on a visible color scale. We also see that, as predicted in Chapter 4, bromine appears to be the best substitute for aldehyde in the host materials because, presumably, of their very similar volumetric sizes.

5.2.2 Halogen-Free Chromophore

Seeing that alterations to the 4 position of Br6A can afford dramatic changes to emission color and knowing that halogen bonding will come primarily from the host molecule, we can make a greater change to the structure, removing the chromophore halogen altogether. By replacing the bromine atom of Br6A with hydrogen we get 2,6-dihexyloxybenzaldehyde (H6A). Figure 5.3 shows the chemical structure of H6A.

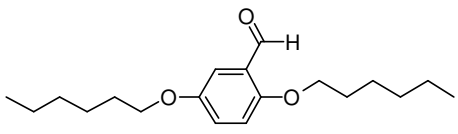

H6A

Figure 5.3 Chemical Structure of H6A.

H6A is cocrystallized with Br6 in samples dropcast from chloroform solutions containing one weight percent H6A to Br6. Figure 5.4 shows the PL emission of one such sample. The phosphorescent peak is clearly shown at λ^{max} = 480 – 495 nm. Hydrogen donates no electron density, significantly less than any halogen, and thus we see a large ca. 30 nm blue-shift from the phosphorescent emission in Br*N*A/Br*N* crystals.

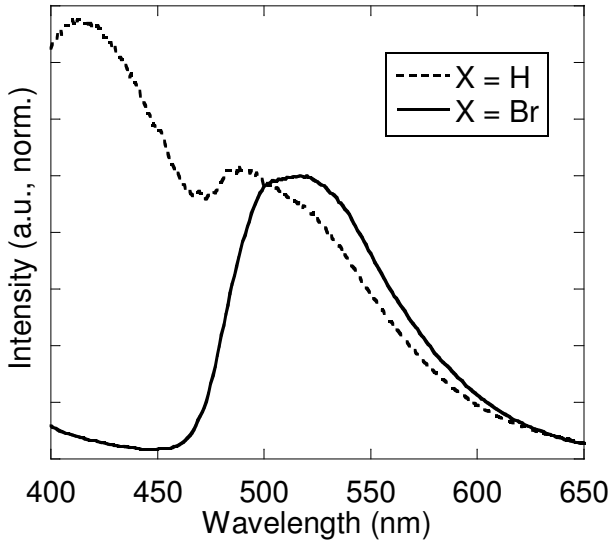

Figure 5.4 PL emission spectrum of H6A/Br6 cocrystal (dotted). Br6A/Br6 cocrystal emission (solid) for reference.

Perhaps the most striking feature of the spectrum in Figure 5.4, however, is the large amount of fluorescence seen as a peak at λ^{max} = 419 nm relative to the phosphorescent peak. This is partially due to poor cocrystallization of H6A and Br6. The two compounds have less structural similarity than others presented thus far because H6A is lacking the large halogen atom. The absence of this halogen also robs H6A of intersystem crossing promoted by the internal heavy atom effect. Figure 5.5 shows PL emission spectra of H6A in solution at 298 K and 77K. Contrary to other aldehydes, such as Br6A (see Figure 3.6), there is no dominant phosphorescent peak from H6A at low temperatures. A third spectrum is made by normalizing the two by their fluorescent peaks and then subtracting the 298K spectrum from the 77K spectrum. The difference shows the moderate phosphorescence intrinsic to H6A at low temperatures.

This study shows us two valuable things. First, making more dramatic changes to electron density of the benzaldehyde alters the emission color more dramatically. The

principles yielding discrete changes from halogen variation are applicable to achieve visibly different colors. Second, we see that removing the halogen from the aldehyde compound is doubly detrimental. It worsens cocrystallization by diverging the structural similarity between phosphor and host and also reduces valuable internal heavy atom effect contributions to triplet generation and phosphorescence. H6A is reported here to demonstrate moderate color tuning, but it is not an optimal approach to do so given the drawbacks.

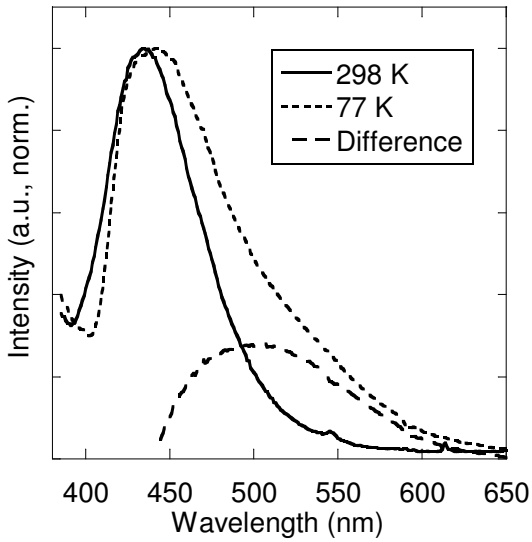

Figure 5.5 PL emission spectra of H6A in solution at 298 and 77K. Both spectra are normalized to their fluorescent peaks. When subtracted (298K from 77K) the difference reveals what phosphorescence is intrinsic to H6A.

5.3 Broad Tuning

With fine-tuning proving successful by altering the electron donation at the 4 position of Br6A, we now move on to altering the 2 and 5 position substitution and extending the chromophore from benzaldehyde to fused ring naphthalenes. The former is achieved while maintaining an alkyl chain structure in an effort to retain the desired crystal packing. In crystals of Br6A and Br6 alkoxy substitutents interdigitate to force tight packing between molecules, which may be assisting to make halogen bonding as strong as is observed for that system. Thus, the strategy was to replace the alkoxy substitutents with other alkyls and ether structures. From lessons learned in Chapter 4 and section 5.2.2, each aldehyde is designed and synthesized along with a dibromo analog that is to

be the host. Cocrystals were grown at a one weight percent concentration aldehyde versus host to achieve highest QY.

5.3.1 Blue

In order to blue shift the phosphorescent emission, chromophore 4-bromo-2,5-diheptylbenzaldehyde (BrAlkyl6A) and host 1,4-diheptyl-2,5-dibromobenzene (BrAlkyl6) are designed as shown in Figure 5.6.[2] BrAlkyl6A has alkyl substitutents in place of Br6A's alkoxy substitutents. The former being alkyls means that they are connected to the central chromophore with carbon atoms and are less electron donating (than the oxygen-connected alkoxys of Br6A). Thus, by the paradigm demonstrated from section 5.2, we expect this compound to have a lower ground state, larger bandgap, and bluer emission than Br6A. BrAlkyl6A and BrAlkyl6 are numbered as six because we view these compounds as variants to Br6A and Br6 with carbon atoms replacing the oxgyens. They have heptyl (seven carbon) chains, but are the same size as Br6A and Br6.

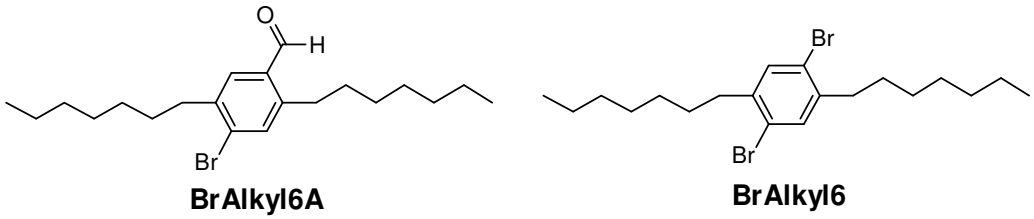

BrAlkyl6A **BrAlkyl6**

Figure 5.6 Chemical structures of BrAlkyl6A and BrAlkyl6.

Samples are dropcast from chloroform solutions containing one weight percent BrAlkyl6A to BrAlkyl6. Figure 5.7 shows the PL emission and excitation spectra observed from one such sample. Large crystals are grown from slow evaporation of the same solution. A photo of one excited under 365 nm light is also shown in Figure 5.7. The spectra contain two striking features reminiscent of the H6A/Br6 crystals in Figure 5.4, blue-shifted emission and significant fluorescence. The shift is dramatic, yielding a phosphorescent emission of λ^{max} = 450-460 nm, which is ideally blue, and an excitation of λ^{max} = 312 nm. These peaks are shifted 50-80 nm relative to Br6A, achieving a dramatic color shift. QYs were measured at 0.5% ± 0.2%, very low, with quantum lifetimes equally low at τ = 100 microseconds (this is here understandable as the two are related by $k_{Ph} = \Phi_{Ph}/\tau_{Ph}$, equation 1.3).

The strong fluorescence peak at λ^{max} = 330, which does not interfere with the observed blue color because it is invisible, is probably the result of poor cocrystallization. The host material, BrAlkyl6, has a very low melting temperature at 35°C and recrystallizes from melts at temperatures very near 24°C. BrAlkyl6A is, at room temperature, a liquid! These factors make generating efficient cocrystals very difficult. Some dropcast samples failed to crystallize even after the solvent had evaporated and several days had past. An attempt to alleviate this was conducted by making samples containing BrAlkyl6A and Br6. The result was very weakly blue emitting crystals that exhibited emission only from their cores (nucleation sites). Figure 5.7 also shows an example of these cocrystals. Despite the visible blue emission, QY were immeasurably low and poorer even than those of BrAlkyl6A/BrAlkyl6. As will be demonstrated in section 5.4.3 also, cocrystallization of compounds with different chain substitutents does not produce bright phosphorescence and should not, in general, be employed as a strategy to enhance phosphor performance.

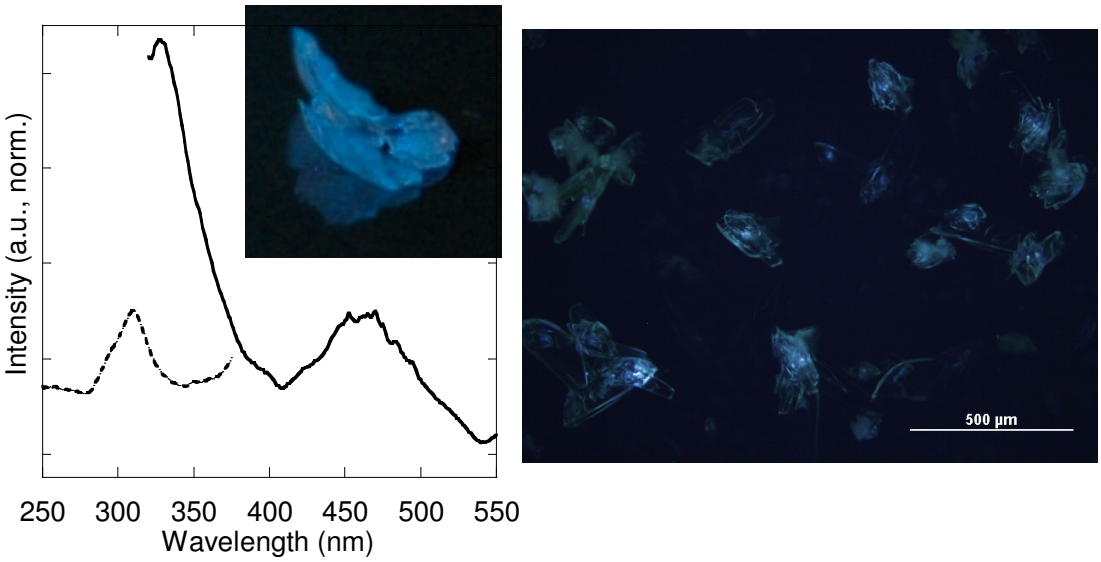

Figure 5.7 Photo, PL emission, and PL excitation spectra of BrAlkyl6A/BrAlkyl6 cocrystals. The BrAlkyl6A/BrAlkyl6 cocrystal is shown as a photo inset on the graph. To the right are shown an optical micrograph of BrAlkyl6A/Br6 cocrystals under 365 nm light. Blue emission is seen from nucleation sites (crystal cores).

Blue metal-free phosphors are of special interest as the blue and near-UV region of the visible spectrum is where many organometallic phosphors being to experience reductions in lifetime and color purity due to intrinsic instabilities. In order to achieve

organometallic phosphorescence at these high energies the metal-ligand bond must be very high energy, i.e. unstable.[3] Thus most color-pure blue organometallic phosphors have very poor QYs, markedly lower than their green and red counterparts.[4] Here the DHAE principle may have a decided advantage as it is not limited in this way. Metal-free phosphors are homogenously organic and more stable at high energies. So despite the low QY from BrAlkyl6A/BrAlkyl6 cocrystals, a working and color pure DHAE blue phosphor holds great promise for further organic phosphor design in the high-energy end of the visible spectrum.

5.3.2 Yellow

In order to enhance electron donation form the chain substitutents at the 2 and 5 positions of Br6A oxygen ethers (alkoxys) were replaces with thiol ethers. 4-bromo-2,5-bis(hexylthio)benzaldehyde (BrS6A) and (2,5-dibromo-1,4-phenylene)bis(hexylsulfane) (BrS6) are designed to this end. Their chemical structures are shown in Figure 5.8. Like those before them, cocrystal samples are made by dropcasting chloroform solutions contains one weight percent BrS6A to BrS6. Larger crystals are grown from the slow evaporation of this solution and are shown in Figure 5.9 along with the measured spectral data for one such dropcast sample and BrS6A in solution.

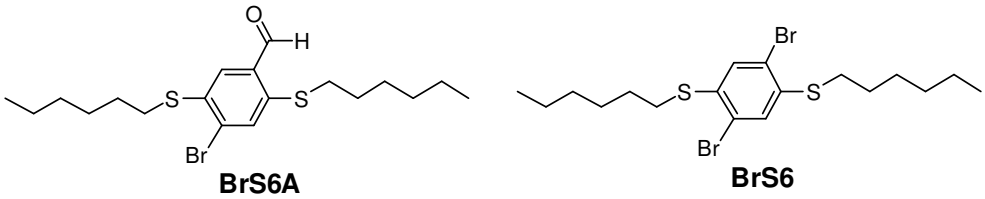

Figure 5.8 Chemical structures of BrS6A and BrS6.

Unlike BrAlkyl6 and like Br6, BrS6 is quite crystalline. The PL emission spectrum shows yellow phosphorescence with a λ^{max} = 540 and no discernable fluorescent peak. This phosphorescence is not spectrally too different from Br6A, which exhibits λ^{max} = 500-530 nm. BrS6A, however, has a spectrum with a sharper cut-on, there is no emission below 500 nm, and a much longer tail making it appear more yellow than the green of Br6A. The excitation spectrum is noticeably more complex. Unlike the neat, blunt peak of Br6A/Br6 cocrystals, BrS6A/BrS6 has a bimodal structure with peaks at λ^{max} = 345

nm and λ^{max} = 419 nm. Reasons for this are uncertain, but both excitation peaks fall within the relatively weak absorption peak of Br6A that spans 320-430 nm with λ^{max} = 370 nm and is presumably the $S_0 \rightarrow S_2$ transition as seen in Br6A. QYs measured for these dropcasts were in the 30-35% range, reasonably high but worse than Br6A/Br6 cocrystals. Quantum lifetimes measured τ = 5.5 milliseconds.

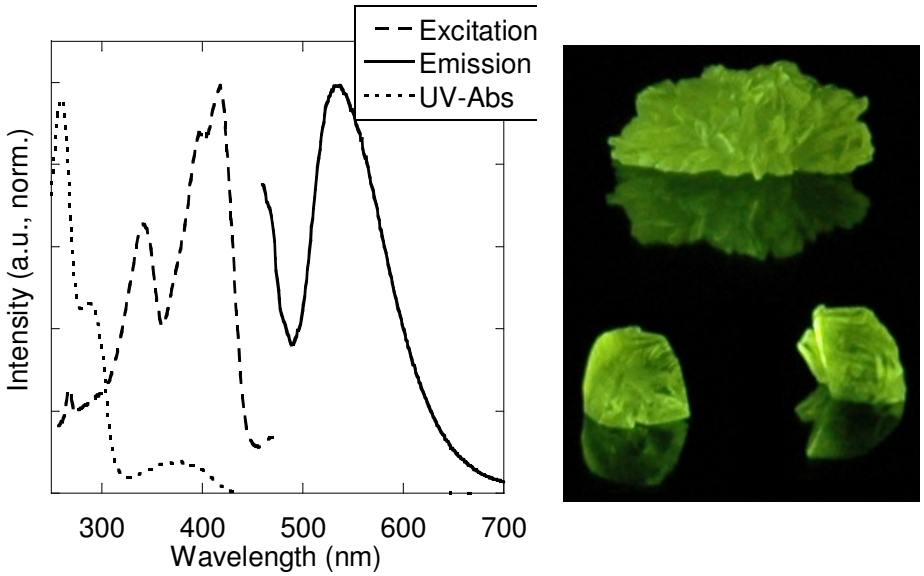

Figure 5.9 Photo, UV-absorption, PL emission, and PL excitation spectra of BrS6A/BrS6 cocrystals.

This study shows us that exchange of oxygen ethers with thiol ethers is both a viable color tuning strategy as well as one that retains high crystallinity as seen from oxygen ethers. QYs are measured somewhat lower, though these cocrystals were not given nearly the attention that the Br6A/Br6 systems were due to both material availability and time constraints. There may be optimizations for this system yet unknown. Attempts to cocrystallize BrS6A and Br6 failed to produce phosphorescent crystals leading us to deduce that cocrystallizing compounds of differing chain substitutents is a failing approach. The high crystallinity and reasonable QY of BrS6A/BrS6 cocrystals stand as very promising evidence that this approach to color tuning and, moreover, the DHAE principle's promise of countless new phosphor designs are very viable.

5.3.3 Orange

In order to push phosphorescent emission further into the red end of the visible spectrum a more dramatic chromophore change is required. Short of attempting selenium

ethers, which would be very difficult given the current state of selenium chemistry[5] and not likely to shift the emission greatly, if the rather subtle green-to-yellow shift of BrS6A is any indication, the core aromatic component must be extended. 5-bromo-2,6-dihexyloxy-1-naphthaldehyde (Np6A) and 1,5-dibromo-2,6-dihexyloxynaphthalene (Np6) are designed to add greater electron density to the central chromophore. Their chemical structures are shown in Figure 5.10.

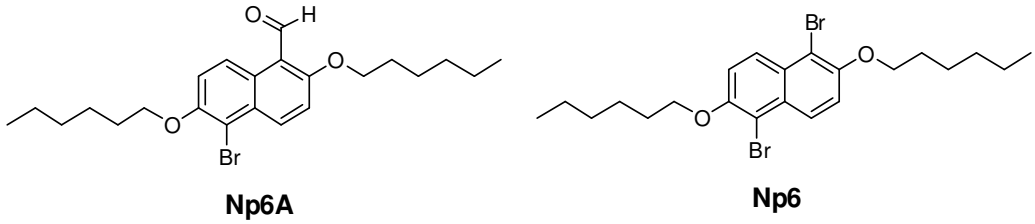

Np6A **Np6**

Figure 5.10 Chemical structures of Np6A and Np6.

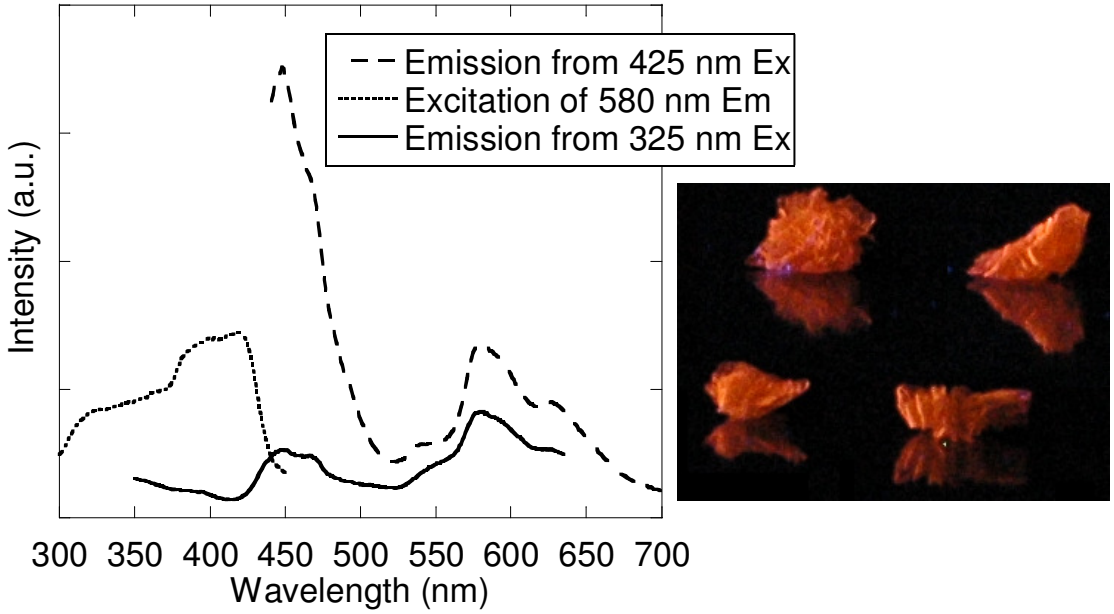

Figure 5.11 Photo, PL emission, and PL excitation spectra of crystals slow grown from 1 wt% solutions of Np6A/Np6.

Dropcast samples of Np6A/Np6 produced very weak phosphorescence, but could be seen to be very weakly orange emitting. Figure 5.11 shows the PL emission spectra from samples slow-grown from chloroform solutions containing one weight percent Np6A in Np6. These samples have a critical difference to those measured thus far: the host material is emissive. Unlike benzene derivatives, Np6 is conjugated and emits

fluorescence at 450 nm, though it is fairly weak emission when in the solid state. This is clearly seen in the emission spectrum of dropcasts excited at λ^{max} = 425 nm. Fluorescence of Np6A is also present, indicating poor cocrystallization, but it is measured only as a shoulder at 470 nm. Phosphorescence is recorded among the peaks at λ^{max} = 540, 580, and 625 nm. Though these samples are only weakly phosphorescent, quantum lifetimes of τ = 640 microseconds were measured, proving the emission to be phosphorescent. (This lifetime was measured from dropcast samples and is likely to be longer in slow-grown crystals.)

Crystals grown from the slow evaporation of the dropcasting solution are larger and much more orange-emitting that dropcasts. Figure 5.11 shows a photo of one of these crystals excited under 365 nm UV light as well as their optical spectra. Here the emission is greatly affected by the choice of excitation wavelength because of the emissive host. Excitation at 380-425 nm yields dominant fluorescence from Np6 and Np6A, but also Np6A phosphorescence. Exciting the sample at 325 nm (note that this, strangely, is significantly bluer than 365 nm excitation of Br6A) emission is predominantly phosphorescent with only small fluorescent Np6A and Np6 peaks.

The Np6A/Np6 system is clearly much more complex than others presented before it, probably due mostly to the optical activity of the host material. In order to understand this compound better we explored the crystal structure of the brightly emissive slow-grown cocrystals. Figure 5.12 shows their crystal structure as determined by XRD. We see that the chromophores are perfectly staggered, that is there is no π-π stacking of the naphthalenes. This precludes excimer formation and may explain why high order single crystals produce such much brighter phosphorescence than those grown from dropcasting. Because the naphthalene unit is so much larger than benzene units in other compounds π-π contact in unordered solids is much more likely. Crystals are more difficult to grow, but once they do excimers are strictly prevented.

The second notable feature of Np6A/Np6 cocrystals is the longer distance between bromine atoms. They contact in a way similar to the Br6 crystals, yet they are spaced at 3.65 Å, which is only slightly closer than their van der Waals distance of 3.7 Å. If we impose an aldehyde moiety in place of one bromine we can calculate a bromine-oxygen contact distance of roughly 2.9 Å, which is excellent for DHAE, but a C=O$^{\cdot\cdot}$Br angle of

147°, which is very steep for a halogen bond. This may also contribute to the low brightness measured from these crystals. QYs measured below one percent even for the brightest crystals.

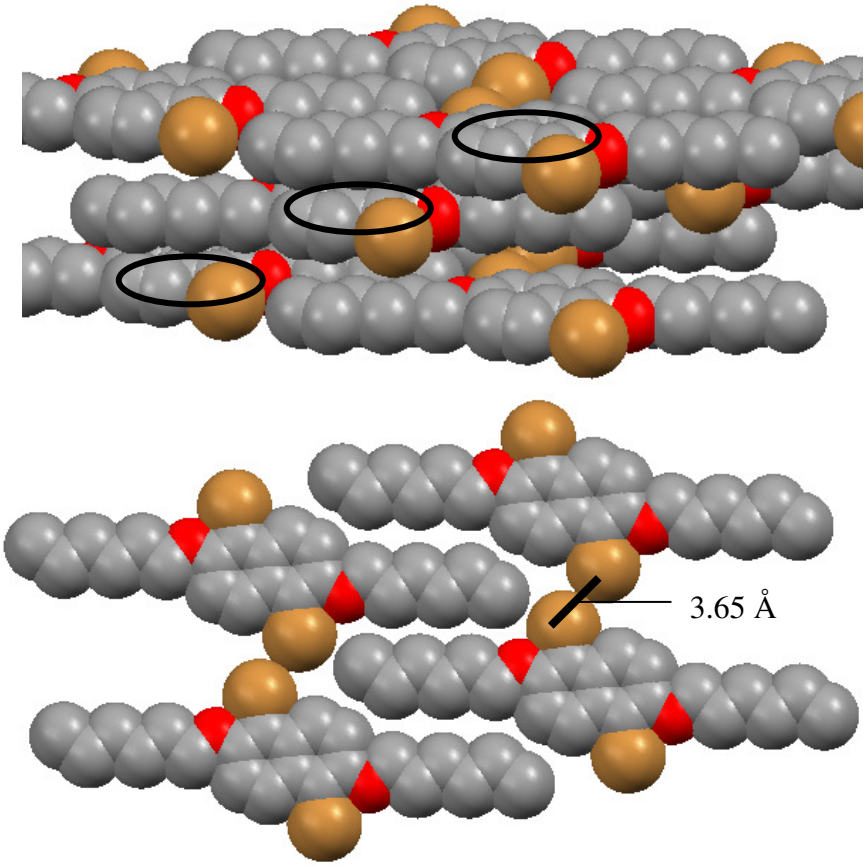

Figure 5.12 Crystal structure of Np6.

NpA6/Np6 crystals are complicated, but for the purposes of color tuning they demonstrate success in dramatic red shifts. Orange phosphorescence that is only visible in the crystalline state and markedly brighter in high quality crystals, both characteristics that we have seen from DHAE phosphors prior, is observed. Though there is much analysis yet to be done on these cocrystals and they are not yet optimized, they lend promise to the design of both redder, and therefore lower energy, chromophores as well as the use of compounds more complex than substituted benzaldehydes.

5.3.4 Red

Trying next to achieve the last visible color, red, the effects of naphthalene and thiol ethers were combined to design 5-bromo-2,6-dihexylthio-1-napthaldehyde (NpS6A) and

1,5-dibromo-2,6-dihexylthionaphthalene (NpS6) whose structures are shown in Figure 5.13. The design targeted achieving the same subtle red shift that BrS6A has relative to Br6A from NpS6A relative to Np6A, turning its orange emission into red. Despite a long and difficult synthesis, this was not successful.

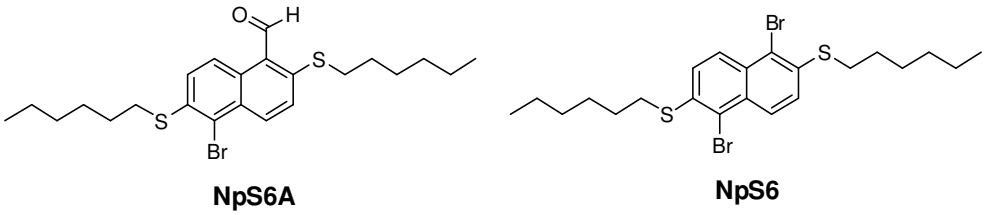

Figure 5.13 Structures of NpS6A and NpS6.

Cocrystals grown from slow evaporation of a chloroform solution containing one weight percent NpS6A in NpS6 were completely non-emissive at room temperatures. XRD reveals the potential reason why. Figure 5.14 shows the crystal structure of NpS6A/NpS6 cocrystals. There is no halogen-halogen interaction at all.

The bromine atoms are spaced far apart at 4.5 Å, which means that the aldehydes are also too distant from bromine atoms to exhibit any halogen bonding nor external heavy atom effect. This demonstrates the greatest challenge to DHAE design; crystal structures are unpredictable. In this case it appears that halogen bonding between the sulfur atoms and bromines may be dominating the crystal matrix though this is apparently not the case in BrS6A/BrS cocrystals.

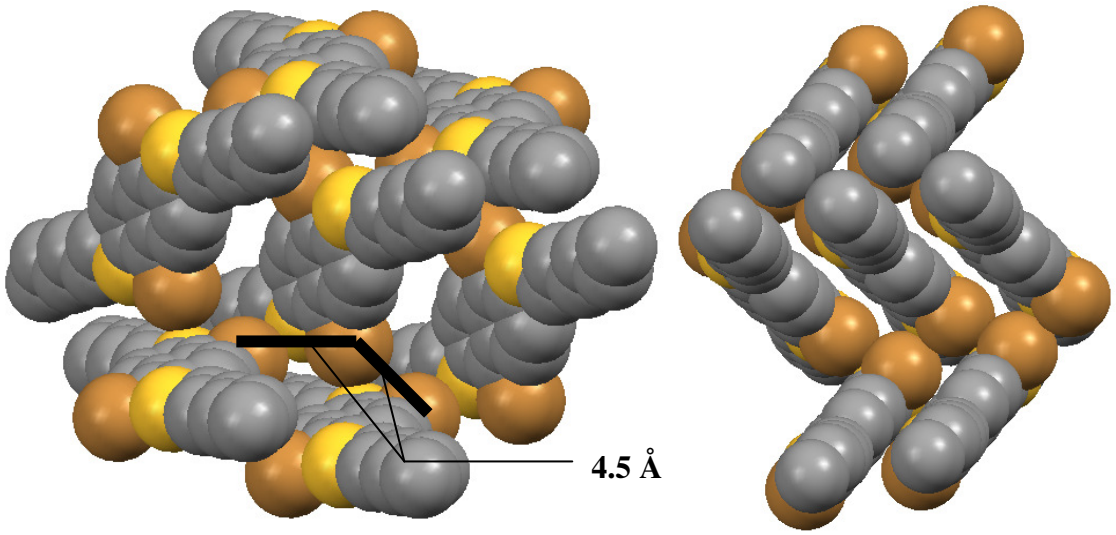

Figure 5.14 Crystal structure of NpS6.

5.4 Experimental

5.4.1 General Methods

All chemicals used were purchased from Sigma Aldrich and used without further purification. Deuterated solvents for NMR were purchased from Cambridge Isotope Laboratories. Proton NMR was conducted on a Varian Inova 500 using $CDCl_3$ solvent with chemical shifts identified relative to 0.05 v/v% tetramethylsilane standard (0.00 ppm). Anhydrous tetrahydrofuran was generated by refluxing over sodium metal and benzophenone collected only from deep purple solution.

UV Absorption measurements were collected using a Varian Cary 50 Bio spectrometer with a solution samples held in a quartz cuvette. PL emission, excitation, and quantum yield data were collected using a Photon Technologies International (PTI) Quantamaster system equipped with an integrating sphere. Quantum lifetime data was collected using a PTI LaserStrobe. Quantum lifetime calculations were carried out on the FeliX32 software partnered with the PTI equipment. XRD was conducted using a Bruker SMART APEX CCD-based X-ray diffractometer as described below. Optical micrographs were collected using an Olympus BX51 optical microscope equipped with a Mercury lamp UV light source and Olympus DP71 color digital camera.

5.4.2 Synthesis and Characterization

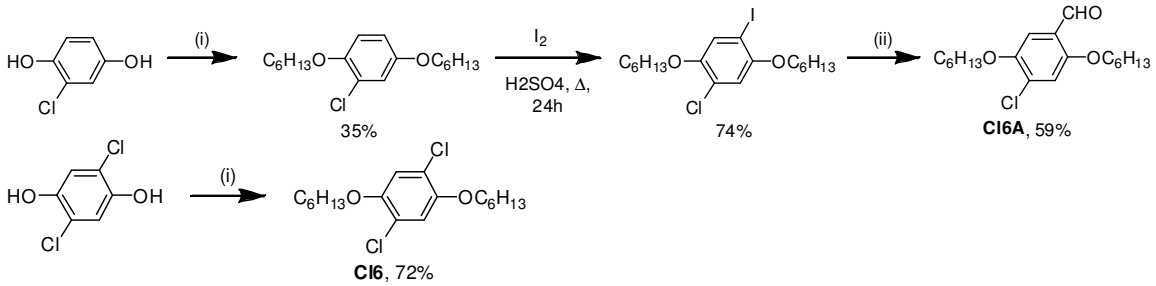

Scheme 5.1 Synthesis route to Cl6A and Cl6. (i) 2.5 equiv. $BrAlkyl_6H_{13}$, 3 equiv. K_2CO_3, DMF, 70-90°C, 24-48h. (ii) *1*. 1 equiv. *n*BuLi, THF, -78°C, 1h, *2*. 4 equiv.

Synthesis of 2-chloro-1,4-dihexyloxybenzne. 2-chlorohydroquinone (1 equiv.) and 1-bromo-n-hexane (2.5 equiv.) is loaded into a two-neck round bottomed glass flask and dissolved into dimethylformamide (ca. 1 ml solvent / g chlorohydroquinone). Potassium carbonate (3 equiv.) is added and the flask is sealed under nitrogen, stirred, and heated to 75°C for 24 hours. The reaction is then cooled, filtered, and rotovaped at high

temperature to remove all solvents. This reaction is referred to as Williamson Ether Synthesis and is referenced in subsequent uses here. The product is purified by column chromatography with hexanes. A colorless oil was collected at a yield of 35%. ^{1}H NMR (500 MHz, $CDCl_3$): δ 6.95 (m 1H), 6.87 (m 1H), 6.74 (m 1H), 3.96 (m 2H), 3.90 (m 2H), 1.85-1.73 (m 4H), 1.47 (m 4H), 1.37 (m 8H), 0.93 (m 6H).

Synthesis of 4-chloro-2,5-dihexyloxy-1-iodobenzne. 2-chloro-1,4-dihexyloxybenzne (1 equiv.) is loaded into a two-neck round bottomed glass flask along with iodine (4 equiv.) and H_2SO_4 (1 ml / g reagent). The reaction is sealed under argon and refluxed for 24 hours. The reaction is poured into ice water. Solids are collected and recrystallized from methanol. White crystals are collected at a yield of 74%. ^{1}H NMR (300 MHz, $CDCl_3$): δ 7.33 (s 1H), 6.85 (s 1H), 3.95 (m 4H), 1.82 (m 4H), 1.52 (m 4H), 1.37 (m 8H), 0.93 (m 6H).

Synthesis of 2-choro-1,4-dihexyloxybenzaldehyde (Cl6A). 1,3-dichloro-2,5-dihexyloxybenzene (Cl6, 1 equiv.) is loaded into a two-neck round bottomed glass flask and vacuum purged with argon three times. Anhydrous tetrahydrofuran is added by syringe (ca. 25 ml solvent / g reagent) and the vessel is placed into a bath of dry ice and 2-propanol (-78^{o}C). *n*-Butyllithium (1 equiv.) is added dropwise via syringe and the reaction is stirred at -78^{o}C for 1 hour. Anhydrous DMF (4 equiv.) is then added and the reaction is allowed to warm to 23^{o}C over three hours. The reaction is quenched carefully with water and extracted with diethylether. The organic layer is collected and dried over $MgSO_4$ before being filtered and rotovaped to remove solvents. This reaction is referenced in subsequent uses here are Lithiation. Purification is done by column chromatography with ethylacetate:hexane (1:30) eluent followed by successive recrystallizations from methanol and acetonitrile at 23^{o}C. White crystals were collected at a yield of 59%. ^{1}H NMR (400 MHz, d_6-DMSO): δ 10.29 (s 1H), 7.40 (s 1H), 7.29 (s 1H), 4.10 (t 2H), 4.03 (t 2h), 1.72 (m 4H), 1.43 (m 4H), 1.30 (m 8H), 0.89 (m 6H).

Synthesis of 1,4-dichrolo-2,5-dihexyloxybenzene (Cl6). 2,3-dichlorohydroquinone is alkylated by Williamson Ether synthesis described above. Products are purified by

column chromatography with hexanes. White crystals were collected at a yield of 72%. ^{1}H NMR (400 MHz, $CDCl_3$): δ 6.92 (s 2H), 3.91 (t 4H), 1.76 (m 4H), 1.42 (m 4H), 1.30 (m 8H), 0.87 (m 6H).

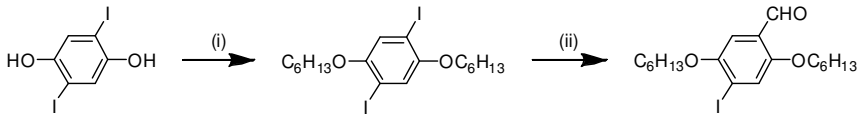

I6, 54% **I6A**, 31%

Scheme 5.2 Synthesis route to I6A and I6. (i) 2.5 equiv. $BrAlkyl_6H_{13}$, 3 equiv. K_2CO_3, DMF, 70-90°C, 24-48h. (ii) *1.* 1 equiv. *n*BuLi, THF, -78°C, 1h, *2.* 4

Synthesis of 1,4-diiodo-2,5-dihexyloxybenzene (I6). 2,5-diiodohydroquinone is reacted with 1-bromohexane via Williamson ether synthesis as described above. Products are purified by column chromatography with hexanes. Large colorless crystals were collected at a yield of 54%. ^{1}H NMR (400 MHz, $CDCl_3$): δ 7.17 (s 2H), 3.92 (t 4H), 1.80 (m 4H), 1.50 (m 4H), 1.34 (m 8H), 0.91 (m 6H).

Synthesis of 2,5-dihexyloxy-4-iodobenzaldehyde (I6A). I6 is reacted to make I6A via Lithiation as described above. Products were purified by column chromatography with ethylacetate:hexane (1:30) eluent followed by successive recrystallizations from methanol at 23°C. White crystals were collected at a yield of 31%. ^{1}H NMR (400 MHz, d_6-DMSO): δ 10.30 (s 1H), 7.68 (s 1H), 7.10 (s 1H), 4.08 (t 2H), 4.00 (t 2h), 1.71 (m 4H), 1.45 (m 4H), 1.32 (m 8H), 0.88 (m 6H).

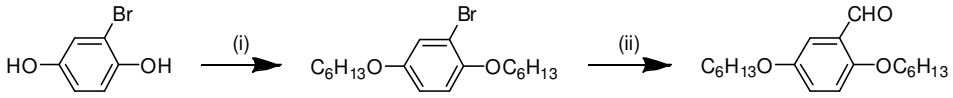

42% **H6A**, 79%

Scheme 5.3 Synthesis route to H6A. (i) 2.5 equiv. $BrAlkyl_6H_{13}$, 3 equiv. K_2CO_3, DMF, 70-90°C, 24-48h. (ii) *1.* 1 equiv. *n*BuLi, THF, -78°C, 1h, *2.* 4 equiv. DMF.

Sythesis of 2-bromo-1,4-dihexyloxybenzene. 2-bromohydroquinone is converted via William Ether Synthesis as described above. Products are purified by column chromatography with hexanes. A colorless oil is collected at a yield of 42%. ^{1}H NMR

(400 MHz, $CDCl_3$): δ 7.08 (s, 1H), 6.79-6.72 (m 2H), 3.91 (t 2H), 3.84 (t 2H), 1.80-1.67 (m 4H), 1.42 (m 4H), 1.30 (m 8H), 0.87 (m 6H).

Synthesis of 1,4-dihexyloxybenzaldehyde (H6A). 2-bromo-1,4-dihexyloxybenzene is reacted to make H6A by Lithiation as described above. Products were purified by column chromatography with ethylacetate:hexane (1:30) eluent followed by successive recrystallizations from methanol at 23°C. White solids were collected at a yield of 79%. ^{1}H NMR (500 MHz, d_6-DMSO): δ 10.51 (s 1H), 7.40 (s 1H), 7.32 (m 2H), 4.22 (t 2H), 4.10 (t 2h), 1.91 (m 2H), 1.85 (m 2H), 1.56 (m 4H), 1.45 (m 8H), 1.05 (m 6H).

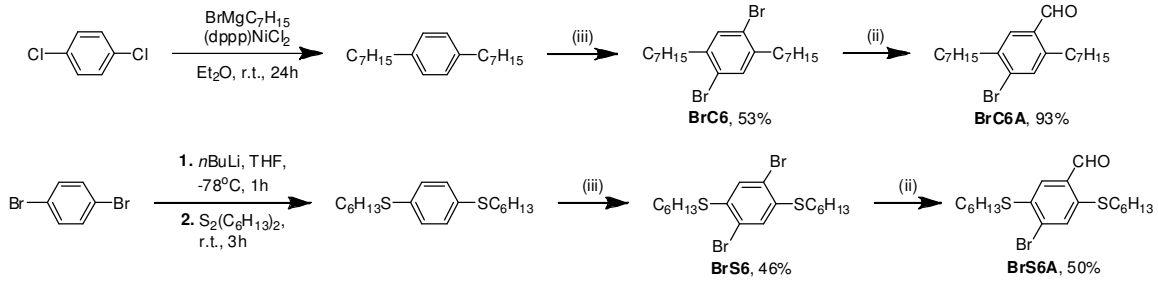

Scheme 5.4. Synthetic route to BrAlkyl6A, BrAlkyl6, BrS6A, and BrS6. (ii) *1.* 1 equiv. *n*BuLi, THF, -78°C, 1h, *2.* 4 equiv. DMF, 23°C, 3h. (iii) 2.05 equiv. Br_2, cat. I_2, CH_2Cl_2, 24h.

Synthesis of 1,4-diheptyl-2,5-dibromobenzene (BrAlkyl6). BrAlkyl6 is synthesized from p-dichlorobenzene following the route reported by Rehahn and coworkers.[6] White crystals are collected at a yield of 53%. ^{1}H NMR (500 MHz, $CDCl_3$): δ 7.71 (s 2H), 2.65 (t 4H), 1.57 (m 4H), 1.37-1.31 (m 16H), 1.08 (m 6H).

Synthesis of 4-bromo-2,5-diheptylbenzaldehyde (BrAlkyl6A). BrAlkyl6 is reacted to make BrAlkyl6A by Lithiation as described above. Products were purified by column chromatography with ethylacetate:hexane (1:30). A colorless oil was collected at a yield of 93%. ^{1}H NMR (500 MHz, $CDCl_3$): δ 10.23 (s 1H), 7.66 (s 1H), 7.47 (s 1H), 2.95 (t 2H), 2.76 (t 2h), 1.61 (m 4H), 1.41-1.28 (m 16H), 0.91 (m 6H).

Synthesis of 1,4-dihexylthiobenzene. 1,4-dibromobenzene is reacted to make 1,4-dihexylthiobenzene by Lithiation as described above with 1,2-dihexyldisulfane added in

place of DMF in step 2. A pungent yellow oil is collected at yields of 20-30%. ^{1}H NMR (400 MHz, $CDCl_3$): δ 7.23 (s 2H), 2.88 (t 4H), 1.61 (m 4H), 1.44 (m 4H), 1.28 (m 8H), 0.86 (m 6H).

Synthesis of 1,4-dihexylthio-2,5-dibromobenzene (BrS6). 1,4-dihexylthiobenzene (1 equiv.) is loaded into a two-neck round bottomed flask along with catalytic iodine (0.05 equiv.) and CCl_2H_2 (10 ml / g reagent.) The vessel is sealed and cooled to 0°C buy an ice bath. Bromine (2.05 equiv.) is added dropwise by syringe and the reaction is stirred at room temperature for 24 hours. The reaction is quenched with 20% potassium hydroxide solution and extracted with CCl_2H_2. Solvents are removed by rotavap and the product is purified by recrystallization from methanol. White crystals are collected at a yield of 46%. ^{1}H NMR (400 MHz, $CDCl_3$): δ 7.36 (s 2H), 2.91 (m 4H), 1.71 (m 4H), 1.46 (m 4H), 1.31 (m 8H), 0.91 (m 6H).

Synthesis of 4-bromo-2,5-dihexylthiobenzaldehyde (BrS6A). BrS6 is reacted to make BrS6A by Lithiation as described above. Products were purified by column chromatography with ethylacetate:hexane (1:30) eluent followed by successive recrystallizations from methanol at 23°C White crystals were collected at a yield of 50%. ^{1}H NMR (500 MHz, $CDCl_3$): δ 10.39 (s 1H), 7.64 (s 1H), 7.61 (s 1H), 2.97 (t 2H), 2.92 (t 2h), 1.71 (m 4H), 1.47 (m 4H), 1.32 (m 8H), 0.89 (m 6H).

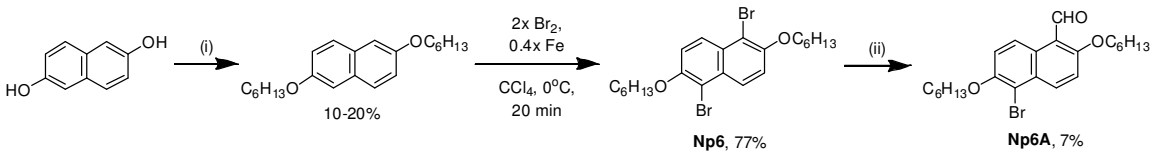

Scheme 5.5 Synthesis route to Np6A and Np6. (i) 2.5 equiv. $BrAlkyl_6H_{13}$, 3 equiv. K_2CO_3, DMF, 70-90°C, 24-48h. (ii) *1.* 1 equiv. *n*BuLi, THF, -78°C, 1h, *2.* 4 equiv. DMF.

Synthesis of 2,6-dihexyloxynaphthalene. 2,6-dihydroxynaphthalene is alkylated by Williamson Ether Synthesis as described above. Products are purified by column chromatography with hexanes. Colorless flake crystals were collected at modest yields

of 10-20%. ^{1}H NMR (500 MHz, $CDCl_3$): δ 7.54 (d 2H), 7.15 (d 2H), 7.11 (s 2H), 4.06 (t 4H), 1.85 (m 4H), 1.53 (m 4H), 1.39 (m 8H), 0.95 (m 6H).

Synthesis of 1,5-dibromo-2,6-dihexyloxynaphthalene (NpS6). 2,6-dihexyloxynaphthalene (1 equiv.) is loaded into a two-neck round bottomed glass flask and is dissolved into carbon tetrachloride (1 ml / g reagent). A solution of powdered iron (0.4 equiv.) in carbon tetrachloride is added to the center of the stirring reaction mix. The reaction is cooled to 0°C by an ice bath and sealed before bromine (2 equiv.) is added dropwise. The reaction is stirred at 0°C for 20-30 minutes then quenched by 10% sodium hydrogen sulfite / water solution. Once all color is gone, the reaction is extracted with CCl_2H_2 and water. This method will be referred to as a Friedel-Crafts reaction in subsequent steps. Organic solvents are removed by rotavap and resulting solids are recrystallized from methanol. White needle crystals were collected at a yield of 77%. ^{1}H NMR (500 MHz, $CDCl_3$): δ 8.21 (d 2H), 7.31 (d 2H), 4.18 (t 4H), 1.88 (m 4H), 1.56 (m 4H), 1.37 (m 8H), 0.93 (m 6H).

Synthesis of 5-bromo-2,6-dihexyloxy-1-naphthaldehyde (Np6A). Np6 is reacted to make Np6A by Lithiation as described above. Products were very carefully purified by column chromatography to isolate them from numerous byproducts with ethylacetate:hexane (1:30) eluent followed by successive recrystallizations from methanol at 23°C. Yellow solids were collected at a yield of 7%. ^{1}H NMR (500 MHz, $CDCl_3$): δ 10.89 (s 1H), 9.30 (d 2H), 9.53 (d 2H), 4.23 (t 2H), 4.17 (t 2H), 1.88 (m 4H), 1.54 (m 4H), 1.37 (m 8H), 0.92 (m 6H).

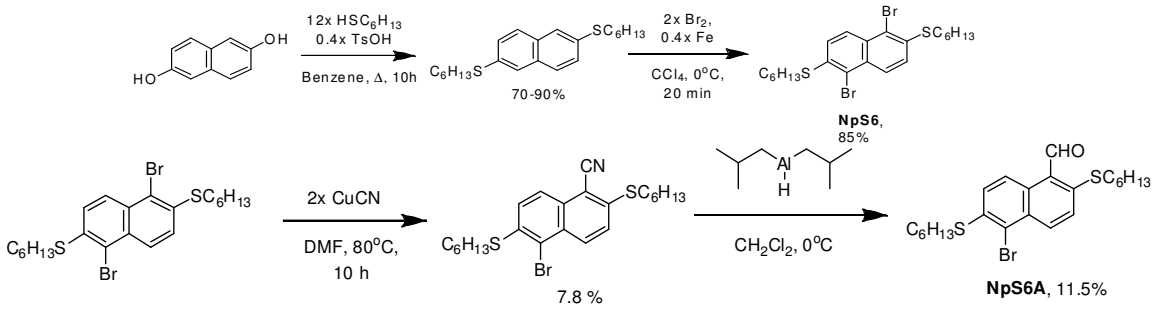

Scheme 5.6 Synthetic route to NpS6 and NpS6A.

Synthesis of 2,6-dihexylthionaphthalene. 2,6-dihydroxynaphthalene (1 equiv.) is loaded into a 2-neck round bottomed glass flask along with hexane-1-thiol (12 equiv.) and Tosyl acid (0.4 equiv.). The solids are dissolved into benzene (5 ml / g reagent) and refluxed for 10-24 hours. The reaction is stopped by removing volatile solvents by rotavap. Products are purified by column chromatography using a diethylether:hexanes (1:10) eluent. A fluffy white powder is collected at yields of 80-90%. ^{1}H NMR (500 MHz, $CDCl_3$): δ 7.66 (s 2H), 7.62 (d 2H), 7.39 (d 2H), 3.00 (t 4H), 1.68 (m 4H), 1.45 (m 4H), 1.28 (m 8H), 0.88 (m 6H).

Synthesis of 1,5-dibromo-2,6-dihexylthionaphthalene (NpS6). 2,6-dihexylthionaphthalene is reacted to make NpS6 by Friedel-Crafts reaction described above. Organic solvents are removed by rotavap and resulting solids are recrystallized from methanol. White powder is collected at a yield of 85%. ^{1}H NMR (500 MHz, $CDCl_3$): δ 8.20 (d 2H), 7.43 (d 2H), 3.05 (t 4H), 1.77 (m 4H), 1.52 (m 4H), 1.33 (m 8H), 0.91 (m 6H).

Synthesis of 5-bromo-2,6-dihexylthio-1-naphthonitrile. NpS6 (1 equiv.) is loaded into a 2-neck round bottom glass flask along with copper cyanide (1 equiv.). The reagents are dissolved in DMF (10 ml / g reagent) and stirred at 80^{o}C for 24 hours. The reaction is quenched when solvents are removed by high temperature rotavap. Products are isolated by careful column chromatography in ethylacetate:hexanes (1:2) eluent. Yellow solids are collected at a yield of only 7.8%. ^{1}H NMR (500 MHz, $CDCl_3$): δ 8.34 (d 1H), 8.07 (d 1H), 9.53 (d, 2H), 4.23 (t, 2H), 4.17 (t 2H), 1.88 (m 4H), 1.54 (m 4H), 1.37 (m 8H), 0.92 (m 6H).

Synthesis of 5-bromo-2,6-dihexylthio-1-naphthaldehyde (NpS6A). 5-bromo-2,6-dihexylthio-1-naphthonitrile (1 equiv.) is loaded into a two-neck round bottom glass flask and dissolved into CCl_2H_2 (10 ml / g reagent) before being cooled to 0^{o}C by an ice bath. Diisobutylaluminum hydride (1.1 equiv.) is added and the reaction is stirred for one hour at 0^{o}C. The reaction is quenched with water, extracted, and dried by rotavap. Products

are carefully isolated by column chromatography using a ethylacetate:hexanes (1:10) eluent. A yellow solid is collected at a yield of 11.5%. ^{1}H NMR (500 MHz, $CDCl_3$): δ 10.96 (s 1H), 8.94 (d 1H), 8.43 (d 1H), 7.66 (d 1H), 7.48 (d 1H), 3.06 (p 2H), 1.73 (m 4H), 1.50 (m 4H), 1.32 (m 8H), 0.92 (m 6H).

Crystal Strcuture of Np6A/Np6 Cocrystals. *The following analysis was conducted and report written by University of Michigan Department of Chemistry staff crystallographer Dr. Jeff W. Kampf as a paid service.* Colorless plates of **NpA6** were grown from a dichloromethane solution at 23 deg. C. A crystal of dimensions 0.28 x 0.24 x 0.04 mm was mounted on a Bruker SMART APEX CCD-based X-ray diffractometer equipped with a low temperature device and fine focus Mo-target X-ray tube (λ = 0.71073 A) operated at 1500 W power (50 kV, 30 mA). The X-ray intensities were measured at 85(1) K; the detector was placed at a distance 5.055 cm from the crystal. A total of 5190 frames were collected with a scan width of 0.5° in ω and 0.45° in phi with an exposure time of 20 s/frame. The integration of the data yielded a total of 23451 reflections to a maximum 2θ value of 56.68° of which 2565 were independent and 2417 were greater than 2σ(I). The final cell constants (Table 5.1) were based on the xyz centroids of 9995 reflections above 10σ(I). Analysis of the data showed negligible decay during data collection; the data were processed with SADABS and corrected for absorption. The structure was solved and refined with the Bruker SHELXTL software package, using the space group P1bar with Z = 1 for the formula $C_{22}H_{30}O_2Br_2$•. All non-hydrogen atoms were refined anisotropically with the hydrogen atoms placed in idealized positions. The cluster lies on an inversion center of the crystal lattice. Full matrix least-squares refinement based on F^2 converged at R1 = 0.0292 and wR2 = 0.0794 [based on I > 2sigma(I)], R1 = 0.0314 and wR2 = 0.0816 for all data.

- Sheldrick, G.M. SHELXTL, v. 2008/4; Bruker Analytical X-ray, Madison, WI, 2008.
- Sheldrick, G.M. SADABS, v. 2008/1. Program for Empirical Absorption Correction of Area Detector Data, University of Gottingen: Gottingen, Germany, 2008.
- Saint Plus, v. 7.60A, Bruker Analytical X-ray, Madison, WI, 2009.

Table 5.1 Crystallographic Data for Np6.

Name	**Np6**
Formula	$C_{22}H_{30}Br_2O_2$
Space Group	P-1
Cell Lengths	**a** 7.6936(11) **b** 8.5442(12) **c** 9.4750(14)
Cell Angles	**α** 108.286(2) **β** 110.770(2) **γ** 102.065(2)
Cell Volume	515.721
Z, Z'	Z: 1 Z': 0
R-Factor (%)	2.92

Table 5.2 Crystallographic Data for NpS6.

Name	**Np6**
Formula	$C_{22}H_{30}Br_2S_2$
Space Group	P 2_1/c
Cell Lengths	**a** 10.8625(6) **b** 14.0253(8) **c** 8.0484(4)
Cell Angles	**α** 90 **β** 110.843(2) **γ** 90
Cell Volume	1145.93

5.5 Conclusions

Here we have taken the DHAE principle and used it to synthesize organic phosphors of varying color by controlling the electron density of the chromophore. By altering the halogen on the aldehyde, fine tuning can be achieved in discrete 5 nm steps. Chlorinated chromophores emit 5 mn bluer than brominated chromophore and iodinated chromophores emit 5 nm redder. Brominated chromophores, though, exhibit the best cocrystallization because they more closely match the volumetric size and shape of their analogous aldehyde. Thus bromine combinations yield the brightest phosphors. The aldehyde can be removed altogether to achieve a broad blue shift of nearly 30 nm, but this comes at the price of inefficient cocrystallization and weakened intrinsic intersystem crossing of the chromophore. Inclusion of halogen-free aldehydes into heavily halogenated hosts is inefficient and, without the benefit of the internal heavy atom effect, fluorescence may dominate singlet decay.

More dramatic changes to the chromophore afford more dramatic changes to the emission color. Alkyl variants donate less electron density and thus exhibit larger bandgaps than the green-emitting Br*N*A/Br*N* family of phosphors. BrAlkyl6A/BrAlkyl6

cocrystals produce very color pure blue phosphorescence, though they exhibit low QYs due in part to their poor crystallinity and low melting temperature. Thiol ethers used in replacement of oxygen ethers red-shift the emission of Br6A slightly while maintaining good cocrystallinity and moderate QYs. BrS6A/BrS6 cocrystals emit yellow phosphorescence, similar spectrally, but not visibly, to Br6A. Finally, Naphthyl variants have even more electron density at their core chromophore, which narrows the bandgap to the point where Np6A/Np6 cocrystals emit visibly orange phosphorescence. Each of these several examples supports the color tuning approach of altering electron density at the aromatic ketone chromophore and can be used as a guide to developing future DHAE phosphors. This work also supports the DHAE design principle's promise to be useful for the design of a broad family of metal-free organic phosphor.

This work does, however, highlight some of the challenges to DHAE phosphor design. First, the blue-emitting BrAlkyl6A/BrAlkyl6 system produces nice color, but very poor QY because its structure has low crystallinity. As the design trends toward certain structures these complications may limit the practical usefulness of blue and near-UV phosphors. Second, cross-mixing of dramatically different chromophores (BrAlkyl6A / Br6 or BrS6A / Br6) failed to produce efficient emission (or any at all in the later case), which highlights that the cocrystallization can be quite difficult to achieve unless the host and aldehyde are ideally sized. Lastly, the weak emission of orange-emitting Np6A/Np6 and the failed attempt to observe red emission from NpS6A/NpS6 show how difficult it is to predict the crystal structure of a given compound. We can design chromophores with the intention that they exhibit strong halogen bonding, but we cannot control this absolutely. Until the efficacy of crystal engineering improves, researchers may be left to trial-and-error when designing new DHAE phosphors.

5.6 References

[1] O. Bolton, K. Lee, K.K. Yien, K.Y. Lin, S.M. Wang, M.T. Gray, J.W. Kampf, and J. Kim *manuscript in preparation.*

[2] O. Bolton, K. Lee, H.-J. Kim, K.Y. Lin, and J. Kim *Nature submitted.*

[3] D. Gebeyehu, K. Walzer, G. He, M. Pfeiffer, K. Leo, J. Brandt, A. Gerhard, P. Stößel, H. Vestweber, *Synth. Met.* **2005**, *148*, 205.

[4] Y. Kawamura, S. Yanagida, and S.R. Forrest *J. Appl. Phys.* **2002**, *92*, 87.

[5] D.M. Freudendahl, S.A. Shahzad, and T. Wirth *Eur. J. of Org. Chem.* **2009**, *11*, 1649.

[6] M. Rehahn, A.-D. Schlüter, W.J. Feast *Synthesis* **2009**, *5*, 386.

Chapter 6

Delayed Phosphorescence

With the DHAE principle now clearly defined and its capabilities demonstrated, this chapter delves into an unexpected discovery from crystals of Br6A, delayed phosphorescence. Here, the phenomenon of delayed emission is described by first explaining the well-established concept of delayed fluorescence. Excimers are then explained in greater detail as they are a critical part of this chapter's finding. Delayed phosphorescence, analogous to delayed fluorescence, is observed and reported here for the first time. As evidenced here, this emission pathway accounts for the phosphorescent emission observed from pure Br6A crystals. The excited state travels through an excimer state before emitting as pure triplets. This holds promise for optical device applications where excimers are generally considered a quenching mechanism. The possibility of delayed phosphorescence demonstrates that emission can be reclaimed from these otherwise detrimental states.

6.1 Introduction

The findings described in this chapter are ancillary to the DHAE design principle, though understanding them draws heavily from the same set of excited state analyses. First we describe two concepts that have not been explained in great detail thus far, delayed fluorescence and excimers. The combination of these two effects, in the discovery described here, yields a pathway to enhance phosphorescent QY for certain systems and optical devices. We present thermally activated delayed phosphorescence.

(Literature has used the term "delayed phosphorescence" to describe a variety of time-dependent phosphorescent observations. The finding reported here is not to be confused with "microwave-induced delayed phosphorescence"[1] or "heat pulse-induced delayed phosphorescence,"[2] which refer to extremely low temperature systems where the three different triplet states T_x, T_y, and T_z can be distinguished dynamically. A report by Lamola comes closest to that reported here, but refers to an inter-species triplet-triplet crossing.[3])

6.1.1 Delayed Fluorescence

When a singlet flips by intersystem crossing into a triplet state there will occasionally occur a process by which the triplet then flips back into the singlet. Triplets, of course, are always of lower energy than their corresponding singlets. With one famous exception,[4] $T_n < S_n$. Thus for a T_1 triplet to convert back to an S_1 singlet, there must be some outside energy assisting the transition. If that singlet then emits the result is emission that is spectrally fluorescent but with the long lifetime of a triplet state. This is the phenomenon of *delayed fluorescence*.[5,6]

There are two main energetic sources that facilitate this up-conversion. One possibility is the interaction of two excited states combining to raise one while relaxing the other. The states are often triplets because they live long enough for this slow intermolecular reaction to occur. In a formula notation: $T_1 + T'_1 \rightarrow S_1 + S'_0$. This is *triplet-triplet annihilation*. This method is intermolecular and is therefore correlated to the square of the chromophore concentration and the square of the exciting emission intensity.[7] Another method of $T_1 \rightarrow S_1$ can occur if the vibrational modes of T_1 overlap with those of S_1. This transition can be facilitated by heat energy. In formula: T_1 + *heat*

$\rightarrow S_1$. This method is, of course, highly dependent on temperature and can be greatly reduced at lower temperatures.

The three critical identifying aspects of delayed fluorescence are 1. emission that is spectrally identical to regular, "prompt" fluorescence, 2. lifetimes that are in the triplet regime, microseconds or longer, and 3. emission intensity that is inversely proportional to temperature. The method of internal up-conversion can be probed by temperature and sample concentration.

6.1.2 Excimers

The concept of delayed fluorescence is sometimes referred to more generally as delayed *emission*, implying that it is theoretically possible that it may occur for phosphorescence as well. This could be the possibility of a triplet up-converting to a singlet before intersystem crossing *back* to a triplet before emitting, but reports of such an observation are absent. The other possibility would be triplets being up-converted from a lower energy state. Almost by definition, T_1 is the lowest excited state of any molecule so a lower energy state could only be an intermolecular state, such as a triplet excimer or exciplex.

Excimers are a concept that has been described only in brief terms here thus far. They, simply, are a combination of an excited state molecule interacting with a ground state molecule to stabilize the overall system. If these molecules are the same species their grouping forms an excimer, otherwise, if they are two different species, they are referred to as an *exciplex*. These typically lead to non-emissive internal conversion through vibrational dissipation. Excimers can occur from either singlet[8,9,10,11] or triplet excited states.[12]

Excimers form because both molecules (excited and ground state) are usually very easily polarized. Once one is exited it becomes highly polarized and imparts opposite polarity in the potential excimer partner nearby. The two align with head-to-toe poles to stabilize the overall energy. Because of this stabilization, excimers typically have longer lifetimes than the monomer excited state, but their lowered energy and the additional vibrational modes associated with two species often lead to non-emissive relaxation.[13,14] Because of this interaction necessary in this relationship, excimer formation requires that

the molecules be aligned ideally for this head-to-toe interaction, or have the freedom to become so. Studies with aromatic systems have demonstrated that the distance between aromatic species necessary for excimer formation is 3-4 Å.[15]

As stated, excimers typically contain very competitive internal conversion mechanisms and, with unusual exception, are non-emissive.[16,17] As such they are seen as a detrimental phenomenon in optical materials for devices, often referred to along with other emission-restricting phenomena as "self-quenching". Because of this they are avoided in material and device design. To this end, chromophores are strictly diluted to prevent any intermolecular interaction of this nature. The prevention of excimers is universally accepted as the proper approach in emissive applications. Our results show the first report of delayed phosphoresce from triplet states repopulated from triplet excimers.[18] This demonstrates the possibility to reclaim emission from these complexes heretofore believed to be unavoidably quenching.

6.2 Results and Discussion

From chapter 3 we see that crystals of pure Br6A emit green phosphorescence at λ^{max} = 500-530 nm. Upon further investigation we can conclude that this emission is actually delayed phosphoresce. Dynamic measurements as well as spectral observations at high and low temperatures support the hypothesis that this emission comes from T_1 states in Br6A that have been thermally repopulated from a lower energy triplet excimer.

Phosphorescent emission from Br6A crystals is spectrally identical to emission seen from the Br6A/Br6 cocrystals from Chapter 4. Figure 6.1 shows the PL emission and excitation spectra of each of these samples. The emissions agree very well (with the exception of the fluorescent emission from the unordered portion of Br6A, which is discussed in Chapter 3). The excitation spectra, on the other hand, are suspiciously divergent. Cocrystals exhibit a very narrow excitation window centered at λ^{max} = 365 nm while pure Br6A crystals exhibit a much broader excitation with two peaks, one at λ^{max} = 320 nm and another with twice the intensity at 390 nm. Taken alone this indicates only that the excitation pathways are not the same in both materials, though the emission from each comes from the same state, T_1 of Br6A. The dramatic differences in the shape of the excitation spectra indicate that the excited state pathways to emission are likely very

different. For example, exposure of the cocrystals to 325 nm light produces no emission, yet pure Br6A crystals exposed to the same light produce significant phosphorescence. Paired with the following evidence, this clearly indicates that the excited states in Br6A crystals travel through an excimer state before finally emitting as triplets.

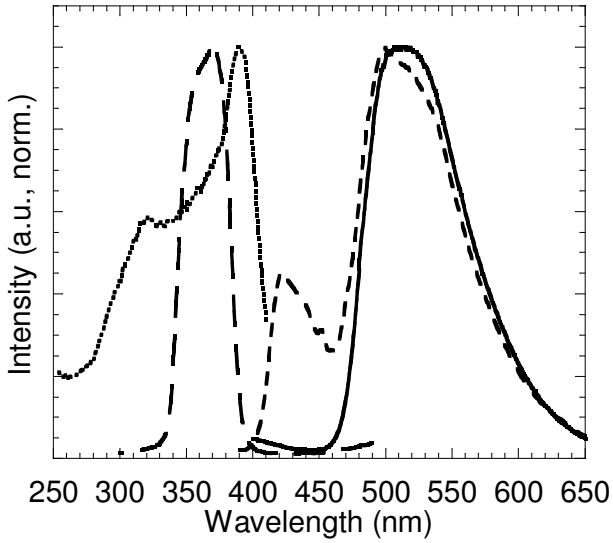

Figre 6.1 PL emission and excitation spectra of Br6A and Br6A/Br6 crystals. Br6A excitation (dotted), Br6A emission (small dash), Br6A/Br6 excitation (long dash), Br6A/Br6 emission (solid).

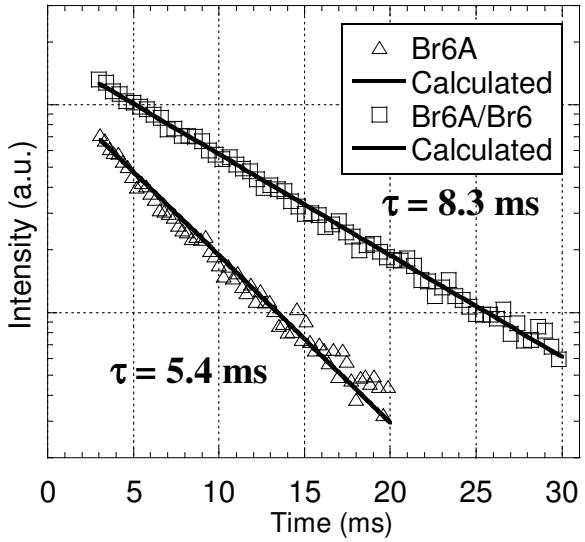

Figure 6.2 Phosphorescent decay curves of Br6A and Br6A/Br6 crystals.

Another very telling finding comes from the phosphorescent lifetimes of these two samples. Figure 6.2 shows the phosphorescent decay curves of both pure Br6A and 0.01 weight fraction (as Br6A) Br6A/Br6 cocrystals. Both are very similar, 5.4 ms and 8.3 ms

respectively, which makes sense until we consider their enormous difference in QY. Equation 1.3 relates the rate of any excited state transition to its QY and lifetime, here $k_{Ph} = \Phi_{Ph}/\tau_{Ph}$. Br6A, in best case, exhibits QY of only Φ_{Ph} = 2.9% (0.029) while the cocrystals yield, in general, Φ_{Ph} = 55% (0.55). From this we see that the phosphorescent rates do not agree: k_{Ph}(Br6A) = 5 s^{-1}, k_{Ph}(Br6A/Br6) = 66 s^{-1}. Emission from pure Br6A is over twelve times slower than from cocrystals though their emission is both from T_1 of Br6A. This is very clear evidence of delayed phosphoresce: phosphorescence from Br6A crystals is much slower than that from cocrystals. One may point to the possibility that the presence of Br6 affects k_{Ph} in cocrystals but, as chapter 4 addresses thoroughly, Br6 is optically non-interacting with Br6A because of its higher energy excited states. Furthermore, Br6 is highly non-polar and non-polarizable precluding the possibility of exiplex formation.

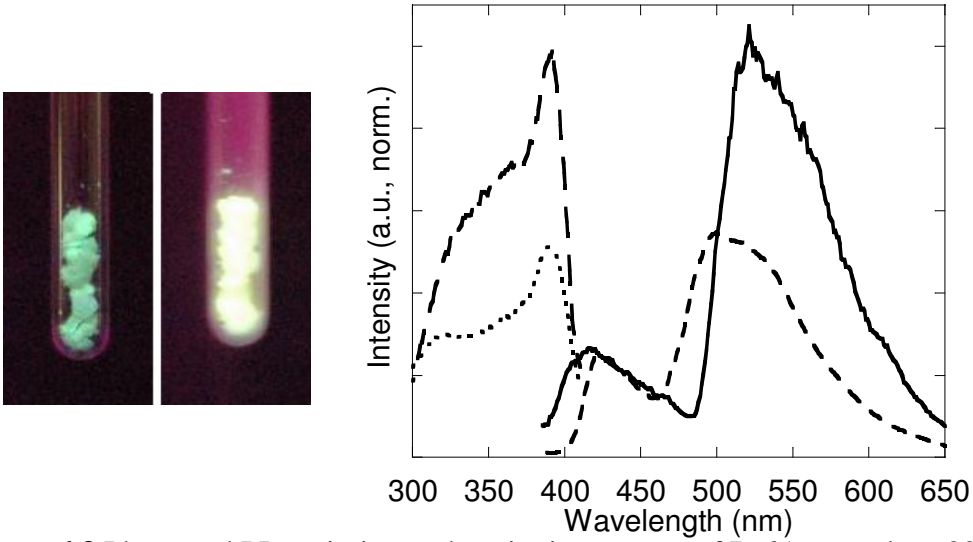

Figure 6.3 Photo and PL emission and excitation spectra of Br6A crystals at 298 K and 77 K. Photos: 298 K (left), 77 K (right). Spectra: 298 K excitation (dotted), 298 K emission (short dash), 77 K excitation (long dash), and 77K emission (solid).

For further evidence low temperature analysis in employed. In delayed phosphorescence (unlike delayed fluorescence) it is likely that the triplet state is repopulated from heat and not triplet-triplet annihilation as final emission comes from a triplet state. Figure 6.3 shows photos of Br6A crystals under 365 nm UV light at 298 K and 77K as well as the PL emission and excitation spectra of these samples. The photo shows an obvious change; at 77 K Br6A crystals emit yellow rather than the green that

they emit at room temperature. The spectral data supports this. Here the data is normalized to the fluorescent emission at 420 nm. This is done because the fluorescent transition $S_1 \rightarrow S_0 + h\nu$ is unaffected by temperature and thus provides a constant between the two samples for comparison.[19] The excitation spectra are not dramatically different, and we can see in emission that a wider portion of the S_1 vibrational modes are now emissive by the broader peak at 420 nm, but the striking change is in the phosphorescent emission. The λ^{max} = 500 nm "green" peak seen at 298 K is entirely gone at 77 K and in its place is a much stronger peak appears at λ^{max} = 530 nm. Though both the green and yellow peaks are close in position, we can be sure that the λ^{max} = 500 nm is gone because it is absent in the normalized spectra. For direct phosphorescence this is counterintuitive. Normally phosphorescence emission is enhanced by low temperatures as vibrational freedoms are restricted to reduce non-emissive relaxation. Here low temperatures extinguish the phosphorescence indicating that it is thermally populated, delayed, phosphorescence. The yellow emission seen only at 77 K is from triplet excimers that are relaxed vibrationally (or converted to T_1) at room temperature and made emissive only when frozen at low temperature. This is represented schematically in Figure 6.4.

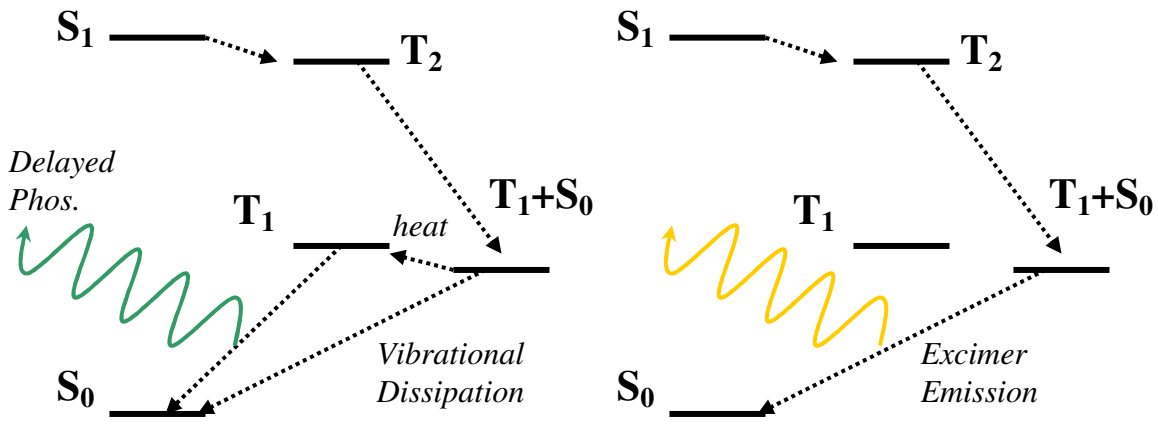

Figure 6.4 Excited state diagrams of Br6A crystals at 298 K and 77 K. 298 K (left) and 77 K (right). T_1+S_0 represents the triplet excimer state. Absorption ($S_2 \rightarrow S_1$) is omitted for simplicity.

The presence of excimers can be speculated by the Br6A crystal structure and proven by controlling intermolecular contact in low temperature samples. Recall from Chapter 4 that crystals of pure Br6A exhibit strong head-to-tow overlap between the benzaldehyde

moieties with inter-aromatic distance of 3.5-3.7 Å, which are sufficiently close for excimer formation. Also note that the head-to-toe arrangement is ideal for excimer polarization stabilization. Empirical evidence comes from comparing Br6A crystals at 77 K to glassy solutions of Br6A also at 77 K as shown in Figure 6.5. In the glassy solution (concentration 0.5 μM) molecules of Br6A are isolated from one another and we see pure green emission at λ^{max} = 500 nm as well as a single thin excitation peak at 360 nm, both in perfect agreement with Br6A/Br6 cocrystals. Clearly the yellow emission comes from an intermolecular excited state species of Br6A as it is absent in solution. Being that this state is lower in energy than T_1 (its emission is redder) we must assume that it is a triplet excimer though the exact pathway from S_1 to T_1-S_0 (excimer) can only be speculated from the data.

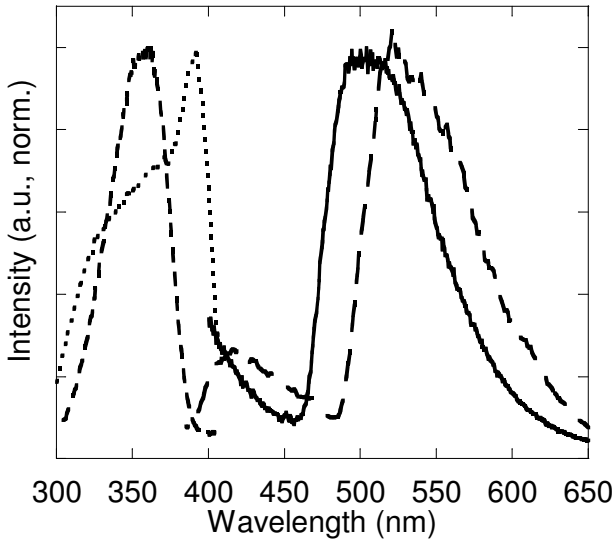

Figure 6.5 PL emission and excitation of Br6A crystals and Br6A in glassy toluene solution each at 77 K. Crystal excitation (dotted), crystal emission (long dash), solution excitation (short dash), and solution emission (solid).

6.3 Experimental

6.3.1 General Methods

All chemicals used were purchased from Sigma Aldrich and used without further purification. Deuterated solvents for NMR were purchased from Cambridge Isotope Laboratories. Proton NMR was conducted on a Varian Inova 500 using $CDCl_3$ solvent with chemical shifts identified relative to 0.05 v/v% tetramethylsilane standard (0.00

ppm). Anhydrous tetrahydrofuran was generated by refluxing over sodium metal and benzophenone collected only from deep purple solution.

PL emission, excitation, and quantum yield data were collected using a Photon Technologies International (PTI) Quantamaster system equipped with an integrating sphere. For low temperature PL measurements a custom made liquid nitrogen dewar specifically designed for the PTI Quantamaster was used. Quantum lifetime data was collected using a PTI LaserStrobe. Quantum lifetime calculations were carried out on the FeliX32 software partnered with the PTI equipment.

6.3.2 Synthesis and Characterization

Br6A and Br6 were both synthesized by the methods reported in Chapters 3 and 4. No new materials were synthesized for this study. Also, referenced crystal structures were collected by the analysis methods reported in Chapters 3 and 4 also.

6.4 Conclusions

Pure crystals of Br6A exhibit delayed phosphorescence. Their phosphorescent emission is much slower than that of Br6A/Br6 cocrystals and they exhibit none of the green, room temperature phosphorescent emission at low temperature. Br6A molecules align in crystals in ideal intermolecular orientations for strong head-to-toe polar interactions such as those seen from excimers. This along with evidence of a low energy excited state seen only from intermolecular species strongly suggests that triplet excimers are formed in Br6A crystals. At room temperature a portion of these triplet excimers transition thermally to pure triplets of Br6A, which then emit this delayed phosphorescence. Delayed phosphorescence from pure Br6A crystals is over twelve times slower than from Br6A/Br6 cocrystals.

Excimers are considered to be detrimental species whose existence only reduces device efficiency. Here, by demonstrating the first report of delayed *phosphorescence*, we prove the possibility that emission can be reclaimed from these otherwise highly quenching excimer states. This provides the potential that phosphors can be designed to experience less detriment from excimer formation and may also present possibilities for dynamic detection methods.

6.5 References

[1] J. Schmidt, W.S. Veeman, and J.H. van der Waals *Chem. Phys. Lett.***1969**, *4*, 341.
[2] A.I. Attia, B.H. Loo, and A.H. Francis *J. Chem. Phys.* **1974**, *61*, 4527.
[3] A.A. Lamola *J. Am. Chem. Soc.* **1970**, *92*, *5045.*
[4] M. Beer and H.C. Longuet-Higgins *J. Chem. Phys.* **1955**, *23*, 1390.
[5] B. Stevensm E. Hutton, and G. Porter *Nature*, **1960**, *185*, 917.
[6] B. Hu, L.A. Yan, and M. Shao *Adv. Mater.* **2009**, *21*, 1500.
[7] A, Yekta and N.J. Turro *Chem. Phys. Lett* **1972**, *17*, 32.
[8] P.P. Wells and H. Morrison *J. Am. Chem. Soc.* **1975**, *97*, 154.
[9] M. Yanagidate, K. Takayama, M. Takeuchi, J. Nishimura, and H. Shizuka *J. Phys. Chem.* **1993**, *97*, 8881.
[10] R.G. Sadygov and E.C. Lim *Chem. Phys. Lett.* **1994**, *225*, 441.
[11] G. Olaso-Gonzalez, D. Roca-Sanjuan, L. Serrano-Andres, M. Merchan *J. Chem. Phys.* **2006**, *125*, 231102.
[12] triplet excimer examples
[13] T. Forster *Angew. Chem.-Intl. Ed.* **1969**, *8*, 333.
[14] H. Beens and A. Weller *Organic Molecular Photophysics,* ed. J.B. Birks, Vol. 2 (Wiley New York, NY 1975).
[15] S. A. Jenekhe & J. A. Osaheni *Science* **265**, 765, (1994).
[16] J. Langelaar, R.P.H. Rettschnick, A.M.F. Lamrooy, and G.J. Hoytink *Chem. Phys. Lett.* **1968**, *1*, 609.
[17] C. Rothe, S. Hintschich, A.P. Monkman, N. Svensson, and M.R. Anderson *J. Chem. Phys.***2002**, *116*, 10503.
[18] O. Bolton and J. Kim *manuscript in preparation.*
[19] Turro, N.J. *Modern Molecular Photochemistry* (University Science Books, Sausalito CA, 1991).

Chapter 7

Dimethoxybromobenzaldehyde

This chapter deals specifically with a unique member of the Br*n* family, 2,6-dimethoxy-4-bromobenzaldehyde (Br1A). This versatile compound was discovered to be not only equally bright to the best combinations of larger Br*n* phosphors but also much simpler to synthesize and purify, highly polymorphic, and readily subliming to create bright and unique microstructures. These benefits make Br1A/Br1 cocrystals uniquely suited to further research in metal-free organic phosphor applications.

7.1 Introduction

Of all of the DHAE phosphors demonstrated so far in this work, it is the Br*n*A/Br*n* family that exhibits the highest quantum yields. The yellow emitting BrS6A/BrS6 phosphor is comparable, but all others fail in initial research to improve upon the 50-60% QY seen from Br6A/Br6. Excellent though these phosphors are, they still exhibit a number of undesirable traits. They are highly electrically insulating due their long alkoxy chain substitutents.[1,2] They can be difficult to purify because of the structurally similar impurities readily generated during the asymmetric lithiation step in their synthesis.[3,4] Finally, their relatively low melting temperatures (55-65^{o}C) lead to problems of practicality in device use and may inhibit efficient cocrystallization during crystal formation.[5,6]

An alternative exists in the smallest members of the Br*n*A/Br*n* family, 2,6-dimethoxy-4-bromobenzaldehyde (Br1A) and 1,4-dibromo-2,6-dimethoxybenzene (Br1), whose chemical structures are shown in Figure 7.1.[7] These compounds exhibit high QYs, have greatly reduced alkyl character, are easier to synthesize/purify, and they do not melt below 100^{o}C. In fact, they do not melt at all but sublime at temperatures of 110^{o}C (for Br1A) and 140^{o}C (for Br1) in atmospheric pressure. From sublimation, monodisperse rod-shaped crystals can be grown with controllable size, which is useful as control of micro and nano-scale fabrication is critical in materials science.[8,9,10] These collected characteristics make Br1A/Br1 an attractive alternative to larger Br*n*A/Br*n* phosphors, but the last gives it unique properties promising for future application development.

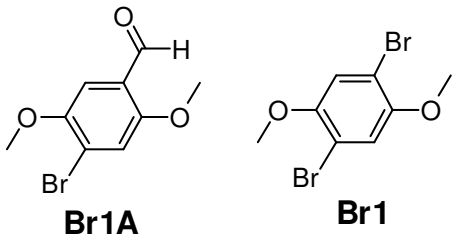

Figure 7.1 Structures of Br1A and Br1.

7.2 Results and Discussion

The synthetic route to Br1A is much simpler than that of Br*n*A (where $n > 1$) given the current state of commercial precursor availability. Rather than using an asymmetric

lithiation step to convert Br1 into Br1A, 2,5-dimethoxybenzaldehyde can be brominated directly to Br1A in a reaction that is non-asymmetric and very clean. Purification can be achieved either by simple recrystallization or sublimation, for stricter purity requirements. Br1 is also synthesized by direct bromination of 1,4-dimethoxybenzene and purified into very large colorless crystals by solvent recrystallization. Both compounds are prepared by bromination without need of additional reagents or catalysts, metallic or otherwise. The fundamental reason that these compounds are so much easier to synthesize is because of their extremely short alkoxy substitutents. Though they are technically alkoxy, methoxy groups are so short they behave as pseudo-functional groups and can be grafted directly to the benzaldehyde in commercial processes. See section 7.3.2 for full synthetic details.

Br1A and Br1 are readily soluble in a wide variety of organic solvents. Unlike longer-chain Br*n* compounds they are poorly soluble in low polarity solvents such as hexanes and diethylether but are, in exchange, more soluble in alcohols. These compounds are also noticeably more crystalline that longer-chain Br*n* compounds, particularly Br1, which forms large millimeter-to-centimeter dimension crystals readily from solvent evaporation.

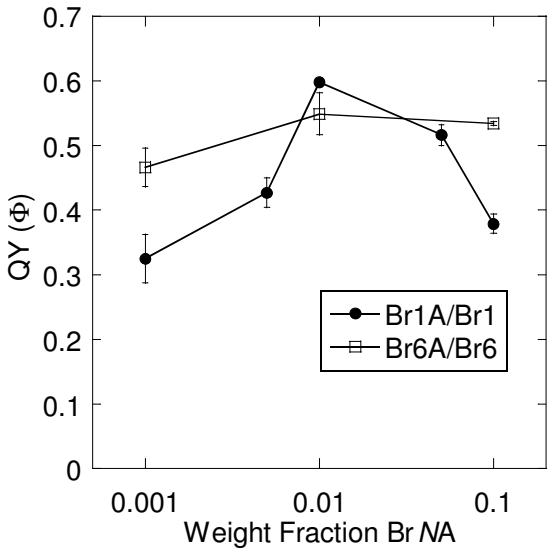

Figure 7.2 Quantum yields of dropcast Br1A/Br1 cocrystals at pertinent weight fractions of Br1A as compared to Br6A/Br6 dropcast cocrystals.

Dropcast samples from chloroform solutions of one weight percent Br1A to Br1 exhibit emission that is spectrally identical to longer-chain Br*n* phosphors and QYs measured as high as 62% as shown in Figure 7.2. This brightness is very competitive with Br6A/Br6 cocrystals, which have exhibited QYs with averages in the 50-55% range. Cocrystals of Br1A/Br1 also appear noticeably brighter than others because of their high chromophore density. Br1A is 36% lighter than Br6A and roughly 66% shorter, meaning that the cocrystal is much denser.

Because the alkoxy substitutents are so short on Br1A and Br1 they no longer play such a large part in crystal packing. Remember that crystals of Br6A, Br6, and Np6, for examples, exhibited interdigitation of the hexyloxy chains. Shorter chain compounds are hypothesized and demonstrated to have less influence on crystal packing.[11,12] Also, the structural difference between Br1A and Br1 are made more dramatic because both compounds do not have large alkyoxy chains in common (as do larger Br*n*A and Br*n* compounds). This may be expected to be a barrier to efficient cocrystallization, however, despite some minor complications, cocrystallization is readily achieved via dropcasting and vapor deposition. Solvent evaporation, however, leads to efficient phase segregation: large emission-less crystals. These effects are also probably the reason for the somewhat noisy nature of the data in Figure 7.2. Cocrystal formation is likely more susceptible to subtle variations in sample preparation.

Another interesting aspect of the Br1A/Br1 system is that crystals of pure Br1A are completely non-phosphorescent. These crystals emit only blue fluorescence when crystalline, which is markedly different from Br6A crystals. If we look at the crystal structure of Br1A we can see why: there is no DHAE working in its pure crystals. Figure 7.3 shows the pertinent contact (or lack thereof) in crystals of Br1A. Figure 7.4 shows the emission spectra of Br1A crystals (fluorescence) and Br1A/Br1 cocrystals (phosphorescence).

Finally, because both components sublime very easily, significant time has been spent on growing bright cocrystal phosphors by sublimation. Long monodisperse crystals can be grown from sublimation of Br1A/Br1 mixes, preliminary data shows. Br1A begins to sublime in atmospheric pressure at 110^{o}C while Br1 does so at 140^{o}C. A series of sublimations were conducted in which a mixed solid containing one weight percent Br1A

to Br1 was heated to 150°C and held for varying amounts of time. Crystals were grown on a glass substrate held perpendicular, approximately one centimeter above the heated source sample. These crystals take on a rod-like appearance and are very bright phosphorescent. Figure 7.5 shows representative samples observed in this study.

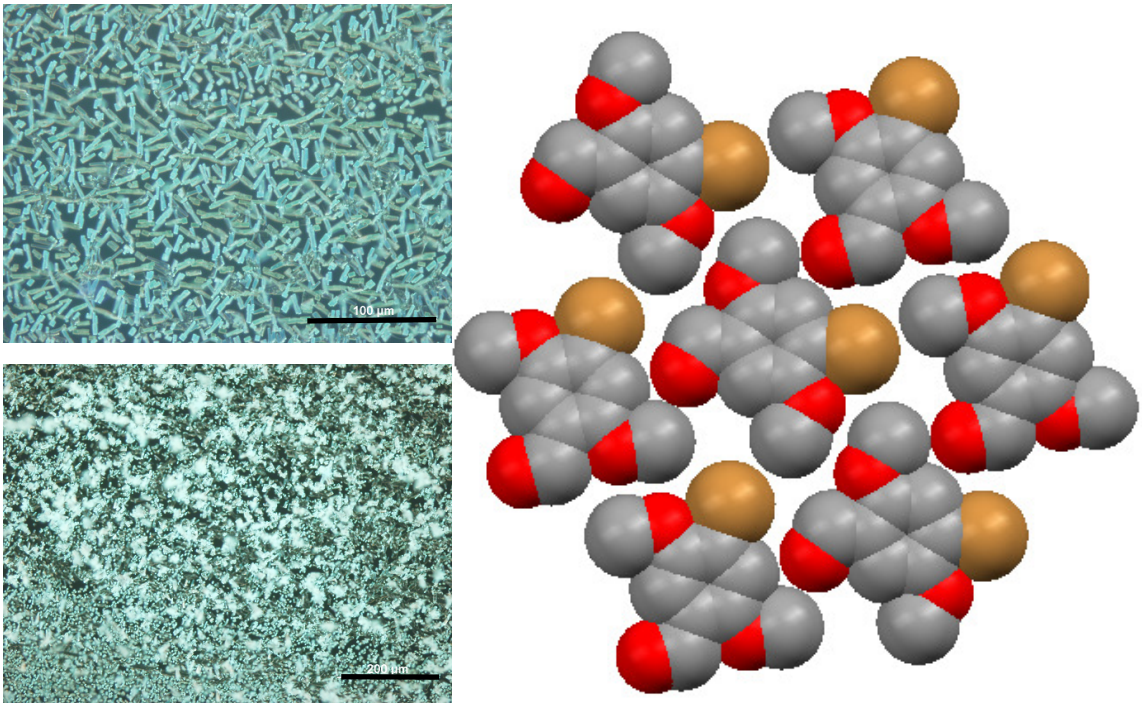

Figure 7.3 Photos and Crystal structure of Br1A. Photos are at differing magnifications to show feature. The top scale bar is 100 µm, the bottom is 200 µm.

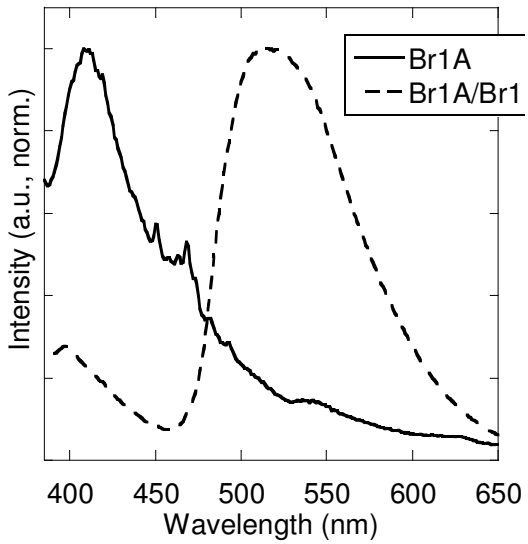

Figure 7.4 PL emission of Br1A crystals and Br1A/Br1 cocrystals.

After fifteen seconds of heating very small crystals form. These crystals are very dimly phosphorescent, though it is unclear whether this is due only to their small size or possible lack of Br1A content. Because of this the sample is shown as a brightfield image in Figure 7.5. Analyzed by imaging software, these smallest crystals are nearly square with aspect ratios of 1.27 ± 0.53 (lengths = 1.52 ± 0.31 micron, widths = 1.30 ± 0.31 micron). The aspect standard deviation comes to 42%.

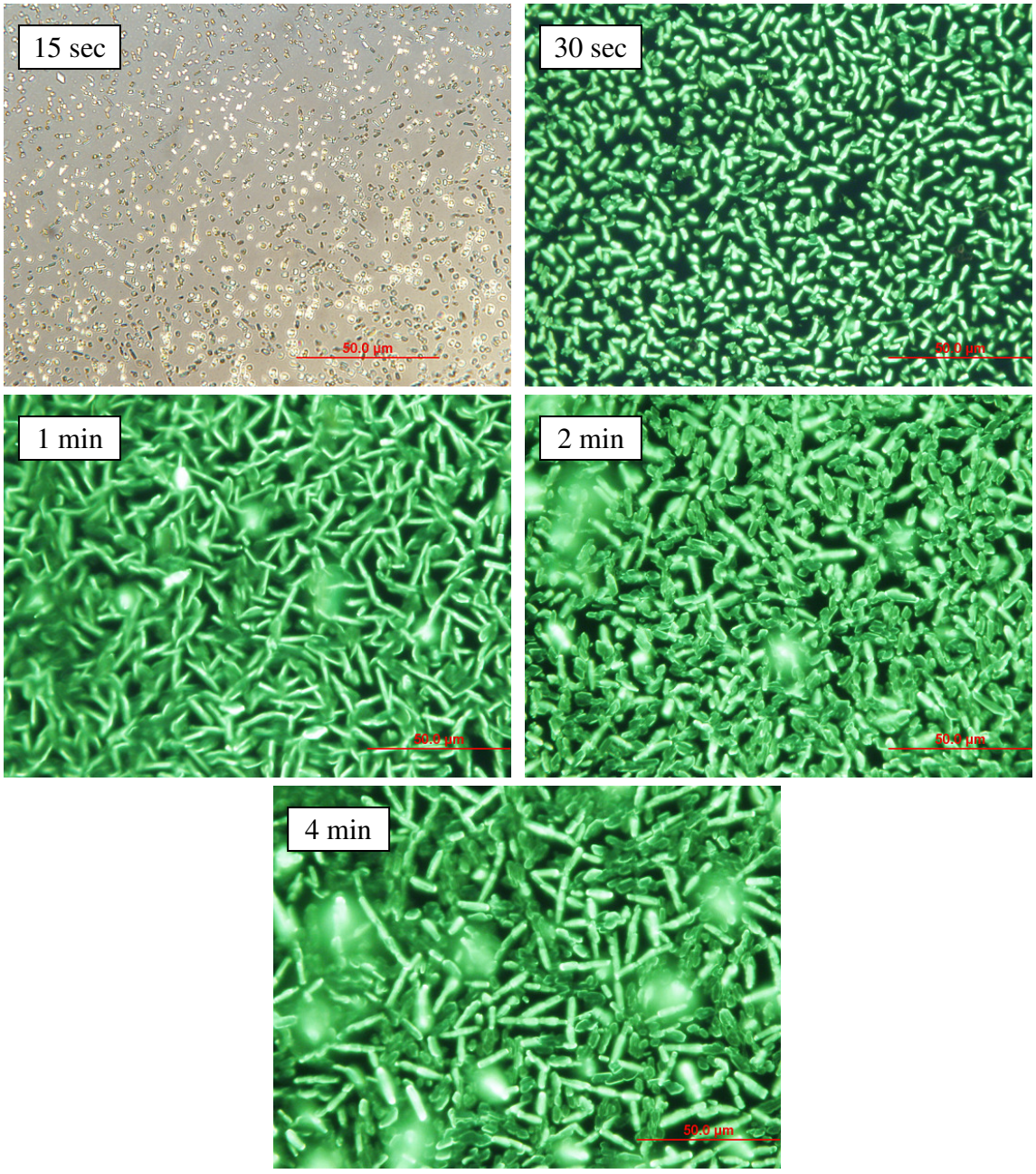

Figure 7.5 Monodisperse crystals grown from 150°C sublimation of Br1A/Br1 for various periods of time. Sublimation is conducted in air at atmospheric pressure.

At longer heating times crystals are noticeably brighter and larger. At thirty seconds the crystals begin to diverge from their square shape into rod-like structures. Lengths measure to 6.70 ± 2.10 micron, which is a standard deviation of 31%, while widths measure 1.57 ± 0.38 micron, a 24% deviation. These crystals exhibited an average aspect ratio of 4.40 ± 1.44, which accounts for a 33% standard deviation, almost 10% better than the fifteen-second samples. Notice also that the widths grow only from 1.30 to 1.68 micron in double the time (15 sec to 30 sec). It appears that the width and length growth are equal until the width reaches a maximum around 1.6 micron.

Samples heated for one minute yield crystals that are longer still but no wider. Lengths measure 8.10 ± 2.59 micron. Widths are 1.64 ± 0.39 micron, which give aspect ratios of 5.18 ± 1.89. This is fairly consistent with shorter heating times. Widths are maximized at 1.6 micron while lengths continue to increase. The dispersity of the system also remains fairly constant as aspect ratios have standard deviations of 42%, 33%, and 37% for 15, 30, and 60 second-heated samples. Lengths have standard deviations of 20%, 31%, and 32% while widths measure slightly more regularly with deviations of 23%, 24%, and 24% (each for 15, 30, and 60 seconds respectively).

Growth and analysis of these monodisperse crystals, created by controlled sublimation, is in its earliest stages but can already be seen to offer a robust route to new phosphorescent materials. Data presented here is rather preliminary but clearly shows that these cocrystals grow anisotropically to form oblong crystals, perhaps micro-rods. The possibility stands that better fabrication methods may allow for more precise control of micro, and perhaps nano, structures of single crystal phosphors.

7.3 Experimental

7.3.1 General Methods

All chemicals used were purchased from Sigma Aldrich and used without further purification. Deuterated solvents for NMR were purchased from Cambridge Isotope Laboratories. Proton NMR was conducted on a Varian Inova 500 using $CDCl_3$ solvent with chemical shifts identified relative to 0.05 v/v% tetramethylsilane standard (0.00 ppm).

UV Absorption measurements were collected using a Varian Cary 50 Bio spectrometer with a solution samples held in a quartz cuvette. PL emission, excitation, and quantum yield data were collected using a Photon Technologies International (PTI) Quantamaster system equipped with an integrating sphere. Optical micrographs were collected using an Olympus BX51 optical microscope equipped with a Mercury lamp UV light source and Olympus DP71 color digital camera.

Sublimations/Vapor depositions were conducted as described above. Homogenous solids were generated by dropcasting chloroform solutions containing one weight percent ratios of Br1A to Br1 onto a glass dish. The dish is then covered with another glass dish distanced approximately one centimeter above the solids (the sublimation flight distance is one centimeter). The bottom dish is then heated to 150°C and the system is left for the experimental time. The cover dish is then removed with the vapor deposited sample attached (the upper dish is the sample substrate). Dishes are cleaned thoroughly with chloroform and acetone and a fresh dropcasting is done for every sample.

7.3.2 Synthesis and Characterization

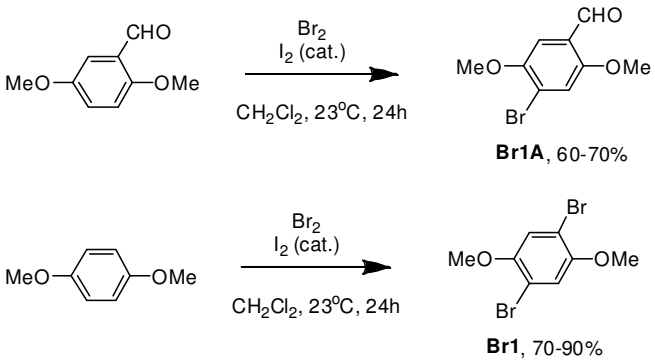

Scheme 7.1 Synthetic routes to Br1A and Br1.

Synthesis of 2,5-dimethoxy-4-bromobenzaldehyde (Br1A). 2,5-dimethoxy-benzaldehyde (1 equiv.) is loaded into a 2 neck round bottom glass flask along with dichloromethane (5 ml / g reagent) and a catalytic amount of iodine (0.01 equiv.). The vessel is sealed under a drying tube charged with potassium carbonate and cooled to 0°C by an ice bath. Bromine (1.1 equiv.) is added dropwise to the reaction, which is then stirred at room temperature for 24 hours. The reaction is quenched by the slow addition

of 20% potassium/water solution until all color is gone. The reaction is extracted with water/dichloromethane. The organic layer is dried over $MgSO_4$, filtered, and rotavaped prior to recrystallization from diethylether at 23°C. Colorless or slightly yellow crystals are collected at 60-70% yields. ^{1}H NMR (300 MHz, $CDCl_3$): δ 10.40 (s 1H), 7.34 (s 1H), 7.25 (s 1H), 3.90 (s 6H).

Synthesis of 1,4-dibromo-2,5-dimethoxybenzene (Br1). 1,4-dimethoxybenzene (1 equiv.) is loaded into a 2 neck round bottom glass flask along with dichloromethane (5 ml / g reagent) and a catalytic amount of iodine (0.01 equiv.). The vessel is sealed under a drying tube charged with potassium carbonate and cooled to 0°C by an ice bath. Bromine (2.2 equiv.) is added dropwise to the reaction, which is then stirred at room temperature for 24 hours. The reaction is quenched by the slow addition of 20% potassium/water solution until all color is gone. The product is extracted with water/dichloromethane. The organic layer is dried over $MgSO_4$, filtered, and rotavaped prior to recrystallization from chloroform evaporated slowly at 23°C. Very large colorless crystals are collected at 70-90% yields. ^{1}H NMR (500 MHz, $CDCl_3$): δ 7.10 (s 2H), 3.85 (s 6H).

Crystal Structure of Br1A. *Crystallographic Data was collected by staff at Seoul National University, Seoul Korea as a paid service. No procedural information was given.*

Table 7.1 Crystallographic Data for Br1A.

Name	**Br1A**
Formula	$C_9H_9O_3Br$
Space Group	P b c a
Cell Lengths	**a** 15.5909(9) **b** 6.8450(5) **c** 18.2697(12)
Cell Angles	**α** 90 **β** 90 **γ** 90
Cell Volume	1949.74

7.4 Conclusions

In Br1A/Br1 there exists a simpler DHAE phosphor that is competitive with earlier reported Br*n*A/Br*n* family phosphors and a material viable for unique vapor phase crystallization. Phosphorescent QYs of Br1A/Br1 dropcasts (of one weight percent

Br1A) are better than those of Br6A/Br6, 59.8 ± 0.5% to 54.9 ± 3.3 respectively, and they exhibit identical emission and excitation spectra. The smaller chromophores in Br1A/Br1 yield crystals that are visibly much brighter because of the higher density of emitting species. Their size also makes their synthesis simpler and cleaner. Difficult-to-remove impurities are easily avoided and large yields are a trivial matter.

Br1A/Br1 cocrystals are easily created by vapor deposition. Both Br1A and Br1 components sublimate in atmospheric pressure at temperatures of 110^{o}C and 140^{o}C, respectively. Crystals grown exhibit good monodispersity and appear rod-like in shape. Rods grow first in both directions equally until they reach a maximum width of 1.6 microns. From that point these rod crystals grown only in length to observed maximums of as much as 10 micron. Relatively uniform collections of these rods are grown via this method with aspect ratios averaging dispersities of around 40%. The good monodispersity and controllable aspect ratios of these cocrystals make them attractive candidates for organic phosphorescent meta-material synthesis and other future micro and nano assemblies.

7.5 References

[1] D.K. Aswal, S. Lenfant, D. Guerin, J.V. Yakhmi, and D. Vuillamume *Anal. Chimica Acta* **2006**, *568*, 84.

[2] Y.D. Park, D.H. Kim, Y. Jang, M. Hwang, J.A. Lim, abd K. Cho *Appl. Phys. Lett.* **2005**, *87*, 243509.

[3] A demonstration of common complications of lithiation (though it is secondary to the article's main focus): R.P. Quirk and J.J. Ma *Polymer International* **1991**, *24*, 197.

[4] Another: R.K. Dieter, C.M. Topping, and L.E. Nice *J. Org. Chem.* **2001**, *66*, 2302.

[5] G. Nenna, G. Flaminio, T. Fasolino, C. Minarini, R. Miscioscia, D. Palumbo, and M. Pellegrino *Macomol. Symp.* **2007**, *247*, 326.

[6] A.R. Buckley, C.J. Yates, and I. Underwood *J. Soc. Information Display* **2009**, *17*, 611.

[7] O. Bolton, Y.-D. Kim, K. Yien, and J. Kim *manuscript in progress*.

[8] T. Asefa, C.T. Duncan, and K.K Sharma *Analyst* **2009**, *134*, 1980.

[9] J.T. Hu, T.W. Odom, and C.M. Lieber *Accounts Chem. Res.* **1999**, *32*, 435.

[10] C.J. Murphy, T.K. San, A.M. Gole, C.J. Orendorff, J.X. Gao, L. Gou, S.E. Hunyadi, and T. Li *J. Phys. Chem. B* **2005**, *109*, 13857.

[11] E. Segerman *Acta Cryst.* **1965**, *19*, 789.

[12] R. Azumi, G. Gotz, T. Debaerdemaeker, and P. Bauerle *Chem. Eur. J.* **2000**, *6*, 735.

Chapter 8

Ester Functionalized Phosphors

Crystal structures are notoriously difficult to predict or design from chemical structures, which is unfortunate as crystal structure is critical to the DHAE principle. As such here is presented BrE*n*A/BrE*n*, a class of DHAE phosphor with functionalized substitutents that crystallize similarly to the brightly phosphorescent Br*n*A/Br*n* family. Phosphorescent QYs of these compounds are similar or slightly better. These compounds are very similar to Br*n*A/Br*n* however they have ester groups at the ends of their alkoxy substituents. Though this alteration is subtle it provides these crystals with additional functionality for potential post-crystallization modifications such as biocongugation. In addition, the crystal motif seen from these compounds agrees so well with Br*n*A/Br*n* analogs that it is reasonable to assume that other chain-end modifications may be possible while maintaining crystal phase halogen bonding and, thus, high efficiency phosphorescence.

8.1 Introduction

To fully utilize the benefits of the DHAE principle is to have complete design freedom over the functionality of phosphorescent compounds made. So far those presented have been compounds designed for brightness, color, or fabrication method. In order to make a DHAE phosphors that can be utilized in specific applications we will need a structure that exhibits the proper crystal structure (halogen bonding) necessary for phosphorescence in conjunction the chemical functionality required for the application. This can be very difficult to achieve if the two are non-compatible in any way.

One such potential incompatibility is the carboxylic acid moiety. Carboxylic acids (as well as other complex carbonyls such as amides) exhibit strong hydrogen bonding, which is very similar to and competitive with halogen bonding. [1,2] In compounds designed to be halogen bonding but containing carboxylic acids, the crystal motif may be driven by the strong hydrogen bonding instead of the halogen bonding. This potential challenge is unfortunate because carboxylic acids and related functional groups are the most common and useful in organic chemistry.[3,4,5] It may be a great challenge to design a DHAE phosphor that has carboxylic character.

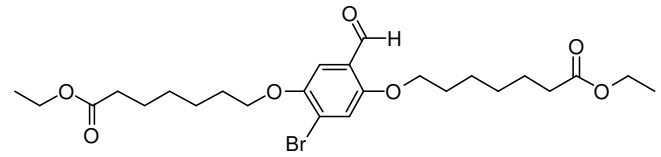

BrE6A

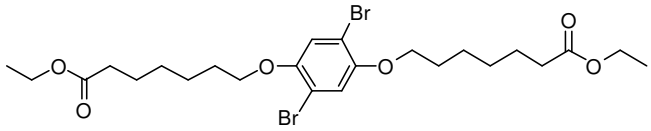

BrE6

Figure 8.1 Chemical structures of BrE6A and BrE6.

One potential approach to this challenge exists with diethyl 7,7'-((2-bromo-5-formyl-1,4-phenylene)bis(oxy))diheptanoate (BrE6A) and its analogous host, diethyl 7,7'-((2,5-dibromo-1,4-phenylene)bis(oxy))diheptanoate (BrE6).[6] These compounds, whose chemical structures are shown in Figure 8.1, are excellent DHAE phosphors. They exhibit bright phosphorescence, crystals with strong halogen bonding, and straightforward cocrystallization yet have ester functionality at the ends of their alkoxy

substitution. These compounds demonstrate one excellent approach to impart additional and potentially incompatible functionalities into DHAE phosphors.

8.2 Results and Discussion

BrE6A/BrE6 cocrystals are very similar optically to cocrystals of Br*n*A/Br*n* phosphors. Because their central chromophore is identical, both are alkoxy substituted borombenzaldehyde, their excitation and emission is identical. Figure 8.2 shows the PL emission and excitation spectra. Just like Br6A/Br6 and Br1A/Br1, BrE6A/BrE6 cocrystals excitation measures as a relatively narrow peak at λ^{max} = 365 nm. Emission is green giving the same blunt peak at λ^{max} = 500-520 nm of the Br*n*A/Br*n* phosphors.

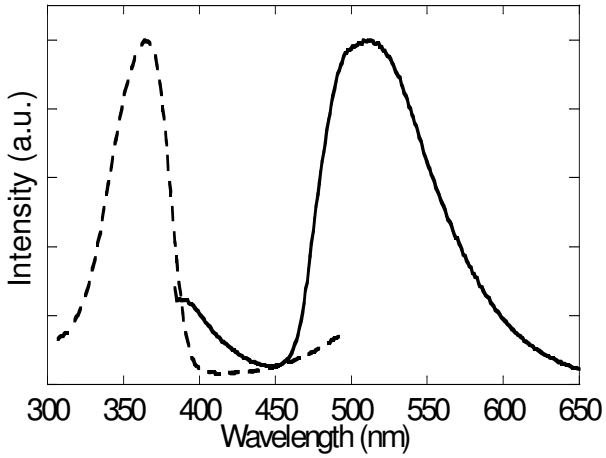

Figure 8.2 PL emission and excitation spectra of BrE6A/BrE6 cocrystals.

Synthesis and cocrystallization of BrE6A and BrE6 is also very similar to Br*n*A/Br*n* phosphors. BrE6 is made by easily by Williamson Ether synthesis from common commercial starting materials. BrE6A is made via ether synthesis from a 4-bromo-2,6-dihyroxybenzaldehyde, which is a precursor made from Br1A. This route is slightly longer than that of Br*n*A, but it is still fairly short and much less likely to produce difficult-to-remove impurities.[7,8]

The crystal structure of BrE6 is shown in Figure 8.3. The crystals exhibit only slight halogen-halogen interaction measured as bromine-bromine distances of 3.7 Å. Though this is only a slight halogen-halogen interaction, the bromine-oxygen distance, when BrE6A is substituted into the matrix, measures at 3.04 Å. This distance is not as close as those in Br6A/Br6, but they are still well below the 3.3 Å maximum for defining a

halogen bond.[9] As is shown later, this longer halogen bond does not reduce the brightness of the crystal phosphor.

Two other features distinguish BrE6A/BrE6 cocrystals from Br6A/Br6 cocrystals. Neighboring aromatic rings are not in plane. There is a 150° angle between C-Br···Br in BrE6 crystals making aromatic rings offset laterally by about 1.8 Å. Also, there is significant π–π overlap/stacking, which is wholly absent in Br6. The stacking in BrE6 is, however, slightly offset distancing each ring at about 4.2 Å. At 4.2 Å these rings are just beyond the active excimer distance of 3.5-4.0 Å.[10]

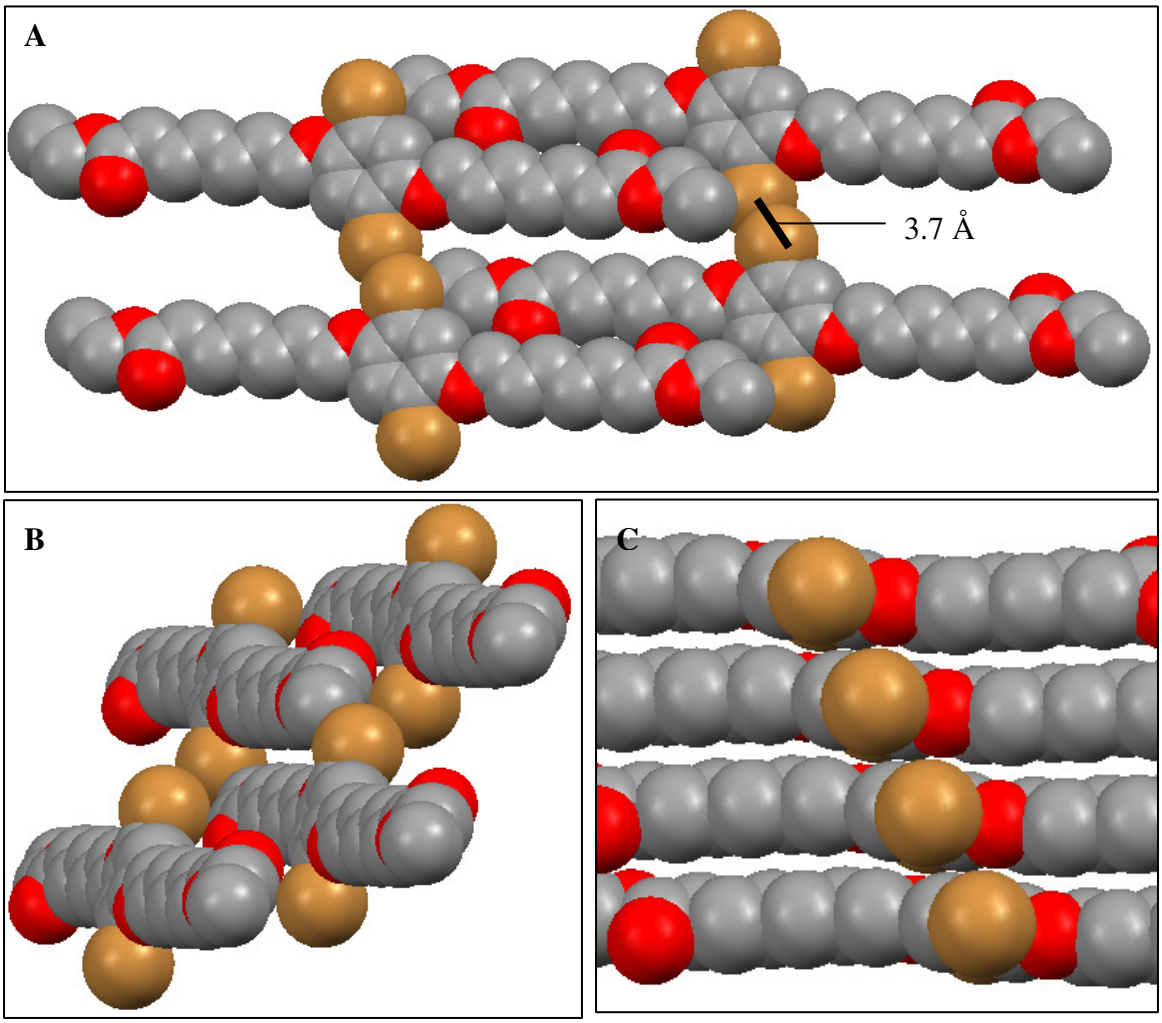

Figure 8.3 Crystal structure of BrE6. (**A**) View showing Br-Br contact. (**B**) View showing staggered rings in the plane parallel to the aromatic rings. (**C**) View showing π–π stacking.

Despite the crystal differences: weaker halogen bonding, non-planar aromatic rings, and subtle π–π stacking, QYs are as good as or better than Br6A/Br6 cocrystals, which

(along with Br1A/Br1) are the brightest DHAE phosphors known at this time. Figure 8.4 shows a sampling of QYs measured from samples dropcasts from chloroform solutions containing BrE6A/BrE6 mixes with BrE6A content in the weight fractions shown. As shown, 0.01 weight fractions (1 wt%) samples present the same QY as Br6A/Br6 samples and even perform better at higher concentrations of the aldehyde. The detrimental factor at these higher concentrations is believed to be chromophore-chromophore contact, self-quenching through excimer formation. It is unclear why this would have less effect in BrE6 crystals as opposed to Br6 cocrystals, but it may be because of more homogenous mixing in cocrystals.

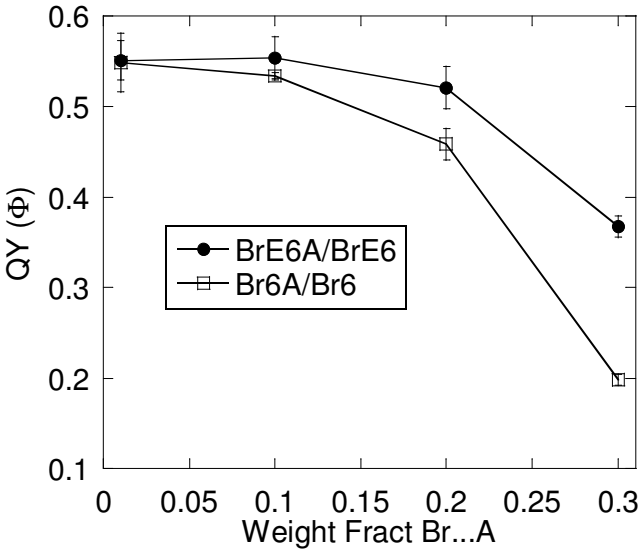

Figure 8.4 Selected QY values of BrE6A/Br6E cocrystals as compared to those of Br6A/Br6 cocrystals.

The additional functionality at the chain ends of BrE6 compounds may help to cocrystallize both aldehyde and host. As compared to Br6A/Br6, BrE6A and BrE6 have more structure in common because of the additional chain similarity, which likely improves cocrystallization and mixing. BrE6 may, thus, also help to isolate the BrE6A chromophore into its crystal, making more homogenous cocrystals. If true, it would explain the enhanced QY at high concentrations but it would also mean that Br6A/Br6 cocrystals must exhibit some degree of phase segregation. This seems like a viable theory, but yet unproven.

Crystals of BrE6 are noticeably different in morphology to the Br*n* family. They appear to take on a spherulite-like structure in dropcasts.[11] Figure 8.5 shows some optical micrographs showing this. Interestingly you can see differences in phosphorescent brightness with the alternating bands in the lamellae. Defect boundaries will occasionally form in the lamellae, and the bright/dark bands in the spherulites will sometimes become discontinuous to form a terraced appearance. It is interesting that in spite of this dramatically different crystal structure (Br*n* crystals form block and needle crystals exclusively) such high QYs are achieved. It may also be an influencing factor in the improved cocrystallization and thus less self-quenching at higher BrE6A concentrations.

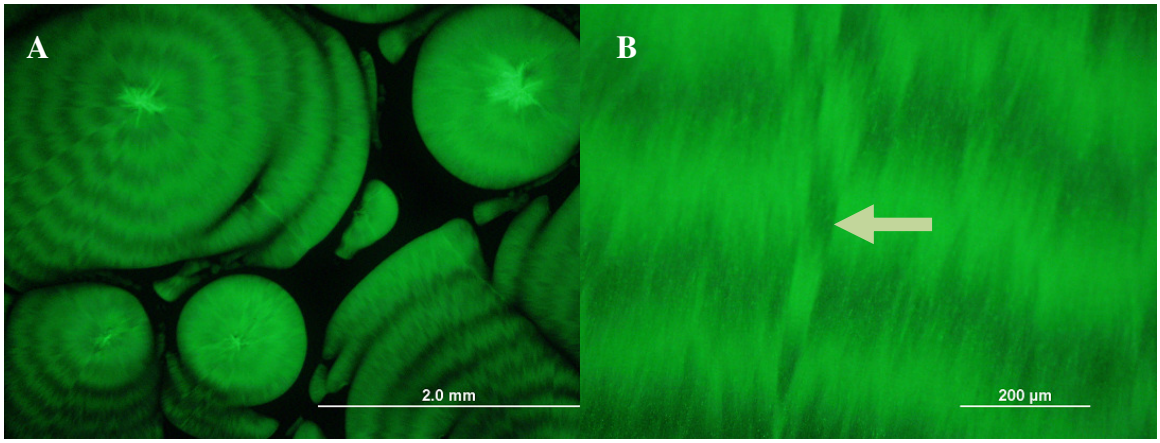

Figure 8.5 Optical micrographs of BrE6A/BrE6 cocrystals. (**A**) Larger-scale image showing the nucleation and growth of BrE6A/BrE6 crystals. (**B**) Smaller-scale image showing a defect in the apparent spherulite structure.

8.3 Experimental

8.3.1 General Methods

All chemicals used were purchased from Sigma Aldrich and used without further purification. Deuterated solvents for NMR were purchased from Cambridge Isotope Laboratories. Proton NMR was conducted on a Varian Inova 500 using $CDCl_3$ solvent with chemical shifts identified relative to 0.05 v/v% tetramethylsilane standard (0.00 ppm).

UV Absorption measurements were collected using a Varian Cary 50 Bio spectrometer with a solution samples held in a quartz cuvette. PL emission, excitation, and quantum yield data were collected using a Photon Technologies International (PTI) Quantamaster system equipped with an integrating sphere. Optical micrographs are

collected using an Olympus BX51 optical microscope equipped with a Mercury lamp UV light source and Olympus DP71 color digital camera.

8.3.2 Synthesis and Characterization

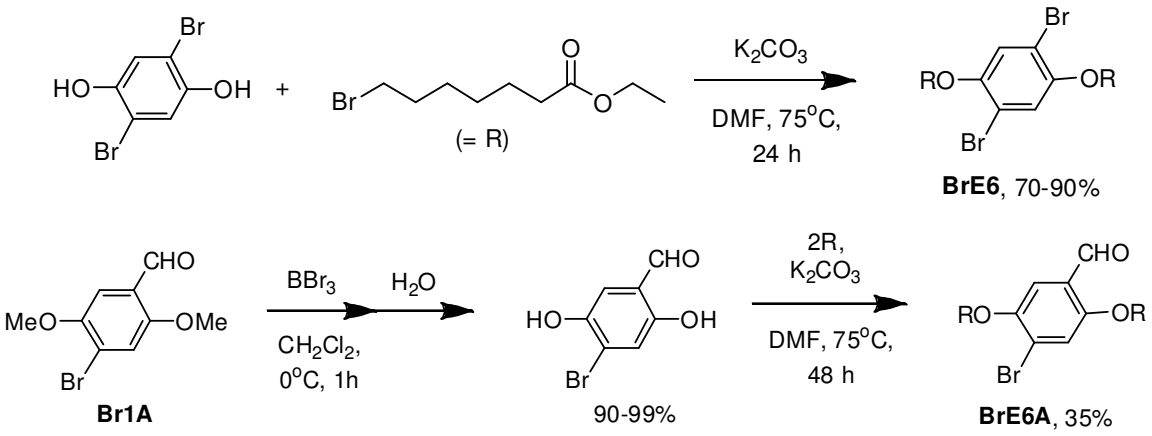

Scheme 8.1 Synthetic route to BrE6A and BrE6.

Synthesis of diethyl-7,7'-((2,5-dibromo-1,4-phenylene)bis(oxy))diheptanoate (BrE6). 2,5-dibromohydroquinone (1 equiv.) and ethyl 7-bromoheptanoate (2.5 equiv.) are loaded into a two-neck round bottomed glass flask and dissolved into dimethylformamide (ca. 1 ml solvent / g dibromohydroquinone). Potassium carbonate (3 equiv.) is added and the flask is sealed under nitrogen, stirred, and heated to 75°C for 24 hours. The reaction is then cooled, filtered, and rotovaped at high temperature to remove all solvents. The product is purified by column chromatography with hexanes. White crystals were collected at yields of 70-80%. For BrE6, ^{1}H NMR (500 MHz, $CDCl_3$): δ 7.08 (s 2H), 4.13 (m 4H), 3.95 (t 4H), 2.31 (m 4H), 1.83 (m 4H), 1.65 (m 4H), 1.55-1.34 (m 8H), 1.26 (m 6H).

Synthesis of 4-bromo-2,6-dihydroxybenzaldehyde. 4-bromo-2,6-dimethoxybenz-aldehyde (Br1A) (1 equiv.) is loaded into a two-neck round bottom flask and dissolved into anhydrous dichloromethane. The reaction is cooled to 0°C in an ice bath and a boron tribromide/dichloromethane solution (1.1 equiv.) is added dropwise. The reaction is stirred at 0°C for an hour as it becomes bright red. The reaction is carefully quenched with water and turns bright yellow. The reaction is extracted with water and dichloromethane, the organic layer is dried over MgSO4, filtered, and rotavaped. The

product is collected as a crystalline yellow solid that becomes dark green/black as it is dried. Yields are 95-99%. For 4-bromo-2,6-dihydroxybenzaldehyde, ^{1}H NMR (500 MHz, $CDCl_3$): δ 10.57 (s 1H), 9.82 (s 1H), 7.19 (s 2H), 5.30 (s 1H).

diethyl-7,7'-((2-bromo-5-formyl-1,4-phenylene)bis(oxy))diheptanoate (BrE6A). 4-bromo-2,6-dihydroxybenzaldehyde (1 equiv.) and ethyl 7-bromoheptanoate (2.5 equiv.) is loaded into a two-neck round bottomed glass flask and dissolved into dimethylformamide (ca. 1 ml solvent / g dibromohydroquinone). Potassium carbonate (3 equiv.) is added and the flask is sealed under nitrogen, stirred, and heated to 75°C for 24 hours. The reaction is then cooled, filtered, and rotovaped at high temperature to remove all solvents. The product is purified by column chromatography with hexanes. White crystals were collected at yields of 70-80%. For BrE6A, ^{1}H NMR (500 MHz, $CDCl_3$): δ 10.41 (s 1H), 7.31 (s 1H), 7.23 (s 1H), 4.14 (m 4H), 4.01 (t 4H), 2.32 (p 4H), 1.85 (m 4H), 1.67 (m 4H), 1.52 (m 4H), 1.41 (m 4H), 1.26 (m 6H).

Crystal Structure of BrE6A. *The following analysis was conducted and report written by University of Michigan Department of Chemistry staff crystallographer Dr. Jeff W. Kampf as a paid service.* Colorless, needle-like crystals of **BrE6** were grown from a methanol solution at 25 deg. C. A crystal of dimensions 0.36 x 0.08 x 0.06 mm was mounted on a standard Bruker SMART 1K CCD-based X-ray diffractometer equipped with a LT-2 low temperature device and normal focus Mo-target X-ray tube (λ = 0.71073 A) operated at 2000 W power (50 kV, 40 mA). The X-ray intensities were measured at 108(2) K; the detector was placed at a distance 4.969 cm from the crystal. A total of 3580 frames were collected with a scan width of 0.5° in ω and phi with an exposure time of 30 s/frame. The integration of the data yielded a total of 16706 reflections to a maximum 2θ value of 56.62° of which 3106 were independent and 2496 were greater than 2σ(I). The final cell constants (Table 8.1) were based on the xyz centroids of 5874 reflections above 10σ(I). Analysis of the data showed negligible decay during data collection; the data were processed with SADABS and corrected for absorption. The structure was solved and refined with the Bruker SHELXTL (version 6.12) software package, using the space group P1bar with Z = 1 for the formula $C_{24}H_{36}O_6Br_2$. All non-

hydrogen atoms were refined anisotropically with the hydrogen atoms placed in idealized positions. The molecule lies on an inversion center in the crystal lattice. Full matrix least-squares refinement based on F^2 converged at R1 = 0.0343 and wR2 = 0.0813 [based on I > 2sigma(I)], R1 = 0.0525 and wR2 = 0.0874 for all data.

- Sheldrick, G.M. SHELXTL, v. 6.12; Bruker Analytical X-ray, Madison, WI, 2001.
- Sheldrick, G.M. SADABS, v. 2.10. Program for Empirical Absorption Correction of Area Detector Data, University of Gottingen: Gottingen, Germany, 2003.
- Saint Plus, v. 7.01, Bruker Analytical X-ray, Madison, WI, 2003.

Table 8.1 Crystallographic Data for BrE6.

Name	**BrE6**
Formula	$C_{24}H_{36}Br_2O_6$
Space Group	P-1
Cell Lengths	**a** 4.1958(12) **b** 9.659)3) **c** 15.714(5)
Cell Angles	α 89.304(6) β 86.772(4) γ 80.397(4)
Cell Volume	626.922
Z, Z'	**Z**: 1 **Z'**: 0
R-Factor (%)	3.43

8.4 Conclusions

BrE6A and BrE6 are a DHAE phosphor combination that is extremely bright and contains additional chemical functionality. Adding esters to the chain ends of the alkoxy substitutents yields crystals that maintain the color and exceptionally high QY of the BrNA/BrN family of phosphors. These cocrystals, in fact, perform better in brightness at higher aldehyde concentrations than do Br6A/Br6 cocrystals. This may be due to the increased similarity between aldehyde and host imparted from the longer, more complex substitutents. A unique spherulite-like crystal structure may also contribute to this enhanced high-concentration QY and gives dropcast samples of BrE6A/BrE6 interesting bands of brightness in their lamellae. Further investigation into these crystals may help researchers to understand how the orientation of the aldehyde affects the direction and brightness of the emission as it escapes the crystal.

This or similar compounds may also prove useful for the chemical incorporation of DHAE phosphor crystals into combinations with other materials. By removing the ethyl

protection of the ester groups post-crystallization a bright organic phosphor crystal with carboxylic functionality would be possible. This would allow scientists to integrate DHAE phosphors into application-specific materials via processes such as bio-conjugation.

8.5 References

[1] B.R. Bhogala and A. Nangia *Crystal Growth & Design* **2003**, *3*, 547.
[2] B.K. Saha, A. Nangia, and M. Jaskolski *Crystal Eng. Comm.* **2005**, *7*, 355.
[3] Example, bio-conjugation: J.H. Wosnick, C.M. Mello, and T.M. Swager *J. Am. Chem. Soc.* **2005**, *127*, 3400.
[4] Example, solubility: E. Nakamura and H. Isobe *Accounts Chem. Res.* **2003**, *36*, 807.
[5] Example, organic-inorganic contact: X.F. Guo et al *Science* **2006**, *311*, 356.
[6] O. Bolton, K. Lee, K.K. Yien, K.Y. Lin, S.M. Wang, M.T. Gray, J.W. Kampf, and J. Kim *manuscript in progress*.
[7] R.P. Quirk and J.J. Ma *Polymer International* **1991**, *24*, 197.
[8] R.K. Dieter, C.M. Topping, and L.E. Nice *J. Org. Chem.* **2001**, *66*, 2302.
[9] Auffinger, P., Hays, F.A., Westhof, E., and Ho, P.S. *Proc. Natl. Acad. Sci.* **2004**, *48*, 16789.
[10] S. A. Jenekhe & J. A. Osaheni *Science* **265**, 765, (1994).
[11] M.T. Lloyd et al *J. Am. Chem. Soc.* **2007**, *129*, 9144.

Chapter 9

Polymer Entanglement

In this chapter emissive, non-crystalline DHAE-like phosphors are presented. Demonstrated here, aldehydes like those presented earlier can become brightly phosphorescent when embedded into certain polymers, entirely removing the requirement of crystallinity. From early results, the versatility of this approach appears quite wide. Even completely amorphous, *liquid* benzaldehydes can become brightly phosphorescent at room temperatures if embedded into a proper polymer matrix, which must be carefully chosen. The key is to choose a glassy polymer that will achieve excellent *entanglement* with the chromophore. As defined here, entanglement is the efficiency at which a polymer backbone mixes with the alkyl substitutents of the benzaldehyde phosphors. Here is shown, by choice of polymer and optical analysis, that polymers whose backbones more closely mimic the chains of the aldehyde produce much brighter phosphorescent emission, presumably due to reduced vibrational freedom of the chromophore. This not only demonstrates a versatile, completely non-crystalline metal-free organic phosphor design principle, it also offers a new means to probe polymer solid state properties and, perhaps, an entirely new paradigm for polymer characterization.

9.1 Introduction

The DHAE design principle has now been proven to be an effective tool for designing metal-free organic phosphors, though its requirements may restrict its use in some situations.[1] The need of not only well-ordered crystal states, but states that exhibit strong halogen bonding can be too demanding to designers in some applications. Here, though, we present a viable alternative to crystals: polymer blends.

DHAE phosphors, substituted benzaldehydes, can be embedded into rigid polymers to achieve a tight packing similar to that in crystals. By restraining the chromophore, polymers can remove vibrational pathways to non-emissive relaxation from T_1, which brings about phosphorescent emission from the chromophore without the need of crystal order.[2] Similar reports exist for organometallic phosphors, whose phosphorescent quantum yields are seen to improve in polymer hosts.[3,4] The difference here is that, rather than simply increasing already high QYs, certain polymers raise room temperature phosphorescent QYs of substituted benzaldehydes up from essentially zero to visible levels of roughly 1%. Thus, polymer hosts can activate phosphorescent emission in otherwise non-emissive metal-free chromophores.

As evidenced, however, not all polymer-phosphor combinations lead to strong phosphorescence. In fact, some combinations will fail to produce any detectable phosphorescent emission. The study presented here identifies the concept of entanglement, which provides a means to determine which polymers will efficiently activate phosphorescent emission. If the polymer backbone is flexible and has structural similarity to the alkyl substitutions of the chromophore and if the polymer has small, non-hindering pendants/sidechains, entanglement with the chromophore is good and emission is strong. If the polymer does not share any structural similarity with the chromophore or if it has a rigid backbone and/or large bulky pendants/sidechains, the polymer and chromophore segregate: poor entanglement and no phosphorescence.

9.2 Results and Discussion

In this study we use a DHAE style chromophore not yet discussed in this volume, 4-bromo-2,5-di((2-ethylhexyl)oxy)benzaldehyde (BrEHA). The structure of BrEHA is shown in Figure 9.1. It is akin to Br6A but has 2-ethylhexyl substitutents in place of

Br6A's hexyloxy. The additional branch in BrEHA makes the compound much, much less ordered/crystalline.[5,6] The bulkiness of the ethylhexyl chains prevent packing so well that BrEHA is an oily liquid at room temperature and remains liquid even at –12°C. At extremely low temperatures (77 K was tested) it does crystallize in thin needles that strongly resemble to spherulite-like structures of BrE6 from chapter 8, though no detailed study of their structure was conducted.

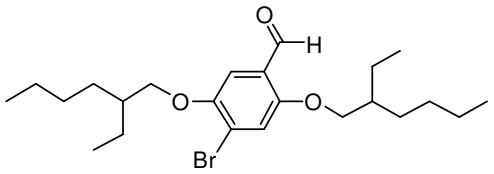

Figure 9.1 Chemical Structure of BrEHA.

BrEHA was designed to be a suitable negative control for DHAE phosphors, specifically Br6A. Like Br6A, BrEHA is an alkoxy-substituted bromobenzaldehyde. Unlike Br6A, it does not crystallize spontaneously, which is desirable here. For, if one were to mix a crystalline DHAE phosphor, such as Br6A, into a polymer there would be a possibility that the small molecule chromophore would simply isolate and crystallize within the polymer. Phosphorescent emission would then be detected even though there is no chromophore/phosphor interaction of interest. BrEHA is a liquid and thus works perfectly to explore chromophore/polymer interactions because it produces none of this potential 'background' phosphorescence. BrEHA alone emits no detectable phosphorescence at room temperature. Figure 9.2 shows the PL emission and excitation of BrEHA. The fluorescent peak at λ^{max} = 410 nm is especially dominant in the emission and the excitation shows a shouldered peak with λ^{max} = 385 nm that is very similar to the fluorescent emission of other Br*n*A compounds such as Br6A (especially when they are observed in chloroform solution).

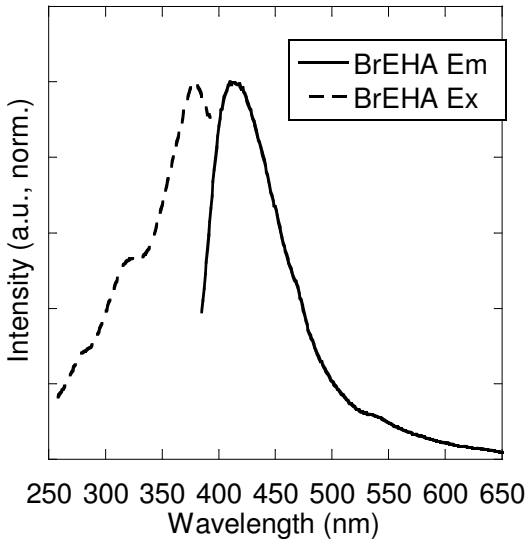

Figure 9.2 PL emission and excitation of BrEHA liquid.

Mixed with certain polymers, BrEHA can begin to emit visibly bright phosphorescence. If the polymer is chosen correctly, this phosphorescence can become very dominant over BrEHA's intrinsic fluorescence. A series of widely varying polymer structures were explored as potential host materials for BrEHA in this capacity. Conjugated and conducting polymers were tried along with a sizeable portion of the poly(methacylic acid) family. Several polymer characteristics were explored as potential variables that could be correlated to the strength of the phosphorescent emission, but no correlation was observed. Density, crystallinity, glass transition temperatures, free volume, and molecular weight were all considered with no observable correlations. In the end of the study, with no quantitative material property following the trend, it appeared to be structural similarity that explained the trends in emission. From this, the notion of entanglement was born.

To best illustrate entanglement, four polymers, some of the brightest phosphorescent-producing polymers tested, are utilized. Poly(methylacrylate) (PMA), poly (methylmethacrylate) (PMMA), poly(styrene) (PS), and poly(α-methyl styrene) (PaMS) are used here, and their chemical structures shown in Figure 9.3. Each is a very simple and common polymer with vinyl backbones and small pendants. Additional methyl substitution on the polymer backbone differentiate PMMA from PMA and PaMS from

PS. For blends with BrEHA, these subtle additions prove to make an enormous difference.

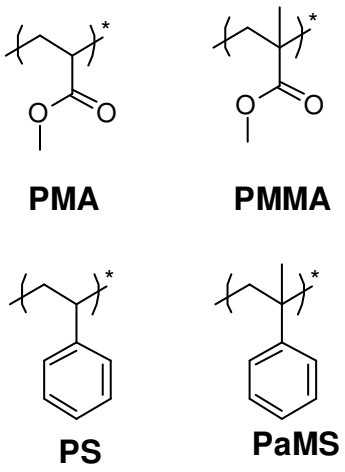

Figure 9.3 Structures of polymers used to embed BrEHA that succeeded in generating phosphorescent emission.

BrEHA is co-dissolved into chloroform with each of the polymers at a ratio of ten weight percent BrEHA (relative to polymer content). Polymer films were dropcast from this solution onto a clean glass substrate and dried in-vacuo for several hours to ensure complete removal of the solvent. The resulting films appeared clear and homogenous (as bulk) though their surfaces were noticeably rough and very clearly terraced. Each sample was excited at 365 nm and their PL emissions measured. The results from these tests are shown in Figure 9.4. The emission of pure, liquid BrEHA is shown also as reference.

Fluorescence is detected from each polymer blend sample. This is not surprising because the polymers are acting only to prevent vibrational freedom of the chromophore. They are not promoting intersystem crossing like the co*crystal* hosts of earlier chapters (these polymers have no halogens to produce the DHAE). Thus they are not affecting singlets in any notable way. The only notable effect these polymers have on the excited state activity of the chromophore is that they act to restrict vibrational loss of the triplet. Because the fluorescent emission is thus expected to be unaffected by the polymer, the peak seen usually at λ^{max} = 410 nm is used as a common feature in each sample and is normalized in Figure 9.4. Data here is given as spectral comparison only because QYs were below the ca. 1% detection limit of our equipment. We suspect that the QYs

measured are lower than actual and that the low numbers may be an artifact of the test method, but at the time of this writing this notion had not been explored extensively.

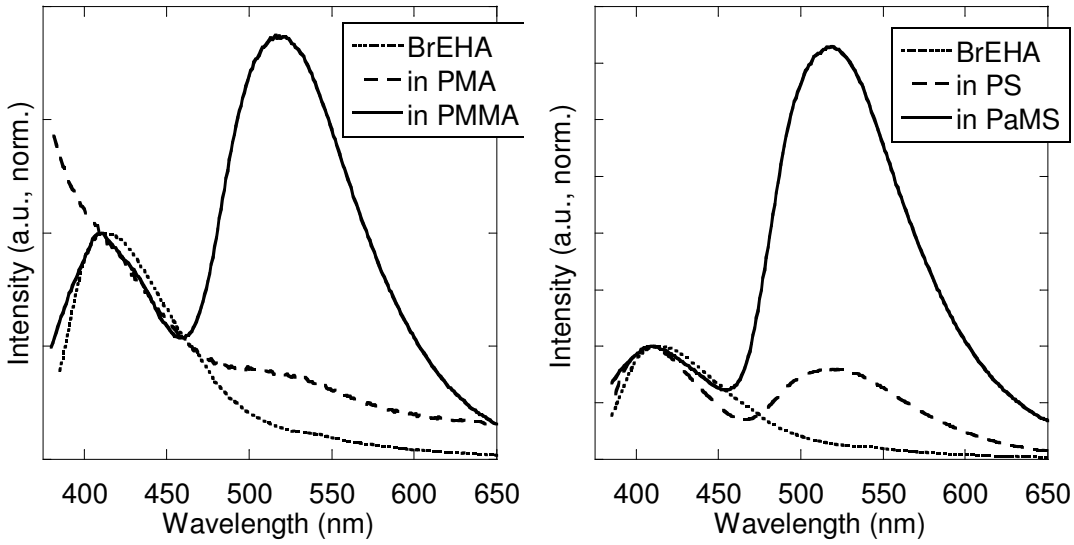

Figure 9.4 PL emission spectra of BrEHA embedded in various polymers.

PMA films produced very little phosphorescence. The PL emission spectrum is predominantly fluorescent with only a small phosphorescent shoulder. The intensity ratio of the phosphorescence (λ^{max} = 500 nm) to fluorescence (λ^{max} = 410 nm) is 0.40. On the other hand, PMMA, different from PMA only in the additional methyl backbone substitution, is very phosphorescent. The intensity ratio of the phosphorescence (λ^{max} = 520 nm) to fluorescence (λ^{max} = 411 nm) is 1.87. As a host for BrEHA, PMMA is 4.67 times brighter in phosphorescence than is PMA.

Brighter than PMA, PS (which is also free of methyl backbone substitution) is moderately phosphorescent. The intensity ratio of the phosphorescence (λ^{max} = 522 nm) to fluorescence (λ^{max} = 410 nm) is 0.80, which is twice the brightness of PMA films. PaMS, though, makes a much brighter phosphor. Its intensity ratio of phosphorescence (λ^{max} = 520 nm) to fluorescence (λ^{max} = 410 nm) is 3.40. As a phosphor host (to BrEHA) PaMS is 4.25 times brighter than is PS. The trend follows both families; methyl substituted backbones are much brighter phosphor hosts than those without. Also, both poly(styrenes) outperform their poly(methacylate) counterparts: PS > PMA and PaMS > PMMA.

Optical micrographs of these polymer-embedded phosphor systems shows select regions of emission. Figure 9.5 shows an optical micrograph of a BrEHA/ PMMA films under 365 nm UV light. The image shows what appear to be diffuse regions of green phosphorescent emission that do not correlate to any feature in the bulk polymer, which forms a homogenous film across the surface. On these view scales it is impossible to tell whether this indicates that BrEHA is isolated into pockets separate from the polymer, but it can be certain that there is some form of phase segregation happening in these blends. The phosphorescent emission is non-homogenous.

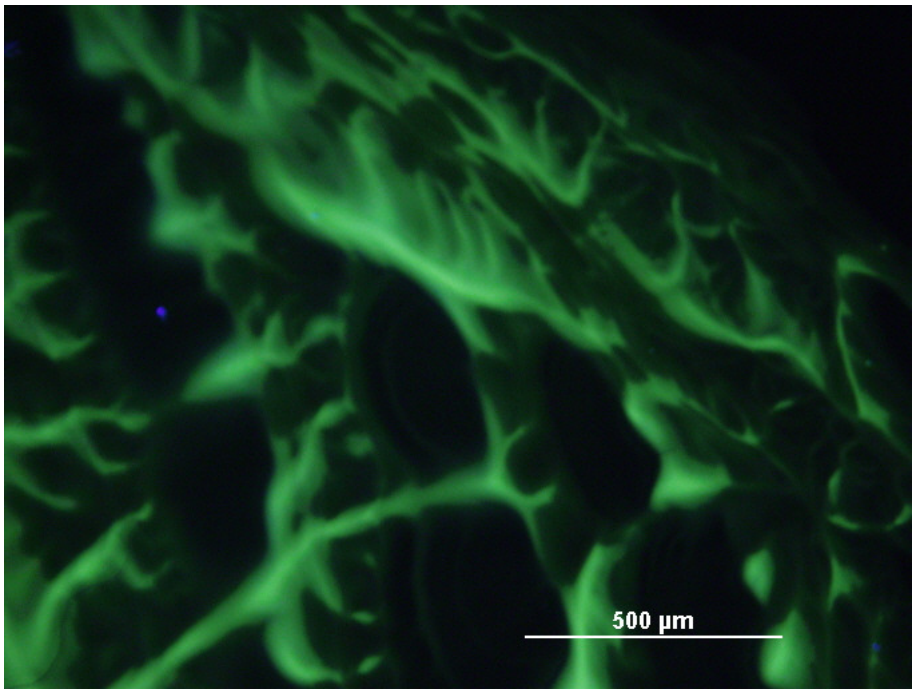

Figure 9.5 Optical micrograph of BrEHA/PMMA film.

From these observations the idea of entanglement is proposed. Figure 9.6 shows schematically what is meant. In order for polymers to succeed as hosts to BrEHA or any DHAE phosphor, they must share some structural similarity with the small molecule. Really this is not unlike determining an adequate crystalline host for DHAE phosphor design in Chapter 3. The polymer must be able to mix well with the chromophore in order to seize its flexible substitutents and prevent vibrational losses.

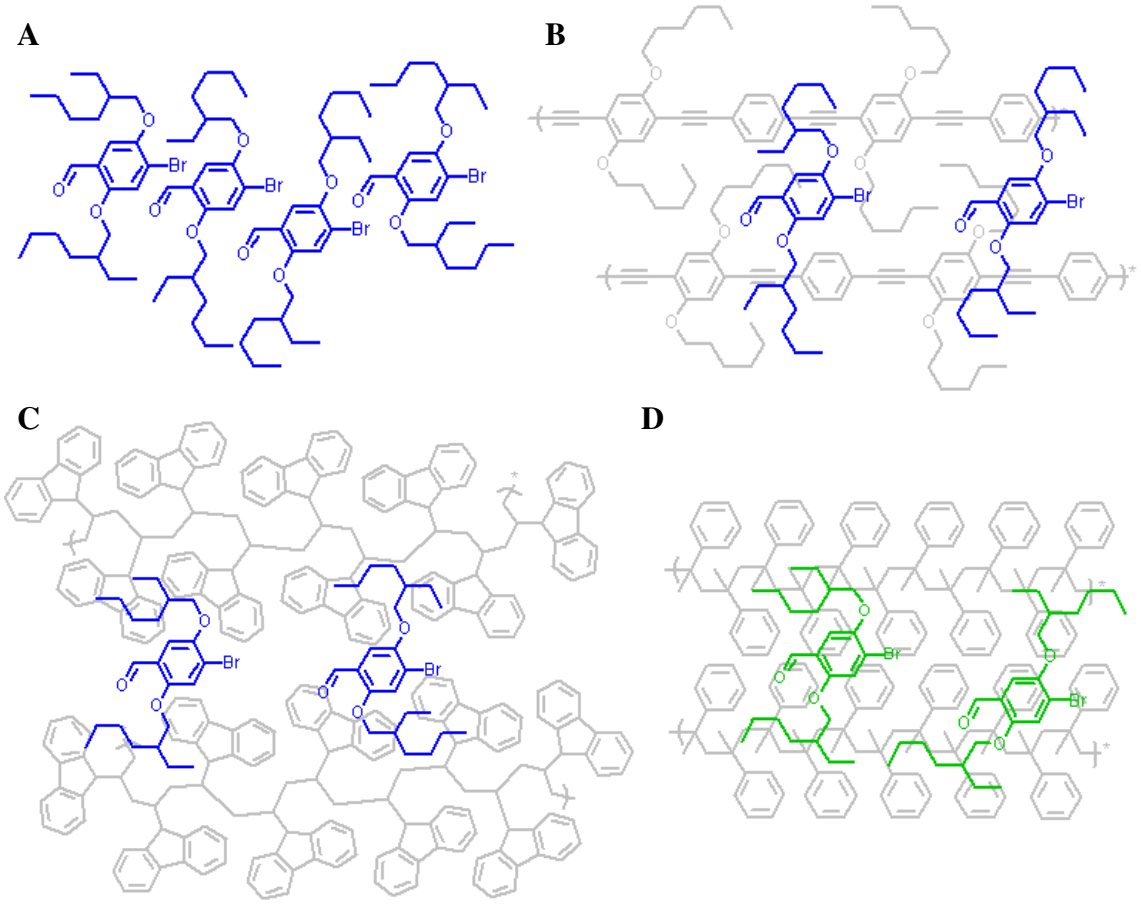

Figure 9.6 Schematic illustrating the idea of polymer entanglement. (**A**) BrEHA liquid has great vibrational freedom so triplets relax non-emissively. (**B**) PPE has a rigid backbone that does not entangle the alkyl substitutents of BrEHA. Triplets relax by vibration here as well. (**C**) PVK has a flexible backbone, but its bulky pendants prevent BrEHA molecules from getting close enough to become entangled. (**D**) PaMS has a flexible, entangling backbone and small pendants. BrEHA mixes well and the glassy polymer prevents vibrational freedoms. Triplets emit strong phorphorescence.

All of the four good host polymers (those shown in Figure 9.4) have some degree of similarity to BrEHA. They all have vinyl backbones, which are like the alkyl substitutents of BrEHA, and they all have relatively small pendants, methyl ester or benzene. The first aspect is important because it allows the ehtylhexyl portions of BrEHA to intertwine with the polymer backbones as they dry into their glassy state in order for the chromophore to be held in place. Rigid-rod polymers such as poly(p-phenylene ethynylenes) (PPE) and poly(p-phenylenes) (PPP) were attempted as hosts and

failed to produce any phosphorescent emission. Their backbones are too unlike any part of BrEHA, and their rigid structures prevent entanglement in any capacity as one cannot tie a knot with sticks. The second aspect, small pendants, is important because it allows the BrEHA molecule to get close enough to the polymer to achieve the substitutent intertwining. Some larger-pendant polyvinyl polymers were used; poly(vinyl carbazole) (PVK), poly(isopropyl methacrylate), and poly(benzyl methacrylate), and failed to produce phosphorescence.[7] These polymers have a proper backbone, but their larger pendants essentially block it from interactions with BrEHA.

Another consideration regarding pendant choice is hinted at in the differences between the poly(methacrylates) and poly(styrenes). Both poly(styrenes) perform better than their poly(methacrylate) counterparts. This could be due to the structural similarity between their phenyl substitutions and the aromatic structure of BrEHA. Methacylate, on the other hand, shares no distinct similarity to BrEHA, which contains no methoxy or ester feature. This may be creating enhanced solid-state interaction between the styrenes, perhaps even some form of π-π interaction[8,9], that is absent in blends with the methacrylates and is likely why those blends are brighter phosphors.

The most surprising finding from this study is the profound effect that the methyl substitution makes. The two polymers presented without methyl substitutents on their backbones, PMA and PS, are markedly less phosphorescent as hosts than those that do have it, PMMA and PaMS. Though this structural difference is rather subtle it has a profound effect on the brightness of phosphorescent emission from BrEHA, which means that it must also have a profound effect on the efficiency of mixing between the polymer and small molecule, work better to suppress vibrational freedom of the system, or both. BrEHA has a branched alkyl chain that may exhibit a favorable solid-state interaction with the additional branching of the methyl-substituted backbones. It is also possible that the additional methyl group helps to fill voids near the polymer backbone, restricting vibrational freedoms better than their methyl-free polymer brothers. Novel polymer design may be a viable means to explore these ideas (perhaps a poly (styrene) with methyl substitutions at both points in the polymer backbone) but has not yet been done.

9.3 Experimental

9.3.1 General Methods

All chemicals used were purchased from Sigma Aldrich and used without further purification. Deuterated solvents for NMR were purchased from Cambridge Isotope Laboratories. Proton NMR was conducted on a Varian Mercury 300 using $CDCl_3$ solvent with chemical shifts identified relative to 0.05 v/v% tetramethylsilane standard (0.00 ppm). Anhydrous tetrahydrofuran was generated by refluxing over sodium metal and benzophenone collected only from deep purple solution.

UV Absorption measurements were collected using a Varian Cary 50 Bio spectrometer with a solution samples held in a quartz cuvette. PL emission, excitation, and quantum yield data were collected using a Photon Technologies International (PTI) Quantamaster system equipped with an integrating sphere. Optical micrographs are collected using an Olympus BX51 optical microscope equipped with a Mercury lamp UV light source and Olympus DP71 color digital camera. Polymer film preparation is described in the text above.

9.3.2 Synthesis and Characterization

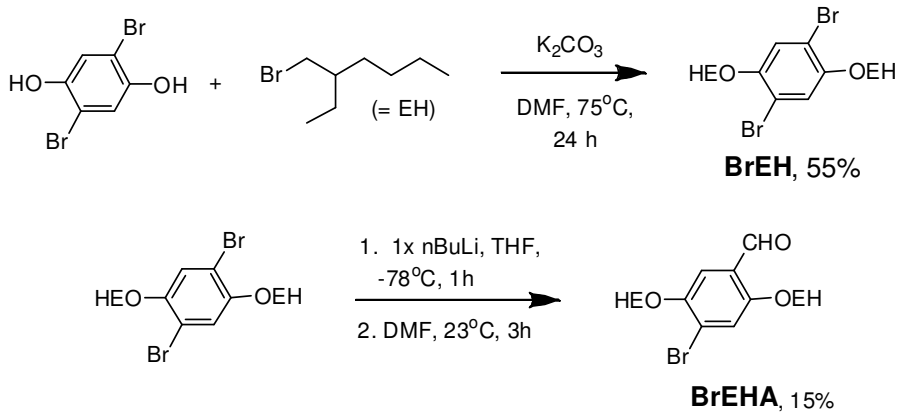

Scheme 9.1 Synthetic route to BrEH6A.

Synthesis of 1,4-dibromo-2,5-di((2-ethylhexyl)oxy)benzene (BrEH) 2,5-dibromohydroquinone (1equiv.) is loaded into a 2-neck glass round bottomed flask along with 1-bromo-2-ethylhexane (2.5 equiv.) and dimethylformamide (ca. 1 ml / g reagent). Potassium carbonate (3 equiv.) is added and the reaction is stirred at 75°C for 24 hours.

The reaction is cooled, vacuum filtered, and rotavaped at 80°C to remove solvents (DMF). The products are then purified through column chromatography using a hexanes eluent. A clear liquid is collected at a yield of 55%. For BrEH, ^{1}H NMR (300 MHz, $CDCl_3$): 7.10 (s 2H), 3.85 (d 4H), 1.77 (m 2H), 1.51 (m 8H), 1.36 (m 8H), 0.95 (m 12H).

Synthesis of 4-bromo-2,5-di((2-ethylhexyl)oxy)benzaldehyde (BrEHA) BrEH (1 equiv.) is loaded into a two-neck round bottomed glass flask and vacuum purged with argon three times. Anhydrous tetrahydrofuran is added by syringe (ca. 25 ml solvent / g Br6) and the vessel is placed into a bath of dry ice and 2-propanol (-78°C). *n*-Butyllithium (1 equiv.) is added dropwise via syringe and the reaction is stirred at -78°C for 1 hour. Anhydrous DMF (4 equiv.) is then added and the reaction is allowed to warm to 23°C over three hours. The reaction is quenched carefully with water and extracted with diethylether. The organic layer is collected and dried over $MgSO_4$ before being filtered and rotovaped to remove solvents. Purification is done by column chromatography with ethylacetate:hexane (1:30) eluent followed by successive recrystallizations from methanol and acetonitrile at 23°C. A colorless liquid is collected at yields of 15%. For Br6A, ^{1}H NMR (300 MHz, $CDCl_3$): δ 10.42 (s 1H), 7.33 (s 1H), 7.24 (s 1H), 3.93 (t 4H), 1.77 (m 2H), 1.50 (m 8H), 1.32 (m 8H), 0.94 (m 12H).

9.4 Conclusions

Common polymers may be suitable replacements to crystalline host materials for the activation of DHAE-style phosphors. Efficient triplet-generating chromophores such as BrEHA, a member of the Br*n*A family, can become brightly phosphorescent when embedded into certain glassy polymers. This effect can be strong even if the chromophore is highly non-crystalline. BrEHA is a liquid yet becomes brightly phosphorescent in certain polymers at ambient temperatures. Glassy polymers, well mixed with DHAE-style small molecule chromophores, can prevent vibrational freedom of the chromophore leading to triplet emission that is dominant over non-emissive relaxation. If the polymer constricts the chromophore efficiently, phosphorescent emission is surprisingly strong.

The critical concept to choosing a good polymer host is the idea of entanglement. In order for the two species to mix well the polymer must have two critical features: a flexible backbone that is structurally similar to the substitutents of the chromophore, and small pendants that do not shield the backbone from the small molecule. If these two conditions are met, the small molecule's substitutents (alkoxy as presented here) can entangle with the polymer backbone, which imparts glassy properties to the chromophore and restricts vibration. This effect can be enhanced if the backbone has a more space-filling structure, such as additional methyl substitutents, and if the pendants have any favorable interaction with the small molecule, such as π-π interactions.

By activating the phosphorescence of DHAE phosphors in non-crystalline and disordered systems we have removed one of the strict requirements of the DHAE design principle: perfect crystal order. This widens the design of metal-free organic phosphors even further and opens their use to a wider variety of applications. Also, the many desirable aspects of polymeric systems; process-ability, homogeneity, dope-ability, etc., are now available to DHAE phosphors. This work also holds promise of a true polymeric metal-free organic phosphor suitable for the fabrication of optoelectronic and optical biological devices.[10,11,12]

This work may also be expanded to improve the phosphorescence brightness by improved polymer-chromophore interaction through secondary bonding.[13,14] Perhaps by designing a polymer/chromophore pair that exhibits complementary groups for strong hydrogen bonding, better mixing and brighter emission can be achieved.

9.5 References

[1] O. Bolton, K. Lee, H.-J. Kim, K.Y. Lin, and J. Kim *Nature submitted* **2009**.
[2] O. Bolton, S. Jeon, and J. Kim *manuscript in progress*.
[3] R. E. Harding, S.-C.Lo, P. L. Burn, and I.D.W. Samuel, *Org. Electron.* **2008**, *9*, 377.
[4] T. Sajoto, P. I. Djurovich, A. Tamayo, M. Yousufuddin, R. Bau, and M. E. Thompson, *Inorg. Chem.* **2005**, *44*, 7992.
[5] W.Y. Huang, S. Matsuoka, T.K. Kwei, and Y. Okamoto *Macromol.* **2001**, *34*, 7166.
[6] D.A.M. Egbe, L.H. Nguyen, H. Hoppe, D. Muhlbacher, and N.S. Saricifci *Macromol. Rapid Comm.* **2005**, *26*, 1389.
[7] Some very weak phosphorescence was occasionally detected for the methyl acrylates listed here, but results were inconsistent and much weaker than the featured polymers listed in Figure 9.4.
[8] K. Li, L. Guo, Z. Liang, P. Thuyagarajan, and Q. Wang *J. Polymer Sci. A: Polymer Chem.* **2005**, *43*, 6007.
[9] U.H.F. Bunz et al *Chem. Mater.* **1999**, *11*, 1416.
[10] J. H. Burroughes et al **1990**, *347*,539.
[11] B.J. de Gans, P.C. Duineveld, and U.S. Schubert *Adv. Mater.* **2004**, *16*, 203.
[12] J. Peet, A.J. Heeger, and G.C Bazan **2009**, *42*, 1700.
[13] D.C. Sherrington and K.A. Taskinen *Chem. Soc. Rev.* **2001**, *30,* 83.
[14] C.R. South, C. Burd, and M. Weck *Acc. Chem. Rev.* **2007**, *40*, 63.

Chapter 10

Conclusions

10.1 Summary

The purpose of this thesis is to explore novel metal-free organic phosphor design through the design principle named the Directed Heavy Atom Effect, DHAE. As the parallel fields of organic materials and phosphorescent materials have been experiencing great surges in interest, they have been united only in a relatively small subset of organometallic compounds.[1,2] The DHAE principle, as is demonstrated in this work, provides a means to create new metal-free organic phosphors that are bright, robust, simple, and can be designed to emit specific colors, exhibit unique materials properties, and possess desired chemical functionalizations.

Phosphorescent materials are desirable in various applications because they emit from triplet states. Because they can emit from any of the three possible triplet states, they are more efficient emitters in light emitting devices than fluorescent emitters, which emit from only one.[3] Also, the long-living triplet states are believed to enhance exciton diffusion lengths in solar cells, allowing for the design of thicker absorbing layers and higher efficiency devices.[4] If these long-living triplets are allowed to emit they produce signals that are easily distinguished from short-living fluorescence, which is useful in certain detection schemes.[5] Triplets are also uniquely susceptible to quenching by other triplets materials, such as oxygen, giving them special use in biological sensing as well.[6]

With so many emerging applications for phosphorescent materials, the need for a versatile design principle to make new phosphors is critical. Previous phosphor design was limited to inorganic materials (mostly ceramics) and a small family of organometallic compounds.[7] The DHAE principle provides the ability to escape these limitations and design bright phosphors that are fully organic and metal-free.

The DHAE principle succeeds by combining two critical phenomena: the heavy atom effect and halogen bonding. The heavy atom effect occurs when a large atom, usually a halogen, enhances intersystem crossing in another molecule in close proximity. The large nucleus of the heavy atom enhances spin-orbit coupling, mixing singlet and triplet states to better produce the later. The DHAE principle enhances this through halogen bonding, which is a non-covalent interaction akin to hydrogen bonding that brings halogens exceptionally close to nucleophilic atoms. If the nucleophile is the carbonyl oxygen atom of a triplet allowing aromatic ketone, excellent triplet generation and bright phosphorescence can be achieved.

DHAE phosphors are brightest in crystal states, where halogen bonding is strongest and tight packing prevents vibrational losses that are otherwise very competitive with triplet emission. Further quenching effects can be eliminated by the introduction of a host material. A host material is structurally very similar to the phosphorescent chromophore but is optically non-interfering. It acts as an optically inert matrix that exhibits the same halogen bonding as the chromophore but also effectively prevents self-quenching by isolating each chromophore molecule in the crystal (co-crystal, as it is).

The most efficient DHAE phosphors presented here are based on a 4-bromobenzaldehyde chromophore coupled with a 1,4-dibromobenzene host. This is the case for nearly every chromophore/host pair in this work. The reasons that benzaldehydes work so well are both the minimal substitution at the carbonyl carbon (all other aromatic ketones contain larger moieties at this site) and the excellent similarity in volumetric size between the aldehyde group and the bromine atom. The former makes access to the aldehyde, for halogen bonding, more favorable while the later makes cocrystallization much more favorable.

Efficient cocrystallization is critical to achieving high quantum yields (QY) in crystalline DHAE phosphors. As chapter 4 demonstrates, low concentrations of the chromophore (relative to the host concentration) leads to inefficient inclusion into the cocrystal and, thus, low QYs. Likewise, large amounts of chromophore lead to self-quenching by excimer formation and triplet-triplet annihilation. Ideal mixes of chromophore and host are seen at concentrations of one-to-ten weight percent chromophore. QYs of cocrystals Br1A/Br1, Br6A/Br6, and BrE6A/BrE6, for examples,

average 55 - 60% and have been measured as high as 68%. These are the highest QYs measured for all DHAE phosphors presented here.

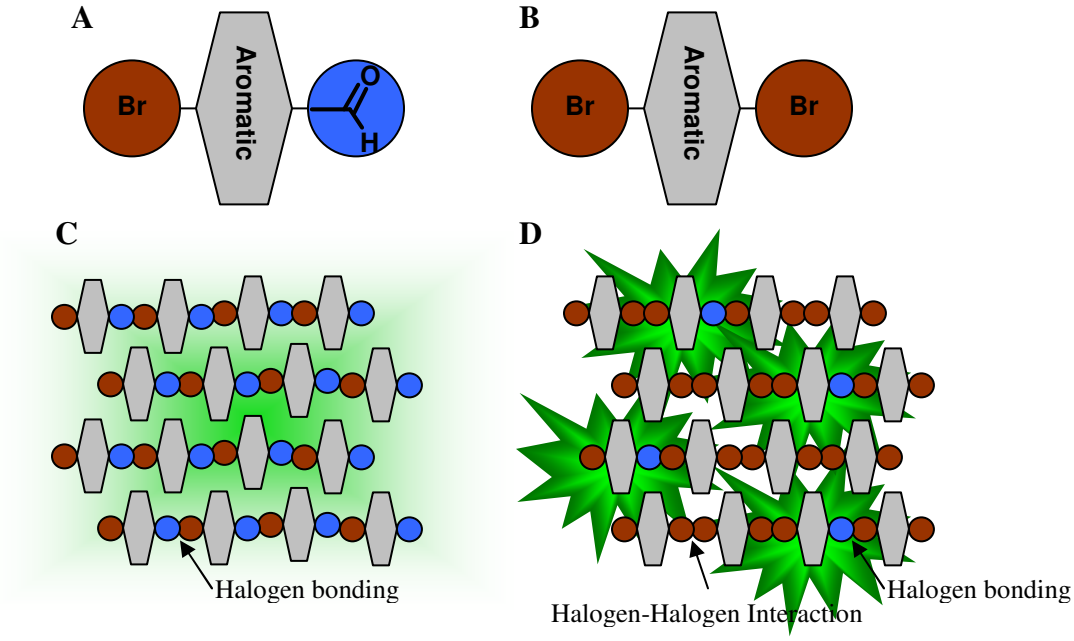

Figure 10.1 Schematic representation of the DHAE design principle. (**A**) The chromophore: a halogenated aromatic aldehyde. (**B**) The host: a di-halogenated analog to the chromophore. The aldehyde group is replaced with a halogen atom. (**C**) Crystals of pure chromophore: the heavy atom effect is directed to the aldehyde by halogen bonding, greatly increasing intersystem crossing. Phosphorescence is emitted though self-quenching is prevalent and QY is modest. (**D**) Cocrystals of chromophore and host, with a majority of host molecules: crystal packing exhibits the same halogen bonding as pure chromophore crystals but the chromophores are now diluted, preventing self-quenching. The phosphorescent QY is extremely high.

The DHAE principle can be used to design organic phosphors of different colors by altering the electron density at the core aromatic unit of the chromophore. As chapter 5 shows, this approach allows for both fine and coarse color tuning. By altering the halogen on the chromophore phosphorescent emission is red-shifted in discrete 5 nm steps from chlorine to bromine to iodine. Removing the halogen altogether, replacing it with hydrogen, shifts the emission roughly 30 nm to the blue, but also makes cocrystallization difficult because of the pronounced difference in chromophore/host structural agreement. Changing the electron donating properties of the chain substituents allows for coarse color tuning. The alkyl substituents of BrAlkyl6A/BrAlkyl6 give their

cocrystals a blue emission while the alkoxy substituents of Br6A/Br6 yield green. BrS6A/BrS6 have thiol ethers that lead to red-shifted yellow phosphorescence. Np6A/Np6 cocrystals have alkoxy substitution but emit orange phosphorescence because their central chromophore is extended from the benzene ring of Br6A to a naphthalene ring, which increases the electron density even more than chain alterations. These demonstrate not only successful application of the general design principles of DHAE, that a brominated aromatic aldehyde cocrystallized with its dibromo variant emit phosphorescence, but that it can be tuned to alter the emission color as well.

In chapter 6 further investigation of the phosphorescent emission from crystals of pure Br6A reveal the novel phenomenon of delayed phosphorescence.[8] Delayed emission occurs when lower-energy excited states are thermally populated into emissive states. This has been observed many times for fluorescence, but until now it has not been seen for phosphorescence, presumably because it would require up-conversion from a normally highly-quenching intermolecular state.[9] Once excited, crystals of Br6A relax to a triplet excimer lower in energy than T_1. With sufficient heat, which is ample at room temperature, electrons in this excimer state are raised to T_1, where they emit in the exact same spectrum as normal, prompt phosphorescence. This emission is only distinguishable from prompt phosphorescence because it occurs at a much slower rate and it is completely absent at low temperature. This finding is noteworthy because it represents a reclamation of emissive triplets from excimer states, normally considered a wholly quenching state.[10] This holds promise for enhancing efficiencies from organic light emitting devices where excimer formation is common and detrimental.

Br1A/Br1, the smallest member of the featured Br*n*A/Br*n* family of DHAE phosphors, exhibits simple synthesis, high QYs, and unique microstructures grown by sublimation. As explained in chapter 7, Br1A and Br1 are extremely simple DHAE phosphors that can be synthesized with fewer impurities and in larger batches than any others in the Br*n*A/Br*n* family. Dropcast samples exhibit QYs as high or higher than Br6A/Br6 cocrystals with some measured as high as 62%. These compounds are also about 66% smaller than Br6A/Br6 making their cocrystals much denser and appearing much brighter. Perhaps most intriguing, Br1A and Br1 sublime readily to form monodisperse needle/rod-shaped cocrystals whose sizes appear to be controllable by

sublimation time. These crystals are very bright, exhibit apparent anisotropic emission, and hold promise for the design of metal-free organic phosphorescent metamaterials.

Extending the usefulness of DHAE phosphors involves adding useful functionality to the crystals so that they can be designed for use in any application desired. Chapter 8 shows one such functionalized material in BrE6A/BrE6 cocrystals. These compounds have ester functionality at the ends of their alkoxy substituents. They cocrystallize very well and achieve QYs on par with Br6A/Br6 cocrystals while actually out-performing their efficiency them at higher chromophore concentrations. The ester functionality does not affect the crystal packing so halogen bonding is still dominant, yet it offers the possibility of post-crystallization de-protection to add carboxylic acid functionality to the cocrystals. This holds promise for attaining useful chemical functionalities in DHAE materials by demonstrating one approach to achieving phosphors that contain functional groups that may otherwise interfere with the desired halogen-bonding crystal motif.

A final study demonstrates that DHAE-style phosphors hold promise for metal-free organic phosphorescence even in the absence of crystal order by instead being embedded into select polymers. Chapter 9 shows that mixing DHAE chromophores into polymers that do not have large pendants and have backbones whose structures are similar to the chain substituents of the chromophore can activate phosphorescent emission. When these conditions are met, the polymer effectively entangles the chromophore to provide the rigidity usually imparted by the crystal. This entanglement prevents vibrational freedom of the chromophore so that triplets are not lost to internal conversion. These systems extend the usefulness of DHAE-style phosphors even further to include non-crystalline materials or those that do not crystallize with strong halogen bonding.

In summary, the DHAE design principle removes the existing limitations on organic phosphor design. This work has shown how bright metal-free organic phosphors can be synthesized through a few simple design requirements: aromatic ketones and halogen bonding. The potential to tune the optical, material, and chemical properties of these phosphors is clearly demonstrated as is a successful approach to reducing the halogen bonding/crystalline requirement altogether. The DHAE principle promises a paradigm shift in the field of phosphorescent materials.

10.2 Future Considerations

The work presented here is only the very beginning of DHAE phosphor research. This phenomenon was discovered through serendipity and most of the time dedicated to it thus far has been to explore its requirements and make small alterations to the first phosphor discovered. Luckily the Br*n*A/Br*n* family of phosphors have been ideal for study because they are bright and easy (and economical) to synthesize. Thus, they were the focus of this work. Uncountable lists of new phosphors and work to be done remains in the field of DHAE phosphors.

Work to integrate these phosphors into OLEDs has begun in earnest, though progress has been slow. Unlike the organometallic phosphors that are currently dominating the field, DHAE phosphors operate best when highly crystalline and sublime at relatively low temperatures. These aspects make it difficult to simply substitute DHAE phosphors into the fabrication techniques of organometallic OLEDs. Achieving bright electro-phosphorescence from DHAE-based devices seems achievable given the high PL QYs observed but it may require entirely new device design and/or fabrication technique. Great promise exists, however, to shorten this process as new DHAE materials with improved and additional functionalities, such as better carrier mobility or higher sublimation temperatures, may accelerate these efforts.

There is also the possibility of using DHAE compounds as efficient triplet sustaining materials to improve the exciton diffusion lengths in organic photovoltaics. Organometallic phosphorescent compounds, "triplet materials," have been employed to this effect with mixed success.[11] DHAE phosphors have the advantage of much longer living triplets (as evidenced by the long, millisecond phosphorescent lifetimes). This can enhance exciton diffusion by allowing the excited states more time to diffuse. The idea of using DHAE materials in this way is especially interesting because it does not require that the triplets emit (in fact it would prefer that they did not), which may make the requirements of strict crystal packing less necessary.

A final future application for which DHAE phosphors may be uniquely suited is in sensor design. Aside from those mentioned in Chapter 1, emissive lifetime and oxygen-quenching approaches, the unique conformational aspect of DHAE phosphorescence may be useful for sensing. This report has shown how the heavy atom effect is so greatly

enhanced when directed by halogen bonding. It may be possible to design benzaldehyde and halogen pairs into compounds that exhibit other forms of conformational recognition, such as in numerous biological compounds. If the conformational recognition is coupled with the formation of a DHAE halogen bond, a strong phosphorescent signal may be generated. Given the high sensitivity of photonic detection, this may offer a way to turn imperceptible biological recognitions into measurable signals. It would also be detectable on a phosphorescent timescale, which would have the added benefits of improved signal-to-noise ratios and measurement by dynamic spectroscopy.

10.3 References

[1] M.A. Baldo, M.E. Thompson, and S.R. Forrest *Pure Appl. Chem.* **1999**, *71*, 2095.
[2] A. Kohler, J.S. Wilson, and R.H. Friend *Adv. Mater.* **2002**, *14*, 701.
[3] M.A. Baldo, D.F. O'Brien, Y. You, A. Shoustikov, S. Sibley, M.E. Thompson, and S.R. Forrest *Nature* **1998**, *395*, 151.
[4] Y. Shao and Y. Yang *Adv. Mater.* **2004**, *17*, 2841.
[5] A.P. de Silva, H.Q.N. Gunaratne, T. Gunnlaugsson, A.J.M. Huxley, C.P. McCoy, J.T. Rademacher, and T.E. Rice *Chem. Rev.* **1997**, *97*, 1515.
[6] W.L. Rumsey, J.M. Vanderkooi, and D.F. Wilson *Science* **1998**, ***241,*** 1649.
[7] E. Baranoff, J.-H. Yun, M. Graetzel, and Md.K. Nazeeruddin *J. Organometallic Chem.***2009**, *694*, 2661.
[8] This is not to be confused with another phenomenon known as "delayed phosphorescence," which is actually dynamically-resolved emission from the T_x,T_y, and T_z triplet states at low temperatures. An example: J. Schmidt, D.A. Antheuni, and J.H. Vanderwa *Mol. Phys.* **1971**, *22*, 1. See Chapter 6.
[9] B. Hu, L.A. Yan, and M. Shao *Adv. Mater.* **2009**, *21*, 1500.
[10] M.A. Slifkin and A.O. Al-Chalabi *Chem. Phys. Lett.* **1974**, *29*, 110.
[11] F. Guo, Y.-G. Kim, J.R. Reynolds, and K.S. Schanze *Chem. Comm.* **2006**, 1887.